MITOCHONDRIAL OXIDATIVE DAMAGE, BASE-EXCISION REPAIR, AND ANTIRETROVIRAL THERAPY

A THESIS SUBMITTED TO THE GRADUATE DIVISION OF THE
UNIVERSITY OF HAWAIʻI AT MĀNOA IN PARTIAL FULFILLMENT
OF THE REQUIREMENTS FOR THE DEGREE OF

DOCTOR OF PHILOSOPHY
IN
CELL AND MOLECULAR BIOLOGY

May 2016

By
Anna Pickering

Dissertation Committee:
Mariana Gerschenson, Chairperson
Peter Hoffmann
Jun Panee
Olivier le Saux
V. Andrew Stenger

ACKNOWLEDGEMENTS

Firstly I would like to express my enormous gratitude to my mentor, Mariana Gerschenson, for all of the tremendous support she has given me. My journey through graduate school has not been the straightest or easiest one, but Mariana helped me along the whole way and has enabled me to be the confident, capable scientist that I am today. Her dedication to my education through writing and presentation assistance, exam preparation, and general advice on life has been invaluable. I would also like to extend my appreciation to our lab manager, Daniel Libutti, for the time he spent instructing me on the ways of the lab. Not only did he teach me many of the experimental techniques I used, he made sure I understood the scientific methods and was kind enough to field all my questions I inevitably had.

All of my fellow lab-mates deserve a round of applause for welcoming me warmly into the lab and for the support they have given me on my project. In particular, I want to thank Heidi Fink for the lengthy training on the 8-oxo-dG Southern blot assay and to Kristen Ewell for the lessons on the Seahorse machine, in addition to all of the day-to-day lab help they provided. Lyn Hamamura needs to be thanked profusely for her tireless administrative support, for keeping me current on all the program requirements, and for always being someone to talk to when I needed. I also want to express my gratitude to my committee members for the time they have committed to my education and for all of the advice they have provided for my project along the way.

Finally, I need to express a sincere appreciation for my husband, Tom Pickering, as he has made my grad student life considerably less difficult. He has provided support in more ways than I can count- mental, logistical, culinary- and having a life partner has made surviving the rough patches that much easier. My family also deserves thanks for their unwavering support- my parents for all of the practical help getting through graduate school, and my sister for the emotional support necessitated- and for their belief in me all along the way.

ABSTRACT

Antiretroviral therapy (ART) has been enabling patients with HIV/AIDS to live longer and healthier, but do cause a number of side effects, including renal and hepatic toxicity, neural dysfunction, and metabolic disorders such as insulin resistance. Complications from ART can be attributed in large part to mitochondrial dysfunction, with decreased oxidative phosphorylation (OXPHOS) and increased oxidative stress, including mitochondrial DNA (mtDNA) oxidative damage. MtDNA damage can be repaired by several mechanisms including base-excision repair (BER), but whether BER is affected by or involved in HIV or ART-associated mitochondrial toxicity has not yet been evaluated.

In this study, three BER enzymes (OGG1, MutYH, and FEN1) and their relationship to mitochondrial function and mtDNA oxidative damage during ART were investigated. First, BER enzyme mRNA levels were evaluated in peripheral blood mononuclear cells (PBMCs) from HIV-negative individuals and HIV-positive, ART-naïve patients at baseline and after receiving ART for 72 weeks (Chapter 2). Next, an *in vitro* model was developed to study ART-induced effects on BER during nephrotoxicity by treating primary human renal cells with protease inhibitor (PI)-based drug cocktails (Chapter 3). The hypothesis to be tested was that ART-induced mtDNA oxidative damage would lead to an increase in BER enzyme expression, and that higher levels of BER enzymes will be associated with decreased mitochondrial function.

In the clinical study, mtDNA oxidative damage was higher in HIV-positive, ART-naïve patients than the HIV-negative participants, while mtDNA content, oxidative phosphorylation (OXPHOS) activity, and MutYH mRNA were lower in HIV patients at baseline. After 72 weeks of ART, these parameters improved. OGG1 and FEN1 mRNA correlated with mtDNA oxidative damage in HIV-negative individuals, but not in HIV-positive, ART-naïve patients. FEN1 mRNA decreased in HIV patients following ART initiation, and those with lower FEN1 levels at baseline showed a greater improvement in mtDNA oxidative damage than those with higher baseline FEN1. In the *in vitro* study, non-mitochondrial respiration and electron transport chain (ETC) proton leak were elevated in ART-treated cells, while both mtDNA oxidative damage and OGG1 mRNA increased during treatment. These results demonstrate that BER is affected by both HIV infection and ART, and the relationship between FEN1 expression and patient outcome could have implications for better personalized ART regimens in the future.

TABLE OF CONTENTS

LIST OF FIGURES AND TABLES

LIST OF ABBREVIATIONS

3TC	Lamivudine
8-oxo-dG	8-oxo-deoxyguanine
ABC	Abacavir
AFRIMS	Armed Forces Research Institute of the Medical Sciences
AIDS	Acquired immunodeficiency syndrome
ART	Antiretroviral therapy
ATP	Adenosine triphosphate
ATV	Atazanavir
ATV/r	Ritonavir-boosted atazanavir
BCA	Bicinchoninic acid
BER	Base-excision repair
BF	Break frequency
BMI	Body mass index
BSA	Bovine serum albumin
CD4	Cluster of differentiation 4
CDC	Centers for Disease Control
cDNA	Complementary DNA
CI	Complex I
CIV	Complex IV
CSPD	Chloro-5-substituted adamantyl-1,2-dioxetane phosphate
CVD	Cardiovascular disease
CYP3A4	Cytochrome P450 3A4
d4T	Stavudine
dGK	Deoxyguanosine kinase
DIG	Digoxigenin
DMEM	Dulbecco’s modified Eagle’s medium
DMSO	Dimethyl sulfoxide
DNA	Deoxyribonucleic acid
DRV	Darunavir

DRV/r	Ritonavir-booster darunavir
ECL	Enhanced chemoluminescence
EDTA	Ethylenediaminetetraacetic acid
ENFD	Epidermal nerve fiber density
EtOH	Ethyl alcohol
FapyAde	4,6-diamino-5-formamidopyrimidine
FCCP	Carbonyl cyanide-p-trifluoromethoxyphenylhydrazone
FEN1	Flap structure-specific endonuclease 1
FTC	Emtricitabine
GI	Gastrointestinal
GPO	Government Pharmaceutical Organization
H_2O	Water
H_2O_2	Hydrogen peroxide
HACRP	Hawaii AIDS Clinical Research Program
HCl	Hydrochloric acid
HDL	High density lipoprotein
HEK	Human embryonic kidney
HIV	Human immunodeficiency virus
HR	Homologous recombination
HRP	Horseradish peroxidase
IgG	Immunoglobulin G
IRB	Institutional Review Board
LDL	Low density lipoprotein
LPV	Lopinavir
MF	Mitochondrial fraction
MMR	Mismatch repair
mRNA	Messenger RNA
mtDNA	Mitochondrial DNA
MutYH	MutY homolog
NaCl	Sodium chloride
NADH	Nicotinamide diamine dinucleotide

NaOAc	Sodium acetate
NaOH	Sodium hydroxide
NEIL1	*Nei*-like DNA glycosylase 1
NHEJ	Non-homologous end joining
NNRTI	Non-nucleoside reverse transcriptase inhibitor
NRF2	Nuclear respiration factor 2
NRTI	Nucleoside reverse transcriptase inhibitor
NTH1	Endo III-homolog 1
NVP	Nevirapine
O_2^-	Superoxide radical
OCR	Oxygen consumption rate
OGG1	Oxoguanine DNA glycosylase 1
OH	Hydroxyl group
OXPHOS	Oxidative phosphorylation
PBMC	Peripheral blood mononuclear cell
PBS	Phosphate-buffered saline
PBST	PBS- Tween 20
PCR	Polymerase chain reaction
PI	Protease inhibitor
PN	Peripheral neuropathy
PNKP	Polynucleotide kinase 3′-phosphatase
Pol	Polymerase
PPIA	Peptidylprolyl isomerase A
PRX2	Peroxiredoxin 2
RIN	RNA integrity number
RNA	Ribonucleic acid
ROS	Reactive oxygen species
SEARCH	South-East Asia Research Collaboration with Hawaii
SOD2	Superoxide dismutase 2
SSC	Saline sodium citrate
TBP	TATA binding protein

TDF	Tenofovir
TE	Tris-EDTA
TFAM	Transcriptional factor A, mitochondrial
TIM	Translocase of the inner mitochondrial membrane
TK2	Thymidine kinase 2
TOM	Translocase of the outer mitochondrial membrane
TRCARC	Thai Red Cross AIDS Research Center
UGT	Uridine 5'-diphospho-glucuronosyltransferase
UNG1	Uracil DNA glycosylase 1
VDAC	Voltage-dependent anion channel
WCL	Whole cell lysate
WHO	World Health Organization
XF	Extracellular flux
ZDV	Zidovudine

CHAPTER 1

Introduction

1.1 MITOCHONDRIAL FUNCTION

1.1.1 The mitochondrion

Mitochondria are fundamentally important for the function of most eukaryotic cells. These organelles are involved in a wide variety of metabolic and cellular processes, including calcium homeostasis [1], heme biosynthesis [2], β fatty acid oxidation [3], the citric acid cycle [4], steroid hormone synthesis [5], and apoptotic regulation [6]. Most significantly, they are the source of the production of a cell's energy in the form of adenosine triphosphate, or ATP, via oxidative phosphorylation (OXPHOS) [7]. Consequently, this results in the majority of the production of a cell's reactive oxygen species (ROS) [8] due to electron slippage during OXPHOS. Individual cells, with the exception of red blood cells, can each contain up to 2000 mitochondria depending on their tissue type and energy requirements, with this number in constant flux due to the processes of mitochondrial fission and fusion [9]. Structurally, mitochondria form a network that is associated with the cytoskeleton and connected to the endoplasmic reticulum, with extensive communicative signaling and tight regulatory control occurring between the organelles [10].

Mitochondria consist of two lipid membranes, the outer membrane and the inner membrane. The inner membrane is folded into multiple cristae for a greater surface area and is the location for oxidative phosphorylation and mitochondrial protein biosynthesis [11] among other systems (Fig. 1.1). The area encapsulated by the inner membrane is called the mitochondrial matrix, the location for most mitochondrial metabolic processes, while that between the inner and outer membranes is known as the inner-membrane space (IMS). The pH and ion concentrations within the matrix and IMS are tightly regulated, creating an electrochemical gradient which is essential for many biological functions [7]. A number of proteins and protein complexes span each of the membranes, including the translocase of the outer membrane (TOM), translocase of the inner membrane (TIM), voltage-dependent anion channels (VDAC proteins) and members of the mitochondrial carrier family, which allow for controlled import and export of proteins, metabolites, and other molecules into and out of the mitochondria [12].

Each mitochondrion contains between two and ten copies of its own small, circular genome, giving rise to the theory that mitochondria originated as prokaryotes which formed a symbiotic relationship with eukaryotic cells [13]. Mitochondrial DNA (mtDNA) is inherited

maternally from oocytes [14]. The mitochondrial genome contains genes for protein synthesis and certain subunits of the electron transport chain and ATP synthase [13]. However, the majority of the proteins that comprise a mitochondrion are encoded by nuclear DNA which must be transcribed in the nucleus, translated in the cytoplasm, and then transported to the mitochondria [15].

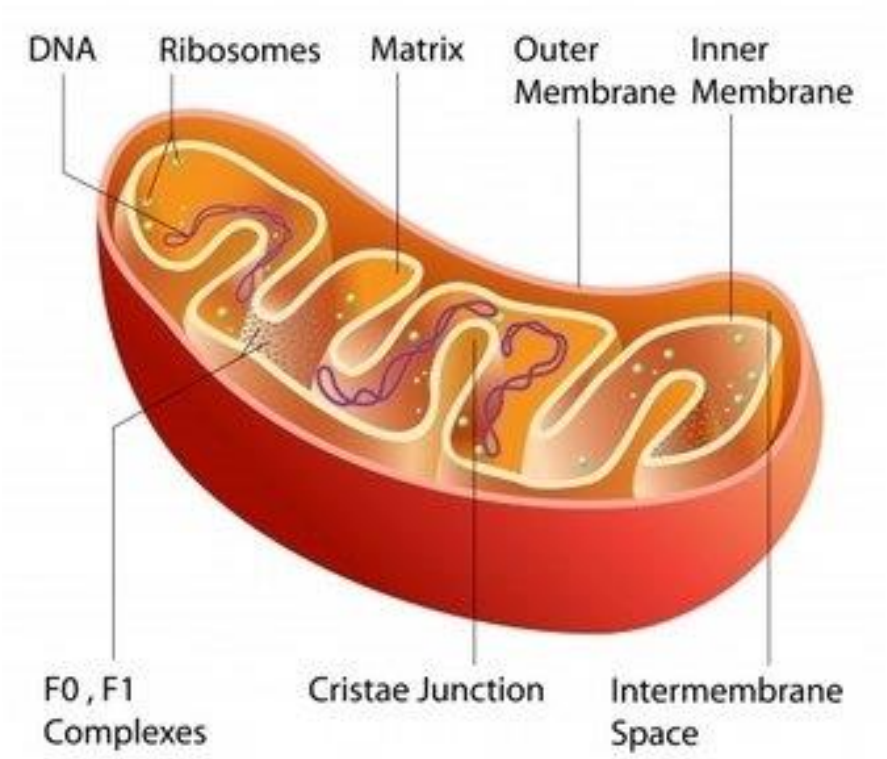

Figure 1.1. Structure of the mitochondrion. A cut-away image of a representative mitochondrion, showing the locations of the inner and outer membranes and membrane localization of mtDNA, mitochondrial ribosomes, and ATP synthase complexes (consisting of the membrane-embedded F_0 and matrix F_1 portions) [16].

1.1.2 Oxidative phosphorylation and respiration

Energy production through oxidative phosphorylation (OXPHOS) is conducted through a series of enzyme complexes that comprise the electron transport chain and ATP synthase, both of which are located within the inner mitochondrial membrane (Fig. 1.2). The four complexes of the electron transport chain are NADH dehydrogenase (complex I), succinate dehydrogenase (complex II), cytochrome *c* reductase (complex III), and cytochrome *c* oxidase (complex IV). Complexes I and II accept electrons from NADH and succinate, respectively, both products resulting from the processing of acetyl-CoA through the citric acid cycle. As the electrons are passed along the transport chain, hydrogen ions are pumped through the complexes from the mitochondrial matrix to the inner-membrane space. This creates both a pH and voltage gradient across the inner membrane, and the resulting potential is what drives the production of ATP [17]. Hydrogen ions are forced back across the inner membrane through the complicated mill-like ATP synthase, which as the hydrogen passes through undergoes a rotation of structural changes that facilitates the addition of inorganic phosphate (P_i) to adenosine diphosphate (ADP) to form ATP [18]. The final net yield is approximately 30-36 ATP molecules per glucose molecule that is catabolized through glycolysis and the citric acid cycle and 14 ATP molecules per round of fatty acid β-oxidation, much more efficient than the 2 ATP resulting from one round of glycolysis alone [9].

As the electrons leave the transport chain after passing through complex IV, they undergo a reaction with hydrogen ions (H^+) to reduce molecular oxygen (O_2) to water (H_2O). It is through this process in the mitochondria where the majority of cellular oxygen consumption occurs [19]. However, electron slippage from the transport chain occasionally occurs, predominantly from complexes I and III, and electrons are prematurely released [20]. The occurrence of this increases if ATP production efficiency is reduced and OXPHOS is performing sub-optimally (such as in cases of drug-induced toxicity) [8]. When this happens, incomplete reduction of oxygen may occur, resulting in oxygen radicals such as superoxide ($\cdot O_2^-$), peroxide ($:O_2^{2-}$), and hydroxyl radicals ($\cdot OH$). These species are highly reactive and can undergo spontaneous redox reactions with a wide variety of molecules they encounter, including DNA, protein, and lipids [21]. Superoxide can be converted by superoxide dismutase (SOD) into O_2 and hydrogen peroxide (H_2O_2), a reactive oxygen species which can cause damage but in low concentrations can also diffuse into the cytoplasm and function in cellular signaling [22].

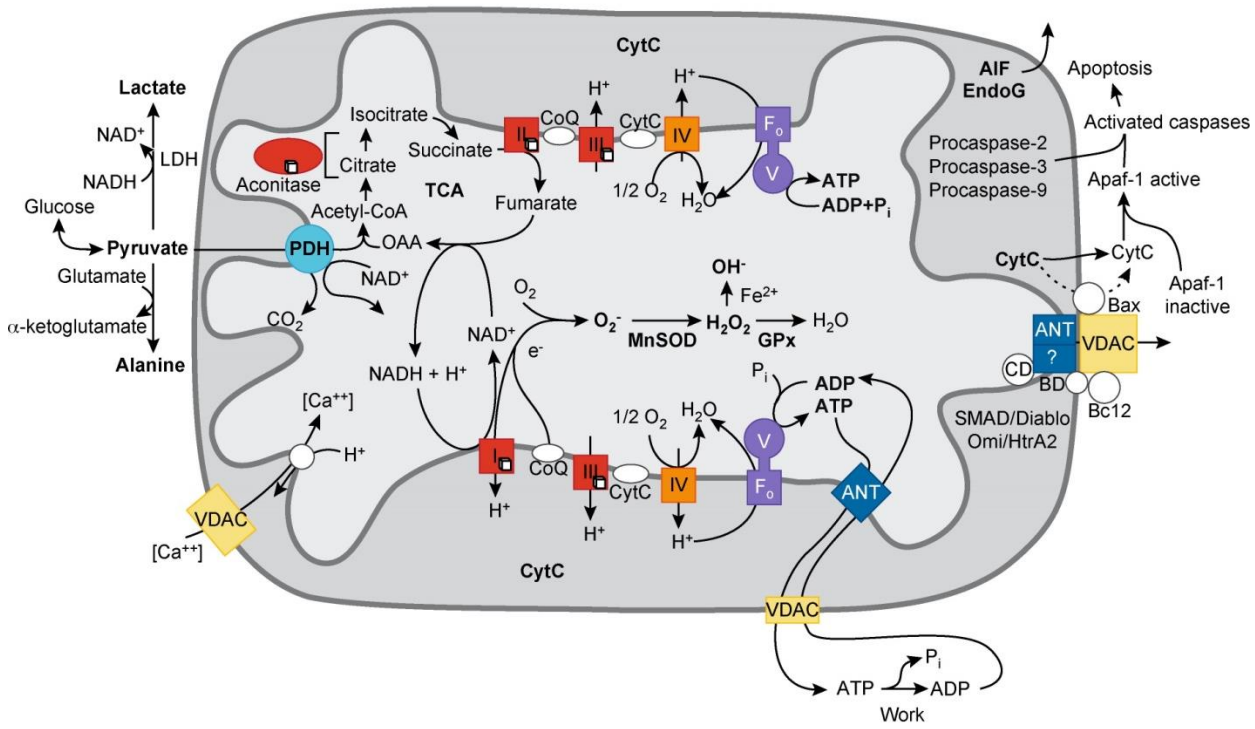

Figure 1.2. Metabolic and signaling pathways of the mitochondria. This figure shows an overview of some of the processes that occur within a mitochondrion, including OXPHOS, apoptosis, the citric acid (TCA) cycle, calcium influx and efflux, and ROS production and processing by antioxidants [14].

1.1.3 Mitochondrial DNA

Each individual mitochondrion contains between two and ten copies of the mitochondrial genome. This genome exists as a small, circular, double-stranded DNA construct approximately 16.6 kb in size in mammals and is highly conserved across other eukaryotes (Fig. 1.3) [14]. The circular structure of mitochondrial DNA (mtDNA) has led to the hypothesis that mitochondria originated from a symbiosis of prokaryotic entities with early eukaryotic organisms [23]. MtDNA does not bind histones like nuclear DNA, but is loosely bound to a number of DNA-binding proteins such as the mitochondrial single-strand binding protein (mtSSB) and the mitochondrial transcription factor A (TFAM). The DNA/protein complex is supercoiled into a structure known as a nucleoid, which is located within the mitochondrial matrix and associated with the inner membrane. Its proximity to the site of OXPHOS and ROS production makes mtDNA especially susceptible to oxidative damage, particularly during replication when it is uncoiled [17].

The two strands of the mtDNA are designated the heavy strand (H) and the light strand (L), based on differences in the guanine:cytosine ratio on each. Both strands contain multiple genes which are transcribed polycistronically. A total of 37 genes are encoded in the mtDNA: 22 transfer RNAs, 2 ribosomal RNAs, and 13 peptides that compose part of complexes I, III, IV, and ATP synthase (Complex V). Only a very small portion of the mtDNA is noncoding, most being in the displacement loop (D-loop), which spans approximately 700-1000 bases in mammals. The D-loop contains the origins for H-strand replication and H- and L-strand transcriptional promotion sites, while the L-strand replication origin exists in a separate site [13]. All enzymes required for mtDNA transcription and replication, including the mitochondrial DNA polymerase (pol) γ, are encoded by nuclear genes and must be transported into the mitochondria after translation.

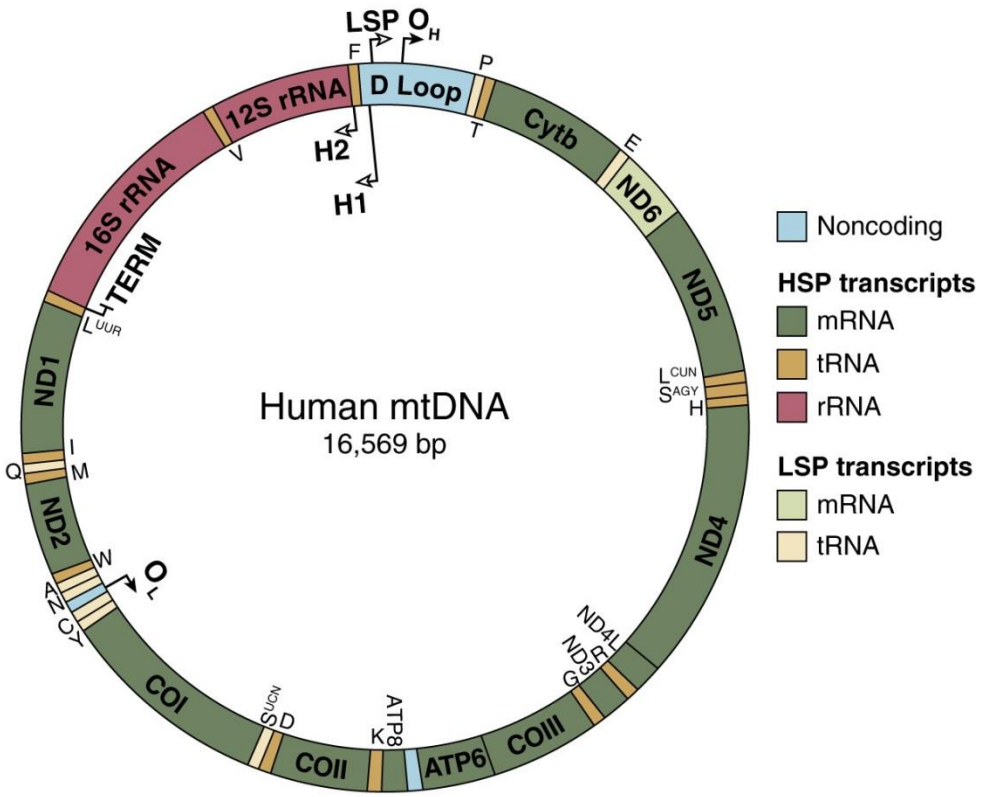

Figure 1.3. Map of human mitochondrial DNA. This figure shows the locations of transcripts, replication origins (O_H and O_L), and transcriptional promoters (H1, H2, and LSP) within the heavy (H) and light (L) strands of the human mitochondrial genome. Regions that are noncoding or that code for mRNA, tRNA, or rRNA are designated by color. Letters designate which OXPHOS complex the mRNA transcripts encode subunits for: cytochrome B (Cytb), NADH dehydrogenase (ND), complexes I, II, and III (COI, COII, and COIII), and ATP synthase (ATP) [13].

1.1.4 Mitochondrial oxidative DNA damage and repair

Being located in the same area as OXPHOS, mtDNA is particularly vulnerable to attack from the ROS that results from the approximately 3% of the electrons that leak prematurely from the transport chain. This number increases when the enzyme complexes of OXPHOS are not functioning optimally or the process is performing less efficiently than normal [8]. As the mtDNA is not as condensed as in chromosomes, it is more open to attack than nuclear DNA, particularly when uncoiled for replication [17]. Oxidative modifications that lead to mutations are especially problematic for mtDNA, as the majority of the DNA is coding and alterations to the genetic code are more likely to have a deleterious effect than in DNA with noncoding

stretches [14]. The most immediate effects of mutations would likely be reduced OXPHOS function, followed by increased ROS production and higher cellular oxidative stress, looping back to more oxidative DNA modifications.

There are many types of oxidative modifications that can arise from reaction of ROS with either the DNA bases or the sugar/phosphate backbone, including strand breaks, inter- or intra-strand crosslinks, adduct formation, spontaneous deamination, or oxidation [24]. Of the mutation-inducing lesions, one of the most common and well-studied is the addition of an OH group to the C8 carbon of guanine, which results in 8-oxo-deoxyguanine (8-oxo-dG). This residue can incorrectly pair with adenine, which if left uncorrected will lead to a G/C → T/A transversion following subsequent rounds of replication [25].

Mitochondria have DNA repair systems in place, including their own forms of base-excision repair (BER), mismatch repair (MMR), and recombinational repair through homologous recombination (HR) or non-homologous end joining (NHEJ) [25]. Due to the difficulty of studying isolated mitochondria, most mechanisms are still not fully understood, though BER was the first pathway to be identified in the mitochondria and is now relatively well characterized.

In the mitochondria, 8-oxo-dG modifications are corrected by a BER pathway similar to that used in the nucleus (Fig. 1.4). It begins with a DNA glycosylase removing the altered or incorrect base from the backbone sugar molecule. This is performed by oxo-guanine glycosylase 1 (OGG1) for 8-oxo-dG [26], and by the mutY homolog (MutYH) for adenine bases incorrectly paired with 8-oxo-dG [27]. Once the base is removed, the DNA strand is cleaved between the 3'OH group of the abasic site and the adjoining 5' phosphate. In the case of 8-oxo-dG this is performed by OGG1 as it has a bi-functional glycosylase/endonuclease activity, while in the case of the incorrectly-paired adenine this is performed by an abasic (AP) endonuclease (APE). APE1 is known to have endonuclease activity in the mitochondria; APE2 has also been found in the mitochondria though its activity there is currently unclear [25].

Two types of mitochondrial BER occur that are distinguished by the DNA synthesis step. In short-patch base excision repair (SP-BER), the AP site is fully removed by an APE, after which DNA pol γ inserts the correct nucleotide and DNA ligase seals the nicks in the DNA backbone. In contrast, in long-patch base excision repair (LP-BER), pol γ inserts the correct nucleotide and then extends a number of nucleotides further, leaving the old strand of nucleotides hanging as a 5' flap structure. The overhang is then removed by the flap structure-

specific endonuclease 1 (FEN1), possibly in tandem with the helicase/nuclease Dna2, after which DNA ligase seals the nick at the ends of the added nucleotides, thus completing the repair process [25].

Other base-excising proteins have been found to exhibit activity in the mitochondria, including uracil DNA glycosylase 1 (UNG1), which removes uracil in DNA, and *nei*-like DNA glycosylase 1 (NEIL1), which removes 4,6-diamino-5-formamidopyrimidine (FapyAde) modifications. Several additional nuclear BER proteins have also been found in the mitochondria, such as the Endo III-homolog 1 (NTH1) and polynucleotide kinase 3′-phosphatase (PNKP), though any mitochondrial repair activity of these has yet to be identified [25]. Most mitochondrial repair proteins found to date have multiple interaction partners in nuclear DNA repair, so it is likely that more nuclear repair proteins, or variants of such, will be discovered in the mitochondria in the future.

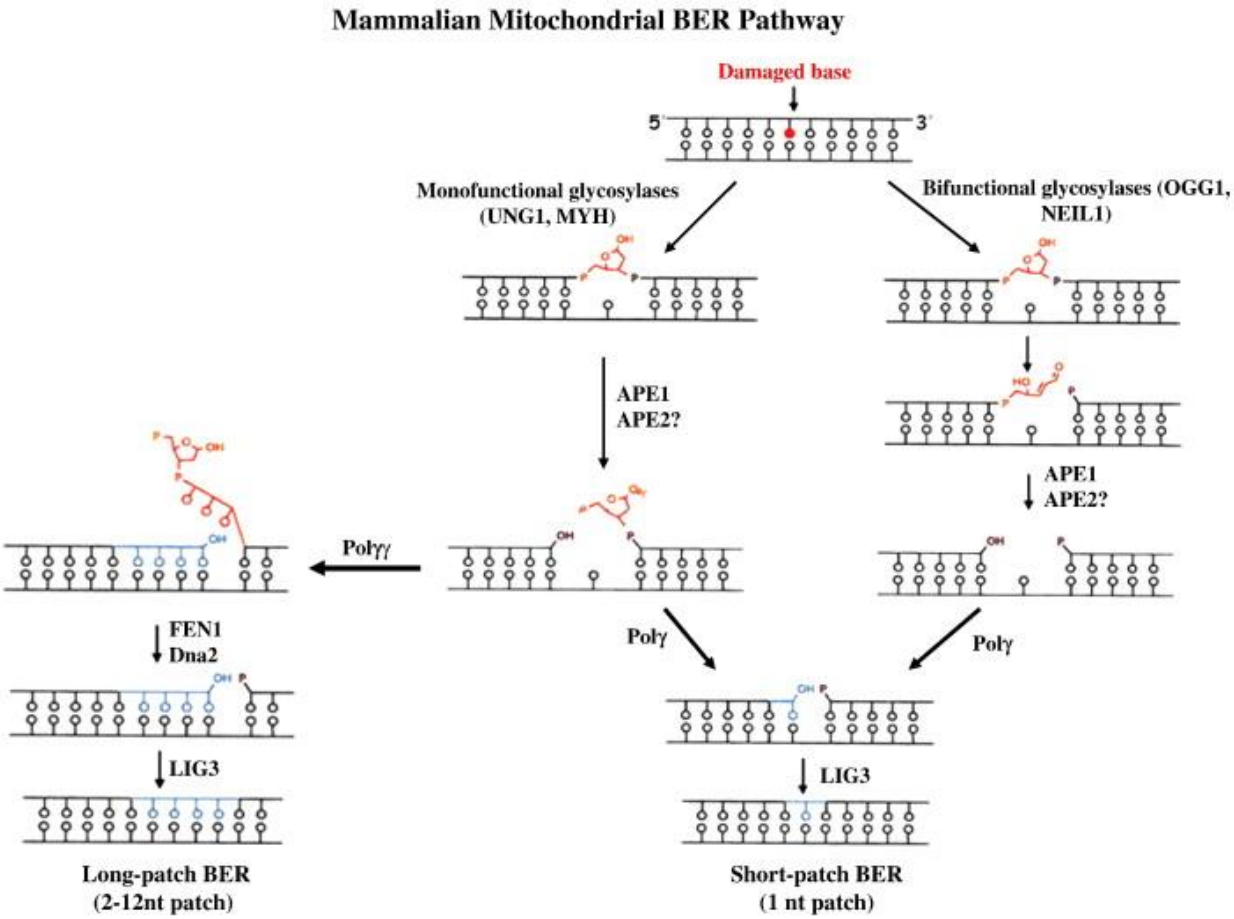

Figure 1.4. Mitochondrial base-excision repair. This diagram shows the steps involved in short-patch (SP) and long-patch (LP) base-excision repair (BER); from the top: removal of modified or incorrect base, cleavage of abasic site from DNA backbone, insertion of correct nucleotide (or multiple nucleotides in LP-BER), removal of 5' DNA flap structure (from LP-BER), and ligation of corrected nucleotide to DNA backbone. Proteins currently known to play a role in each step are also indicated: uracil-DNA glycosylase 1 (UNG1), mutY homolog (MutYH), oxoguanine-DNA glycosylase 1 (OGG1), nei-like DNA glycosylase 1 (NEIL1), apurinic/apyrimidinic endonucleases 1 and 2 (APE1 and APE2), DNA polymerase γ (Polγ), flap structure-specific endonuclease 1 (FEN1), DNA replication helicase/nuclease 2 (Dna2), and DNA ligase 3 (LIG3) [25].

1.1.5 Mitochondrial BER enzymes

All proteins involved in mtDNA repair are encoded in the nucleus, translated in the cytoplasm, and imported into the mitochondria via a variety of mitochondrial translocases [28]. The BER enzymes in this study, OGG1, MutYH, and FEN1, are all active in both nuclear and mitochondrial DNA repair. The protein isoforms are created by alternative splicing or translation initiation accounting for differences in localization patterns [25]. The gene for OGG1 encodes at least seven different splice variants of the enzyme, each with a unique C-terminal region but all containing an N-terminal mitochondrial targeting sequence, though some isoforms localize more strongly to the mitochondria than others while some are more strongly targeted to the nucleus [29]. At least ten splice variants of MutYH have been identified, belonging to three major groups of isoforms of which one is mitochondrial-targeted and the other two nuclear-targeted [30]. Recently, a truncated version of FEN1 produced by an alternative translation initiation site was found to be enriched within the mitochondria compared to the full-length form [31]. In most cases for these enzymes, the degree to which the product is targeted to each particular organelle varies by each variant, though the differentiation between nuclear and mitochondrial isoforms is not absolute.

The predominant role of OGG1 is the bi-functional activity of 8-oxo-dG base glycosylase and cleavage of the resulting abasic site from the adjacent 5'-phosphate group [26]. In the nucleus, this is initiated and carried out in conjunction with multiple other proteins, such as the DNA scaffolding protein XRCC1 [32]. Though some of these proteins have been found in the mitochondria as well, whether OGG1 interacts with them or an equivalent protein for mitochondrial BER is unknown as of yet [25]. Recently, OGG1 has also been shown to serve a function in cell signaling through activation of a pro-inflammatory pathway in response to oxidative stress: when bound to 8-oxo-dG, either from the free nucleotide pool or released during DNA repair, OGG1 gains function as a guanine exchange factor and can activate members of the RAS and RHO kinase families [33]. Transcriptional regulation of OGG1 can occur through multiple means, including the EGFR/Akt/mTOR pathway [34] and the HIV TAT protein [35], via the transcription factor AP-4 (activating protein 4).

MutYH serves as a mono-functional glycosylase, removing the adenine bases that are incorrectly paired with 8-oxo-dG. Like OGG1, MutYH is known to interact with a number of DNA repair-associated proteins [27], but such interactions have not yet been demonstrated in the

mitochondria [25]. Only recently has the regulation of MutYH expression or activity begun to be elucidated, with the discovery of MutYH ubiquitination by the E3 ligase Mule [36], and much remains to be learned.

FEN1 removes the 5' flap structure created during long-patch BER [37]. In the nucleus, it also processes the 5' end of Okazaki fragments during DNA replication [38], and is involved in leading strand telomere replication [39]. Thus, FEN1 can be regulated through multiple DNA-related cellular pathways, including stimulation by the Fanconi anemia (FA) pathway [40], phosphorylation by various cyclin-dependent kinases (CDKs) [41], and acetylation by the transcriptional coactivator p300 [42]. Activity of FEN1 has even been shown to be affected by HIV integrase, and FEN1 may play a role in the integration of viral DNA into the host genome [43].

1.2 HIV

1.2.1 Virology of HIV

Human Immunodeficiency Virus (HIV) is a lentivirus that infects immune cells of its host. Two types of this virus are known to exist: HIV-1 and HIV-2, though HIV-2 is relatively uncommon and generally the term "HIV" is specifically referring to HIV-1. There are many strains of HIV-1 divided into four groups, with group M causing the majority of the pandemic [44]. If unmanaged, HIV infection will lead to progressive loss of immune function and the condition known as Acquired Immune Deficiency Syndrome, or AIDS [45]. This disease can contribute to a number of complications, particularly opportunistic infections due to the suppressed immune system, and other effects related to immune system and inflammatory dysfunction, such as gastrointestinal upset [46] and neuropathies [47]. Approximately 37 million people are currently living with HIV, with an estimated 2 million new infections and 1.2 million HIV/AIDS related deaths occurring annually. The virus is spread through blood, semen, vaginal secretions, or breast milk, and can be passed via unprotected sexual intercourse, sharing contaminated needles, transfusion of infected blood, or from mother to infant either during pregnancy, childbirth, or through breastfeeding. Treatment exists which can prevent or reduce the progression or transmission of the disease, though currently no complete cure is available [48]. The numerous strains of the virus and high mutation rate have made attaining a vaccine exceedingly difficult [49].

The HIV retrovirus is a spherical virion, with an exterior consisting of a lipid bilayer coated with glycoprotein complexes known as Envelope, containing two copies of the double-stranded RNA genome enclosed in a protein capsid and further surrounded by a protein matrix [50]. It infects immune cells including $CD4^+$ T-cells, macrophages, and dendritic cells. Virions dock to these cells onto CD4 and a chemokine receptor such as CCR5 or CXCR4 using Envelope, then fuse with the host cell membrane [51]. The viral RNA is converted into DNA via the viral reverse transcriptase, and then inserted into the host genome by viral integrase (Fig 1.5). Here the virus can remain latent for an extended period of time, up to many years, or immediately begin producing more viral particles [52].

When certain conditions are met, the viral DNA begins to be transcribed and translated by host cell enzymes. The viral proteins are produced initially as poly-proteins called Env and Gag-Pol. Env is processed by the Golgi body and cleaved by the host protein furin into glycoproteins gp41 and gp120, which form the heterotrimeric Envelope complexes, and sent to the surface of the cell [53]. Gag-Pol is cleaved by the viral enzyme Protease into the remaining viral structural, enzymatic, and regulatory proteins. Copies of the viral RNA are condensed and encapsulated, then move to the inner cell membrane. New virions coated with Envelope and containing the viral RNA, capsid, and matrix are budded from the surface membrane of the host cell [54].

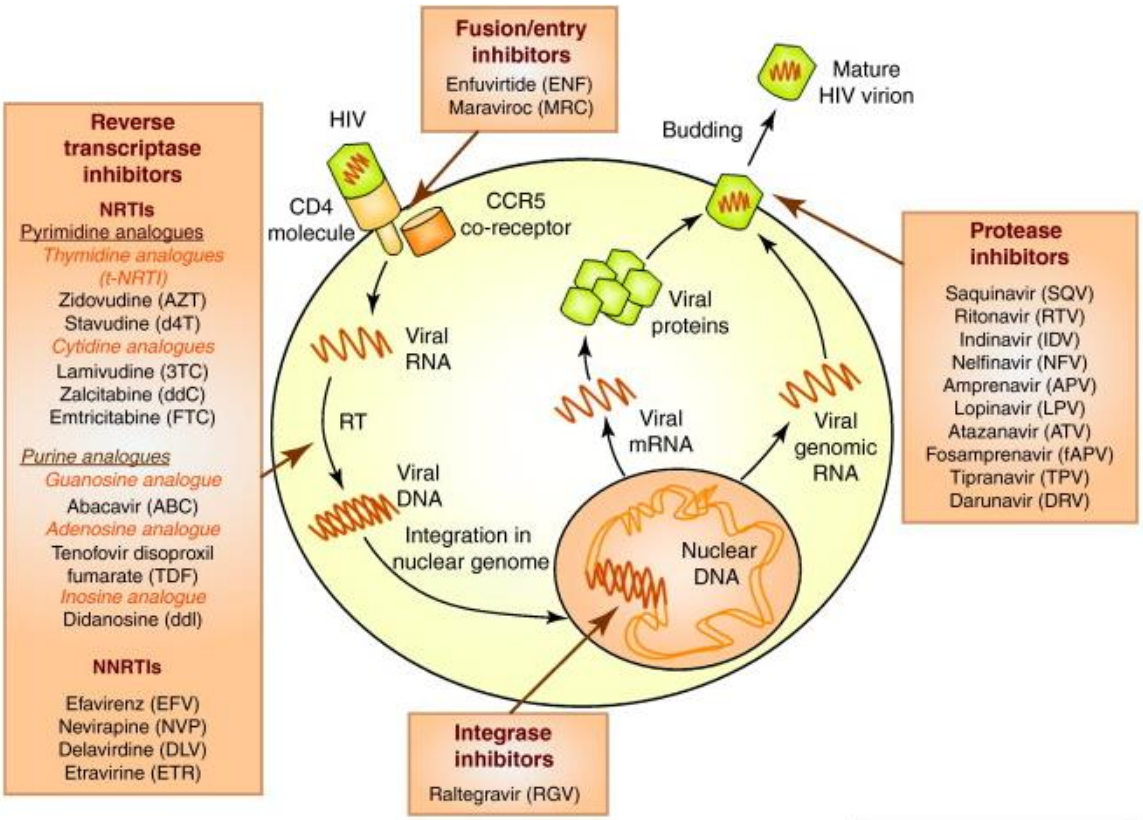

Figure 1.5. HIV replication cycle and the targets of antiretrovirals. This diagram illustrates the replication cycle of an HIV virion: docking to host cell surface proteins, fusion with cell membrane, injection of viral RNA, reverse transcription of viral RNA into DNA, integration of viral DNA into host cell genome, expression of viral mRNA and genomic RNA, transcription of viral polyproteins, cleavage of polyproteins into mature viral proteins, encapsulation of viral genomic RNA into viral proteins, and budding of mature virions from the host cell membrane. Classes of antiretroviral drugs and the viral replication cycle event they target are indicated [55].

1.2.2 HIV-induced mitochondrial dysfunction

Effects of HIV on cells are complex and multifaceted, though their mechanisms are not fully understood, particularly with regard to their impact on mitochondria. Such effects are not limited to immune cells but are also observed in various tissues, notably in muscle and adipose tissue [56]. Studies examining mitochondrial complications due to HIV infection show changes to mitochondrial number and function, with altered mtDNA copies per cell (mtDNA/genomic DNA ratio) [57] and reduced activities of mitochondrial enzymes such as cytochrome *c* oxidase. These differences could be due to a chronic state of inflammation due to HIV infection, which would increase ROS damage, or a more direct cause from the virus itself. In either case,

mitochondrial dysfunction is thought to be a driving force behind long-term associated metabolic disorders.

Among the gene expression changes found in HIV-infected cells, a number of mitochondria-encoded genes have been shown to be down-regulated in PBMCs, muscle, and adipose tissue [58]. This could be due to indirect influences of viral infection or direct impacts through regulating mitochondrial transcriptional machinery or viral microRNAs. HIV miRNAs from the viral TAR element potentially regulate nuclear-encoded genes involved in apoptosis and cell survival, while viral regulatory proteins enhance the transcription of viral genes and can control the expression of some host genes as well [59]. Indeed, the viral *tat* gene product has been shown to reduce cellular levels of Mn-SOD (manganese-containing superoxide dismutase, a mitochondrial antioxidant) and increase expression of pro-survival Bcl-2 [60] and the DNA repair protein OGG1 [35], among others, while HIV integrase can stimulate activity of the DNA repair and processing enzyme FEN1 [43]. Many of these HIV-induced cellular and mitochondrial alterations may serve the purpose of creating a more hospitable environment for viral replication.

1.3 ANTIRETROVIRALS

1.3.1 Use of antiretrovirals in treating HIV

A major turning point in the history of HIV/AIDS occurred in 1987 with the development of the first antiretroviral drug zidovudine (AZT or ZDV), followed by the introduction of highly-active antiretroviral therapy (HAART) in 1996, which heralded the change of HIV infection from a death sentence to a manageable chronic condition [61]. The safety and efficacy of antiretrovirals has improved over time, with modern drugs having less severe side-effects than those used in the beginning of HIV/AIDS treatment. Several of the earliest drugs on the market are no longer currently given as first-line therapy in the United States; however, they continue to be used in other countries worldwide, particularly in developing regions where cost-effective medicines are essential [62]. In addition, drug delivery has improved, with fewer daily doses required and pharmaceutical companies now offering fixed-dose drug cocktails in single-capsule forms, reducing the pill burden and increasing convenience for patients, with a resulting improvement in patient adherence [63].

Currently there are three predominant classes of antiretroviral drugs (ARVs) used in therapy: nucleoside reverse transcriptase inhibitors (NRTIs), consisting of nucleoside analogs which inhibit the viral reverse transcriptase and thus block conversion of viral RNA into DNA; non-nucleoside reverse transcriptase inhibitors (NNRTIs), comprised of other small-molecule inhibitors of viral reverse transcriptase; and protease inhibitors (PIs), which inhibit the viral protease and prevent the cleavage of viral polyproteins into mature proteins (Fig. 1.5) [64]. Other more recent and less frequently-used classes of drugs include integrase inhibitors, which block viral integrase and prevent viral DNA from being incorporated into the host genome [65]; entry inhibitors, which bind to immune cell receptors to block the virus from docking [66]; and fusion inhibitors, which target viral surface proteins to prevent the virus from fusing with the host cell [61].

Presently, the National Institutes of Health (NIH) recommend initiation of antiretroviral therapy (ART) for all HIV positive patients regardless of their stage of disease progression. Treatment typically involves a cocktail of three or more drugs, usually two NRTIs and either an NNRTI or a boosted PI, with the intention of preventing HIV resistance to any one drug [61]. The drugs are most often intended to be taken continuously, as non-adherence or intentional treatment interruptions can lead to virus reemergence or drug resistance [67], though patients showing strong virological suppression can be switched to different treatment regimens with lesser complications [68]. ART can also be prescribed for pre- or post-exposure prophylaxis for people at a high risk of HIV exposure, such as intravenous drug users [69] or those with HIV positive sexual partners [70]. Pregnant mothers with HIV and their newborn infants are usually placed on ART to prevent mother-to-child transmission, with a high success rate [71]. Through treatment with modern antiretrovirals, given proper medication adherence, patients are able to achieve near-complete virological suppression and virtually eliminate risk of viral transmission, which is essential to current efforts to eradicate the disease [72].

1.3.2 Nucleoside and non-nucleoside reverse transcriptase inhibitors

NRTIs were the first class of antiretroviral developed and are still used in nearly all combinational therapies for HIV/AIDS today. Anti-replication activity of 3’-azidothymidine (ZDV) against HIV was first identified in 1985, just a year after the discovery of HIV as the cause of AIDS, and AZT was approved for clinical treatment of the virus in 1987 [73]. As of

today, a total of eight NRTIs have been approved by the FDA to treat HIV [74], though only seven are still currently used, including tenofovir (TDF), emtricitabine (FTC), stavudine (d4T), and lamivudine (3TC) [75]. Several of these medications may also be used to treat other retroviruses, such as hepatitis B [76]. Before becoming active, NRTIs must enter a host cell and be phosphorylated three times by intracellular kinases [74], with the exception of tenofovir, which already possesses one phosphate group prior to processing (thus termed a nucleotide reverse transcriptase inhibitor) [73]. The metabolized drugs are dNTP analogs, lacking the 3'-OH group, which can be incorporated by viral reverse transcriptase and cause premature termination of the nascent viral DNA strand [74].

NNRTIs first became FDA-approved in 1996 with the introduction of nevirapine (NVP), with the same year seeing the beginning of combinational therapy and HAART [74]. As their name implies, these drugs are not dNTP analogs and are not incorporated into the extending viral DNA strand. Instead, they are small compounds which function by inhibiting the reverse transcriptase enzyme itself, permanently binding the a pocket near the active site and causing a conformational change which blocks the enzyme from further DNA production [77]. Currently, there are six NNRTIs approved for clinical use [75], which are usually given in combination with two NRTIs for first-line HIV therapy [78].

1.3.3 Protease inhibitors

PIs were first introduced to the HIV treatment repertoire in 1995 with the approval of saquinavir (SQV). To date, nine PIs have been approved by the FDA [79] with eight currently being used in ART, including atazanavir (ATV), darunavir (DRV), and ritonavir (RTV) [75]. Generally, PIs are given in combination with two NRTIs for first-line treatment [61]. This class of drugs targets a later step in the viral life cycle than NRTIs and NNRTIs, competitively binding the viral protease in its active site and preventing the cleavage of newly-translated viral Gag and GagPol precursor proteins into their mature forms. PIs are peptidomimetics, acting as the viral protease substrate but contains a hydroxyethylene group in the place of a normal peptide bond in the molecule's core, which the protease is unable to catalyze [79].

During the early days of PI use in ART, PIs were more weakly effective and required higher dosages due to their quick metabolism by the liver enzyme cytochrome P450-3A4 (CYP3A4) and the subsequent low rate of cellular uptake [77]. However, the molecular structure

of RTV was found to be a potent inhibitor of CYP3A4, significantly reducing the rate at which it processes other PIs. Therefore, in a method known as "boosting," most PIs are usually given together with RTV, which greatly increases their serum concentrations, cellular uptake, and medicinal strength [80].

1.3.4 Antiretroviral-induced mitochondrial toxicity

With a cure for HIV currently unavailable, patients must continue taking ART for the entirety of their lives. This unfortunately allows for any antiviral-related negative effects to build over time, with a number of clinical complications arising in people on long-term ART [81]. Side effects range widely, with notable pathologies including: peripheral neuropathy; metabolic disorders such as lactic acidosis, hyperlipidemia, decreased HDL cholesterol levels, and insulin resistance with increased cardiovascular disease (CVD) risk; less-common but severe complications including hepatic, renal, and neuronal toxicities and neurocognitive dysfunction; down to mild but discomforting symptoms such as gastrointestinal upset, headaches, and rashes. Earlier-developed antiretrovirals have more severe effects including myopathy, lipodystrophy, lactic acidosis, and pancreatitis; this is rarely an issue in the United States today, although is a concern in resource-poor nations which continue to use these drugs[82]. These side-effects concern patients and can decrease a patient's comfort and quality of life. This may result in treatment non-adherence which increases the risks of viral reemergence, drug resistance, and possibly transmission to other persons.

The toxic effects of ART were first described in 1988, with the observation of ragged red fibers, a hallmark of myopathy, in patients taking AZT [83]. As myopathy was known to be a symptom of mitochondrial toxicity, the mitochondria themselves were examined in association with the drug. Misshapen mitochondria and decreased OXPHOS activity and mtDNA levels were found in muscle biopsies of HIV patients on AZT [84]. Eventually it was learned that antivirals in the NRTI class, in addition to viral reverse transcriptase, had an affinity for the mitochondrial polymerase pol γ, leading to a reduction in mtDNA quantities in the cell, with earlier drugs such as didanosine (ddI), AZT, and d4T having stronger inhibitory effects on mtDNA synthesis than the more recently-developed NRTIs including abacavir (ABC), TDF, and 3TC [85]. This mtDNA depletion and associated decrease in mitochondrial respiratory capacity has been linked to several ART-related pathologies in addition to the initially-discovered

myopathy, including lipoatrophy, lactic acidosis, and peripheral neuropathy [86]. Given that the degree of mitochondrial toxicity induced by NRTIs does not always correlate exactly with the mtDNA loss, and the specificity of complications such as the renal toxicity associated with TDF, it is possible that other modes of mitochondrial impairment by NRTIs exists besides just pol γ inhibition [55]. Other possible means for mitochondrial off-target effects include uncoupling, OXPHOS impairment, altered membrane potential or permeability, or disruption of the metabolic cycles that occur within the matrix (Fig. 1.6).

NNRTIs and PIs have not been found to cause as much toxicity as NRTIs, but still exhibit some amount of negative side effects. The exact cause of these have yet to be elucidated, partly due to the fact that NNRTIs and PIs are usually administered in combination with NRTIs, making their specific effects difficult to distinguish. NRTIs as a group can induce rashes, while PIs can cause gastrointestinal problems, hyperlipidemia, and insulin resistance [87]. Patients taking PI-based therapies often have elevated levels of LDL cholesterol and triglycerides with lowered HDL cholesterol, suggesting alterations to lipid metabolic pathways [82]. ATV in particular has been associated with renal toxicity in addition to the standard PI side effects [88]. *In vitro* studies have pointed to a relationship between PIs and NRTIs and increased ROS production or altered mitochondrial membrane potential ($\Delta\psi_m$) and apoptotic regulation, though which precise mechanism is eliciting these changes is unknown [55].

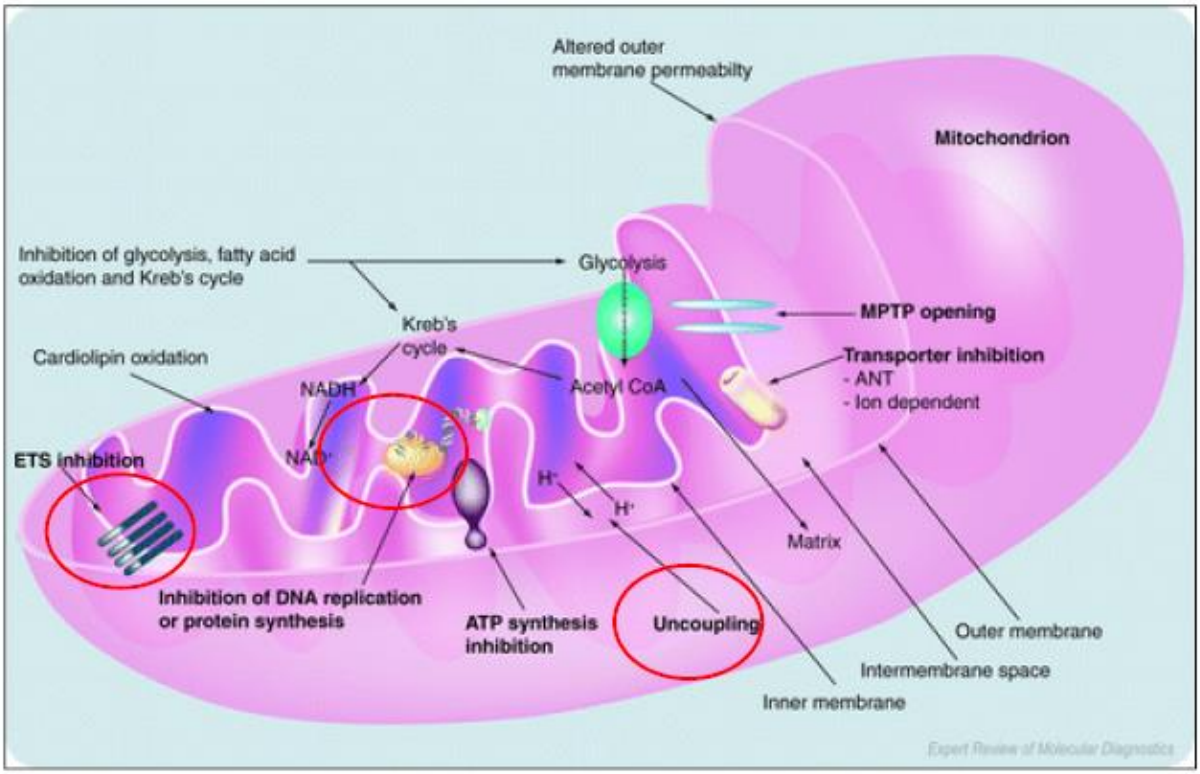

Figure 1.6. Potential targets for drug-induced mitochondrial toxicity. This diagram depicts possible mechanisms for drug-induced toxicity, showing mitochondrial functional areas which could be impacted by off-target effects of antiretroviral agents. Major potential effects include inhibition of mitochondrial DNA replication or protein synthesis, respirational uncoupling, or OXPHOS impairment [89].

1.4 SUMMARY

Much has been improved in the treatment and prevention of HIV since its discovery in the 1980's, yet neither a cure nor vaccine exists. Current treatment by ART has done much to increase the length and improve the quality of life for patients living with HIV, yet antiretrovirals have a number of clinical complications, some of them serious toxicities. Many of these side effects are attributable to mitochondrial dysfunction, which can initiate a vicious cycle of molecular consequences: reduced mitochondrial respiratory function causes an increase in ROS production, elevated levels of ROS induce oxidative damage to mtDNA, damaged or mutated mtDNA leads to decreased OXPHOS function, and so forth. NRTIs are known to cause toxicity by inhibiting polγ and depleting mtDNA, but the molecular mechanism behind other antivirals including NNRTIs and PIs still needs to be elucidated.

The following studies focus on the role of mitochondrial BER in ART-induced mtDNA oxidative damage and mitochondrial dysfunction. The first will investigate the long-term effects of ART on mitochondrial health and BER in a cohort of HIV patients from Thailand initiating therapy (with HIV seronegative control subjects). BER enzyme mRNA expression in frozen PBMCs will be quantified and compared to mtDNA content and oxidative damage and OXPHOS activity level measurements already obtained from these patients. This will allow an examination of mitochondrial BER expression in HIV- and HIV+ patients without the compounding factor of ART, as well in HIV+ patients both with and without antiretrovirals, and whether it is related to alterations to mitochondrial function due to ART.

The second study will be an *in vitro* experiment using renal cells to examine the molecular mechanism of ART-induced nephrotoxicity without the compounding interference of HIV infection. This will assess how two currently used PI-based drug cocktails affect mitochondrial respiration, mtDNA oxidative damage, and the expression of three enzymes essential to mitochondrial BER: OGG1, MutYH, and FEN1.

With a better understanding of the mechanisms behind ART-induced mitochondrial toxicity, improved methods for mitigating side effects of essential HIV medications could be developed. Additionally, researchers and pharmacologists can be better informed when designing new potential drugs and treatments, with future antivirals having even lower toxicities than those available today. During the wait for a more complete cure for HIV, this knowledge could help improve health and quality of life for those currently relying on ART to treat this disease, which in turn would lead to greater patient adherence to medication, and possibly reduced transmission rates, vital to the mission of HIV eradication.

CHAPTER 2

Mitochondrial oxidative damage and base-excision repair in HIV patients before and after initiating antiretroviral therapy

2.1. ABSTRACT

Long-term treatment of HIV infection with ART has been linked to various clinical complications, such as neuropathy, lipodystrophy, and various metabolic disorders. In NRTIs, many of these side effects are attributable to mitochondrial dysfunction, with decreased OXPHOS activity and increased mtDNA oxidative damage, though whether mitochondrial BER is involved in or affected by ART-induced toxicity is currently unknown. This study sought to investigate expression of mtDNA BER enzymes in HIV patients before and after initiating ART treatment.

Banked PBMCs from two different cohorts from the South-East Asia Research Collaboration with Hawaii (SEARCH) in Thailand were used for this study: SEARCH 014, consisting of HIV seronegative participants, and SEARCH 003, consisting of ART-naïve HIV-positive patients who were enrolled on an ART regimen for 72 weeks. The SEARCH 003 patients were randomly sorted into three drug arms: 24 weeks on d4T + 3TC/NVP followed by 48 weeks on ZDV + 3TC/NVP; 72 weeks on ZDV +3TC/NVP; or 72 weeks on TDF/FTC + 3TC/NVP. Baseline and 72 weeks SEARCH 014 (n=37) and SEARCH 003 (n=56) PBMCs were assayed for OGG1, MutYH, and FEN1 mRNA transcript levels. Mitochondrial 8-oxo-dG break frequency (BF), mtDNA copies/cell, and OXPHOS complexes CI and CIV enzyme activities had previously been measured for each participant. Wilcoxon or Mann-Whitney Rank-Sum tests for non-parametric data was used for analysis with significance set at $p \leq 0.05$. Relationships between parameters were evaluated by Spearman's Correlations.

MutYH expression was found to be decreased in ART-naïve HIV patients compared to the controls, but increased after ART initiation. OGG1 expression correlated with 8-oxo-dG levels in both the controls and HIV patients after 72 weeks of ART. FEN1 expression decreased after ART initiation, and expression correlated with 8-oxo-dG in the controls but not the HIV positive patients at either time point. Patients whose 8-oxo-dG levels increased from baseline to 72 weeks had higher amounts of FEN1 mRNA at baseline than those whose 8-oxo-dG decreased. It is possible that antiretroviral drugs may affect the normal response of FEN1 regulation to oxidative damage, and baseline FEN1 expression could influence the outcome of ART treatment.

2.2. INTRODUCTION

2.2.1. Antiretroviral therapy and mitochondrial oxidative stress

Antiretrovirals act by targeting specific points in the replication cycle of HIV. Treatment with antiretroviral compounds is effective in virtually eliminating HIV viral load, which reduces transmission and attenuates symptoms of AIDS. Most HIV therapy involves at least three compounds of two different drug classes to avoid development of drug resistance by the virus [74]. A patient must remain on an ART regimen for the rest of their life, as a pause in therapy in most cases leads to a re-emergence of the virus, often with drug-resistant mutations [67]. This long-term treatment induces a buildup of toxicities over time which causes a gradual development of complications over the course of months or years [82].

Many of these clinical complications are attributable to mitochondrial toxicity. One of the hallmarks of mitochondrial dysfunction is increased ROS production and elevated mitochondrial and cellular oxidative stress [8]. Indeed, patients receiving ART have been found to have increased levels of ROS production, including superoxide and hydrogen peroxide [90], as well as antioxidant enzyme dysfunction in monocytes and cerebrospinal fluid [91]. MtDNA is particularly vulnerable to attack by ROS [25], and elevated levels of mtDNA oxidative damage have been found in ART-treated HIV patients with symptoms of neurological degeneration [92] and increased CVD risk factors [93]. Several systems for DNA damage repair exist in the mitochondria which are capable of correcting various types of mtDNA oxidative damage [25], though the extent to which mitochondrial BER is involved in or affected by HIV or ART is currently unknown. To elucidate this, we will examine mRNA expression levels of mitochondrial BER enzymes and their relationship to mtDNA oxidative damage in HIV-positive, ART-naïve patients before and after initiating therapy and compare them to age, ethnicity, and gender-matched HIV seronegative control subjects.

2.2.2. HIV and ART in Thailand

As of 2014, an estimated 450,000 individuals in Thailand were HIV positive, amounting to approximately 1.1% of the adult population [94]. From the first case in 1984 to 2012, more than one million people had been infected in total [95]. To address this, in the 1990's the Thai government began a program, known as the Government Pharmaceutical Organization (GPO), which began manufacturing generic antiretrovirals to provide at low cost to its citizens living

with HIV [96]. The government has been successful in nearing its coverage goal of 80%, with the World Health Organization (WHO) estimating 76% of people in need of HIV medications receiving treatment in 2012, up from 60% in 2005 [97]. However, this still leaves many infected individuals without the treatment they require to remain healthy and prevent transmission.

Up until as recently as 2008, the Thai national recommendations for antiretroviral therapy included d4T in first-line drug regimens [98]. Due to numerous complications, in particular a high mitochondrial toxicity, d4T is no longer recommended for therapy in the United States [78], though it continues to be used in low-resource nations due to its cost effectiveness (in 2013, the cost per person-year for a d4T-containing regimen in low-income countries was $53, compared to ≥$99 for more highly-recommended regimens [99]). In 2010, the Thai national recommendations switched d4T regimens from preferred to alternative therapies [100], though the preferred therapies still include ZDV which has also largely been discontinued in the United States due to toxicity concerns [78].

In 2003, the South East Asia Research Collaboration with Hawaii (SEARCH) program was founded to facilitate research on HIV and AIDS in the Southeast Asia world region. It consists of a partnership between the Thai Red Cross AIDS Research Center (TRCARC), the University of Hawaii – Hawaii AIDS Clinical Research Program (HACRP), and the United States Department of Defense Armed Forces Research Institute of the Medical Sciences (AFRIMS) Department of Retrovirology and is based in Bangkok, Thailand. Over the years SEARCH has led multiple clinical trials on the safety and efficacies of ART regimens in Thailand, and has participated in basic research on HIV immunology and virology as well as the molecular basis of antiretroviral toxicities. Ongoing projects include studies on neural and metabolic toxicity, vaccine development, research into opportunistic infections and co-morbidities, and social advocacy [101].

2.2.3. SEARCH 003

The SEARCH 003 cohort [102] consisted of 150 participants in Thailand who were HIV-positive and had not yet begun ART. The aim for the study was to determine whether starting patients on a d4T-containing regimen for the first six months before switching to a ZDV-based regimen could reduce the risk of developing anemia, which had the tendency to occur in patients starting ZDV while CD4+ T-cell counts were low (<350 cells/mm^3). Participants were

randomized 1:1:1 into three different drug arms for the duration of 72 weeks: Arm A received d4T (30mg) with lamivudine (3TC, 150mg) and nevirapine (NVP, 200mg twice daily) for 24 weeks, followed by a switch to ZDV (150mg) + 3TC + NVP for the remaining 48 weeks. Arm B received ZDV + 3TC + NVP for the whole 72-week duration, while Arm C received tenofovir (TDF) + 3TC + NVP for 72 weeks. Blood samples were collected from each patient at weeks 0, 24, and 72 of the study, from which peripheral blood mononuclear cells (PBMCs) and plasma were isolated and frozen at -80°C prior to shipping to the University of Hawaii. At the times of blood draw, clinical measures were taken, including body mass index (BMI), blood pressure, blood metabolic profile, hemoglobin, HIV viral load, and CD4 count.

Inclusion criteria for the cohort were a minimum age of 18 years, positive HIV status, CD4 count <350 cells/mm^3, a Thai national identity card, signed consent with an understanding of the consent forms, no allergy to anesthetics, and no prior exposure to ART, while exclusion parameters were current AIDS-defining or other illnesses, abnormal blood laboratory values, peripheral neuropathy (PN), and pregnancy or breastfeeding. IRB approval was received from Queen Savang Vadhana Memorial Hospital, Chulalongkorn University, University of Hawaii, and University of California San Fransisco. Informed consents were completed and obtained in Thai language from all participants.

Ultimately the study found that participants who received d4T initially had both reduced anemia and higher CD4 counts at the end of the 72-week period than those who started with ZDV, suggesting that short-term d4T treatment could be beneficial to patients initiating ART with low CD4 counts. A repository of plasma and PBMC samples remains from this study at the University of Hawaii, providing future opportunities to study a demographic that is otherwise difficult to study in the United States: HIV-infected patients who are ART-naïve.

2.2.4. SEARCH 014

The SEARCH 014 cohort [103] consisted of 125 participants who were either HIV-positive and receiving d4T-based ART or who were HIV seronegative, both with and without PN. Patients were enrolled into one of four groups: Group 1 included 25 HIV positive patients on ART who displayed symptoms of PN; Group 2 included 25 HIV-positive patients on ART without symptoms of PN; Group 3 included 50 HIV-seronegative individuals without symptoms of PN; and Group 4 included 25 HIV-positive patients on ART with asymptomatic PN. IRB

approval was received from Queen Savang Vadhana Memorial Hospital, Chulalongkorn University, University of Hawaii, and University of California San Fransisco. Informed consents were completed and obtained in Thai language from all participants.

Our current study focuses specifically on Group 3, which has been used as an HIV negative control for the SEARCH 003 cohort. Inclusion criteria for Group 3 included minimum age of 18 years, negative HIV status, a Thai national identity card, signed consent with an understanding of the consent forms, no allergy to anesthetics, no current exposure to ART, no symptoms of PN, and no current pregnancy. Blood samples were drawn from Group 3 participants at the beginning of the study, after which plasma and PBMCs were isolated and frozen at -80°C prior to being shipped to the University of Hawaii. At this time, clinical measurements were also taken, including BMI, blood metabolic profile, hemoglobin, HIV viral load, and CD4 count. A repository of plasma and PBMC samples from SEARCH 014 exists for use in future studies at the University of Hawaii.

2.3. METHODS

2.3.1. Sample Selection

From the SEARCH 003 cohort, samples for this study were selected based on participants' change in 8-oxo-dG from baseline to 72 weeks. Most individuals experienced a decrease in 8-oxo-dG break frequency 72 weeks after initiating ART- from them, those with a decrease in break frequency of 0.05 or greater (34 individuals in total) were selected. A total of 17 individuals experienced an increase in 8-oxo-dG break frequency; these were all also chosen. Selection based on these criteria encompassed all individuals who had break frequencies of 0.05 or higher at either baseline or at 72 weeks. Five individuals who experienced no change (with a break frequency of 0.0 at baseline and 72 weeks) were chosen at random. A final total of 112 samples from SEARCH 003 (PBMCs from 56 participants at weeks 0 and 72) were processed.

All participants from Group 3 in the SEARCH 014 cohort who had a positive 8-oxo-dG break frequency, 21 in total, were chosen for this study. Among those with no detectable 8-oxo-dG, 11 were selected at random, for a final total of 37 PBMC samples processed from the SEARCH 014 cohort as controls.

2.3.2. DNA, RNA, and protein extraction and quantification

For RNA extraction, frozen PBMCs were thawed in a 37°C water bath, added to 5mL 1X PBS (Amresco, Solon, OH), then spun down for 5 minutes at 500xg, 4°C. Cell pellets were lysed with buffer RLT+ (Qiagen, Valencia, CA) then processed using Qiagen's AllPrep DNA/RNA Mini Kit according to manufacturer's instructions. RNA was eluted with RNAse-free H_2O and used directly for quantification and cDNA synthesis. RNA quantity and quality were measured on an Agilent 2100 Bioanalyzer using the RNA Nano or RNA Pico Lab-on-a-Chip Kits (Agilent Technologies, Santa Clara, CA) according to manufacturer's instructions. An RNA integrity number (RIN) of 7.0 or higher was the standard requirement for further RNA experimental use.

Prior to DNA purification, frozen PBMCs were thawed in a 37°C water bath, then pelleted by spinning down for 15 minutes, 300xg, 4°C. After decanting, the cell pellets were brought up in 1X PBS then spun down again, and finally re-suspended in MDT tissue lysis buffer with 10% proteinase K (FujiFilm Corporation, Tokyo, Japan). DNA extractions were performed by Heidi Fink and Julia Choi of the Gerschenson Laboratory at the University of Hawaii on the QuickGene-610L personal genome extraction system using the DNA tissue kit S (FujiFilm) according to manufacturer's instructions. DNA concentrations were measured on a NanoDrop 2000 spectrophotometer (Thermo Scientific, Waltham, MA).

For protein lysates, frozen PBMCs were thawed in a 37°C water bath and re-suspended in 400µL cold 1X PBS. Afterwards, 200µL buffer A (Abcam) and 1X Protease Inhibitor Cocktail (Thermo Fischer Scientific) was added, and samples were incubated on ice for 20 minutes with brief vortexing every 5 minutes. Lysates were centrifuged for 20 minutes at 14,000xg, 4°C to remove cellular debris, then flash frozen and stored at -80°C. Prior to use for ELISA assays, protein content was quantified using the Pierce BCA protein assay (Thermo Scientific, Rockford, IL) using a serial dilution of bovine serum albumin (BSA) for a standard curve and calculated on PRISM software version 5.0d (GraphPad Software, Inc., San Diego, CA).

2.3.3. Mitochondrial 8-oxo-dG quantification by Southern blot

Mitochondrial 8-oxo-dG Southern blots were performed by Heidi Fink of the Gerschenson Laboratory at the University of Hawaii. Oxidative damage to mtDNA was evaluated by measuring the number of 8-oxo-dG modifications per mtDNA strand using a gene-

specific repair assay. MtDNA was detected using a DNA probe specific for the mitochondrial gene encoding human cytochrome b, labelled with digoxygenin (DIG) by PCR amplification (primer sequences: DigFor: 5'-GCT ACC TTC ACG CCA A-3'; DigRev: 5'-CCG TTT CGT GCA AGA AT-3').

The following ethanol precipitation procedure was used for each DNA concentration step: 0.1 volume of 3.0M NaOAc (Sigma-Aldrich) then 2.5 volume cold 100% EtOH was added per sample. DNA was then incubated at -80°C for a minimum of 40 minutes (up to overnight), then centrifuged for 15 minutes, 16,000xg, 4°C. The supernatant was aspirated, then 500µL 70% EtOH was added followed by another centrifugation for 3 minutes, 16,000xg, room temperature. The supernatant was removed again, and the DNA pellet allowed to air-dry in a 40°C heat block before re-suspending in the desired solvent at the desired concentration.

After the appropriate amount of starting DNA was concentrated in DNase/RNase-free H_2O, mtDNA was linearized by a two-hour incubation at 37°C with 1X NEBuffer 2 and 20U/mL PVUII (New England BioLabs, Ipswich, MA). Samples were precipitated again, re-suspended in TE buffer (Qiagen), and divided equally into two parts. One half remained at 4°C while the other half was digested for one hour at 37°C with 1X NEBuffer 2.1, 200µg/mL BSA, and 100U/mL hOGG1 (New England BioLabs). The digestion reaction was terminated by incubating at 65°C for one hour, followed by another precipitation and re-suspension in TE buffer.

Both halves of each DNA sample were re-quantified, and equal amounts for each half were used for alkaline gel electrophoresis. Each sample pair was brought to equal volumes using TE+ (Tris-EDTA, Sigma-Aldrich, with extra 0.2mM EDTA, Amresco), mixed with 1X alkaline loading dye (Boston BioProducts, Ashland, MA), and dry-loaded onto a 0.75% SeaKem Gold agarose gel (Lonza Group Ltd., Basel, Switzerland) along with a DIG-labelled, HINDIII-digested λ DNA molecular weight marker (Roche Diagnostics Corporation, Indianapolis, IN). The gel was dry-run at 50V for 30 minutes until the loading dye had completely left the wells and entered the gel. Electrophoresis continued at 50V for another 3 hours after adding 1X alkaline electrophoresis buffer (50mM NaOH, Fisher Scientific, 1mM EDTA, Amresco), using a Mini-pump Variable Flow recirculating system (Fisher Scientific) to keep cool. After the first two hours, DNA complimentary to the detection probe was loaded into an unused well as a positive control.

The DNA gel was transferred onto a Nylon+ membrane (Roche) using a Vacugene XL vacuum blotting unit (GE Healthcare Bio-Sciences, Pittsburg, PA) at 50mbar. A series of solutions was used to facilitate transfer: 15 minutes with depurination solution (0.25M HCl), 15 minutes with denaturation solution (1.5M NaCl, 0.5M NaOH), 7 minutes with neutralizing solution (1M Tris, 1.5M NaCl, pH 7.5), and 30 minutes with 20X SSC (Teknova, Hollister, CA). After transfer, the blot was auto-crosslinked with 1200μJ/cm^2 UV using a Stratalinker 1800 UV crosslinker (Stratagene, La Jolla, CA). The blot was incubated in pre-hybridization buffer (dissolved DIG Easy Hyb granules, Roche) at 45°C for 20 minutes in a Shake 'N' Bake hybridization oven (Boekel Scientific, Feasterville, PA), then incubated overnight at 45°C in DIG probe hybridization buffer (pre-hybridization buffer with 15μL denatured probe).

Prior to detection, the blot was washed twice for 5 minutes at room temperature with low-stringency wash buffer (2X SSC, 0.1% SDS, Sigma Aldrich) then twice for 20 minutes at 65°C with high-stringency wash buffer (0.5X SSC, 0.1% SDS), and rocked in 1X Blocking Buffer in 1X Maleic Acid Buffer (Roche DIG Wash and Block Buffer Set, Roche) between 30 minutes and 3 hours at room temperature. A solution of 0.15U anti-DIG Fab (Roche) in 1X Blocking Buffer , 1X Maleic Acid Buffer was added, and incubation proceeded for another 30 minutes. The blot was then washed and incubated in 1X Detection Buffer (Roche) for 5 minutes, then incubated under a thin layer of CSPD solution (Roche) 5 minutes at room temperature then 20 minutes at 37°C while blocked from light. Two overlaid images were taken at 30 minutes each on a G:BOX gel doc system using GeneSys software (SynGene, Cambridge, UK).

Band quantification by densitometry was performed using GeneTools software by SynGene. 8-oxo-dG modifications were quantified by calculating the mtDNA strand break frequency (BF) based on Poisson distributions of undigested and hOGG1-digested mtDNA using the following formula:

$$BF = l_n\left(\frac{undigested\ mtDNA}{hOGG1-digested\ mtDNA}\right)$$

2.3.4. cDNA synthesis

Purified RNA was converted into cDNA by reverse transcription PCR using the Transcriptor First Strand cDNA Synthesis Kit (Roche) according to manufacturer's instructions using the following parameters: for each reaction, 11μL RNA eluate was combined with 2μL Random Hexamer Primer, then denatured at 65°C for 10 minutes, followed by a 1 minute

incubation on ice. Reverse transcription reaction protocol was: 25°C, 10 minutes; 50°C, 60 minutes; 85°C, 5 minutes. Two duplicate reactions were run separately per RNA sample, then combined and stored at -20°C.

2.3.5. MtDNA quantification by real-time PCR

MtDNA quantification by the Mt/Gen qPCR assay was performed by Julia Choi of the Gerschenson Laboratory at the University of Hawaii. For each amplification, 30ng sample DNA was combined with SYBR Green Master Mix (Life Technologies, Carlsbad, CA) and 1μM each primer and brought to a total volume of 20μL using purified H_2O. The primer sets were for a nuclear housekeeping gene (Fas Ligand; GenDIR: 5'-GGC TCT GTG AGG GAT ATA AAG ACA-3'; GenREV: 5'-CAA ACC ACC CGA GCA ACT AAT CT-3') and a mitochondrial-encoded gene (NADH dehydrogenase subunit II; mtDIR: 5'-CAC AGA AGC TGC CAT CAA GTA-3'; mtREV: 5'-CCG GAG AGT ATA TTG TTG AAG AG-3'). A positive control reaction was prepared using a control plasmid containing the 90bp NADH dehydrogenase subunit II gene and the 98bp Fas Ligand gene which had been diluted to $1x10^6$ DNA copies per μL. The cycling conditions for the reactions were: pre-incubation at 95°C for 5 minutes; amplification for 30-36 cycles with denaturing at 95°C for 3 seconds, annealing at 58°C for 5 seconds, and extension at 72°C for 5 seconds per cycle; and a melt curve analysis beginning at 65°C and increasing 0.1°C/s up to 95°C. Each sample and control reaction was run in duplicate. Analysis was performed using LightCycler software version 4.0 (Roche). The absolute number of mtDNA copies per cell was calculated for each sample by dividing mean mtDNA value by mean genomic DNA value, then multiplying by 2 to account for the duplicate copies of nuclear genes in each cell.

2.3.6. OGG1, MutYH, and FEN1 mRNA quantification by real-time PCR

Quantification of OGG1, MutYH, and FEN1 mRNA was performed by real-time PCR with hydrolysis probes on a LightCycler 480 instrument using LightCycler 480 Software version 4.0 (Roche). Custom primers were ordered from Life Technologies (primer sequences: OGG1F: 5'-CCC CAG ACC AAC AAG GAA C-3'; OGG1R: 5'-AGG TCG GCA CTG AAC AGC-3'; MutYHF: 5'-AAC TAT GAG CCC GAG GCC TT-3'; MutYHR: 5'-AGC GGC TTC CCA GAG GTA G-3'; FEN1F: 5'-ACC CCG AAC CAA GCT TTA G-3'; FEN1R: 5'-GGG CCA

CAT CAG CAA TTA GT-3'). Fluorescent hydrolysis probes from the Universal ProbeLibrary (Roche) used for each primer pair were: Probe #20 (OGG1), Probe #14 (MutYH), and Probe #82 (FEN1). The Universal ProbeLibrary Human TBP Reference Gene Assay (Roche) was used for normalization. For each cDNA sample, four separate reactions, one for each target and reference gene, were run in duplicate on the same 96-well plate. Each reaction mixture was composed of the following: 25-100ng cDNA (diluted to 5µL in PCR-grade H_2O), 10µL ProbesMaster mix (Roche), 1µL (reference) or 2µL (target) primers (10µM forward and reverse primers in TE buffer, Sigma), 0.4µL probe, PCR-grade H_2O up to 20µL total volume per well. Cycling conditions were: a 10 minute pre-incubation at 95°C; amplification over 55 cycles of denaturing at 95°C for 10 seconds, annealing at 55°C for 30 seconds, and extension at 72°C for 1 second; and a final cool-down at 40°C for 30 seconds. Each target gene was normalized to TBP for each sample, and calibrated to a control sample of cDNA from untreated HEK-293 or RPCT cells included on each plate.

2.3.7. OXPHOS Complex I and Complex IV enzyme activity by ELISA

NADH dehydrogenase (CI) and cytochrome *c* oxidase (CIV) activity ELISAs were performed by Julia Choi of the Gerschenson Laboratory at the University of Hawaii using the Complex I and Complex IV Human Enzyme Activity Microplate Kits (Abcam, Cambridge, MA) according to manufacturer's instructions. For the CI assay, 75µg protein was used per well, while 25µg protein per well was used for the CIV assay. Buffer A (Abcam) was used as a negative control while control PBMC protein lysate (Astarte Biologicals, Redmond, WA) was used as a positive control, with all controls and samples being plated in duplicate. Plates were read on a SpectraMax 190 absorbance microplate reader (Molecular Devices LLC, Sunnyvale, CA) at 450nm every 30 seconds for 30 minutes at 27°C for the CI assay and at 550nm every 1 minute for 40 minutes at 30°C for the CIV assay.

Specific activities were calculated by averaging replicates then plotting over time, giving raw slope values by linear regression. These slope values were divided by the protein quantity per well then multiplied by 1,000,000 for the final absorbance values. CI and CIV specific activity values are expressed as the change in absorbance per minute per microgram of sample ([OD/µg/min]x10^6).

2.3.8. Statistical Analysis

Wilcoxon or Mann-Whitney Rank-Sum tests for non-parametric data were run to compare 8-oxo-dG BF, mtDNA copies per cell, OXPHOS enzyme activity levels, and DNA repair gene mRNA values between the HIV-seronegative, baseline HIV-positive, and 72-week HIV-positive participant groups. Relationships between parameters were evaluated by Spearman's Correlations. Statistical probability values of $p \leq 0.05$ were considered significant while those of $0.06 \leq p \leq 0.10$ were considered a trend. Analyses were performed using SigmaPlot version 12.0 software.

2.4. RESULTS

2.4.1. Participant characteristics of the SEARCH 003 and 014 cohorts and study samples

A total of 37 samples from SEARCH 014 Group 3 (HIV-) and 56 samples from SEARCH 003 (HIV+) at both baseline and 72 weeks were examined in this study. Average ages, genders, and baseline vital statistics of individuals of the selected subgroups are presented in Table 2.1. The two cohorts were similar at baseline in terms of male/female ratio ($p=0.19$), body mass index (BMI, $p=0.54$), blood pressure ($p=0.34$), and triglycerides ($p=0.44$). Patients from the SEARCH 003 cohort were slightly older than the participants from the SEARCH 014 cohort ($p=0.058$) and higher levels of lactate ($p=0.036$) and lower total cholesterol ($p<0.001$) and fasting glucose levels ($p=0.022$, Table 2.1). Three of the measured mitochondrial parameters mtDNA content, OXPHOS enzyme activities) from the selected samples were not vastly different from those of the cohorts as a whole (Table 2.2), indicating that the chosen samples are representative of the larger cohort in terms of mitochondrial function. However, the selected samples from the SEARCH 003 cohort at both baseline and 72 weeks after therapy initiation had higher 8-oxo-dG BFs than the total cohort ($p=0.029$ and $p=0.022$, respectively), as samples had been selected based on changes in 8-oxo-dG BF from 0 to 72 weeks (Table 2.2).

Table 2.1. Baseline characteristics of SEARCH participants selected for the current study

	SEARCH 014 (n=37)	SEARCH 003 (n=56)	Difference (*p*-value)
Age (Years ± SD)	33.8 ±5.1	37.2 ±8.5	0.058
#Female/Male (%Female)	20/17 (54.1)	31/25 (55.4)	0.19
BMI ±SD	22.2 ±2.4	23.1 ±3.7	0.54
Systolic blood pressure ±SD	116.5 ±10.7	114.3 ±11.6	0.35
Fasting glucose (mg/dL ±SD)	87.2 ±8.2	83.7 ±11.9	0.022
Total cholesterol (mg/dL ±SD)	207.4 ±36.1	174.2 ±40.5	<0.001
Triglycerides (mg/dL ±SD)	104.2 ±62.9	113.3 ±73.8	0.44
Lactate (mmol/L ±SD)	1.11 ±0.51	1.30 ±0.54	0.036

Table 2.2. Mitochondrial parameters of the SEARCH 003 and 014 cohorts and the subset of participants selected for the current study.

	MtDNA copies per cell		8-oxo-dG (BF)	
	Mean ±SD	Cohort/Subset *p*-value	Mean ±SD	Cohort/Subset *p*-value
SEARCH 014 (n=50)	251.31 ±70.10		0.09 ±0.16	
Study subset (n=37)	238.40 ±60.64	0.33	0.11 ±0.18	0.35
SEARCH 003 baseline (n=150)	198.70 ±83.15		0.12 ±0.17	
Study subset (n=56)	179.87 ±69.62	0.23	0.19 ±0.21	0.029
SEARCH 003 72wk (n=150)	336.23 ±132.62		0.04 ±0.08	
Study subset (n=56)	316.38 ±119.77	0.19	0.07 ±0.10	0.022
	CI Activity (OD/µg protein x 10^6)		CIV Activity (OD/µg protein x 10^6)	
	Mean ±SD	Cohort/Subset *p*-value	Mean ±SD	Cohort/Subset *p*-value
SEARCH 014 (n=50)	34.60 ±4.75		68.97 ±6.18	
Study subset (n=37)	33.84 ±4.31	0.50	68.60 ±6.42	0.63
SEARCH 003 baseline (n=150)	32.94 ±9.65		58.99 ±13.97	
Study subset (n=56)	31.72 ±10.63	0.37	57.80 ±14.73	0.60
SEARCH 003 72wk (n=150)	32.98 ±8.63		63.04 ±11.29	
Study subset (n=56)	34.44 ±9.28	0.25	63.74 ±10.95	0.55

2.4.2. Mitochondrial parameters are negatively impacted by HIV infection but improve after ART initiation

Oxidative mtDNA damage, as measured by 8-oxo-dG BF, was higher in HIV+ patients at baseline (mean BF ±SD = 0.19 ±0.21 breaks/16.6kb) than in HIV- participants (0.11 ±0.18, p=0.032) but decreased after 72 weeks of ART (0.07 ±0.10, p=0.003, Fig. 2.1). MtDNA copies per cell, conversely, was lower in HIV+ patients at baseline (179.9 ±69.9 copies/cell) than in HIV- participants (238.4 ±10.6, p<0.001) but increased after 72 weeks of ART (316.4 ±119.8, p<0.001). MtDNA content was also higher in HIV+ patients at 72 weeks than in HIV- participants (p<0.001, Fig. 2.2). Likewise, CI and CIV enzyme activities were similarly lower in the baseline HIV+ group (31.7 ±10.6 and 57.8 ±14.7, respectively) than the HIV- group (33.8 ±4.3, p=0.085; and 68.6 ±6.4, p<0.001) but were increased at week 72 (34.4 ±9.3, p=0.034; and 63.7 ±11.0, p=0.001). CIV enzyme activity was slightly lower in HIV+ patients at 72 weeks than in the HIV- participants (p=0.073, Fig. 2.3). Specific enzyme activities are given in (OD/µg protein/min)x10^6.

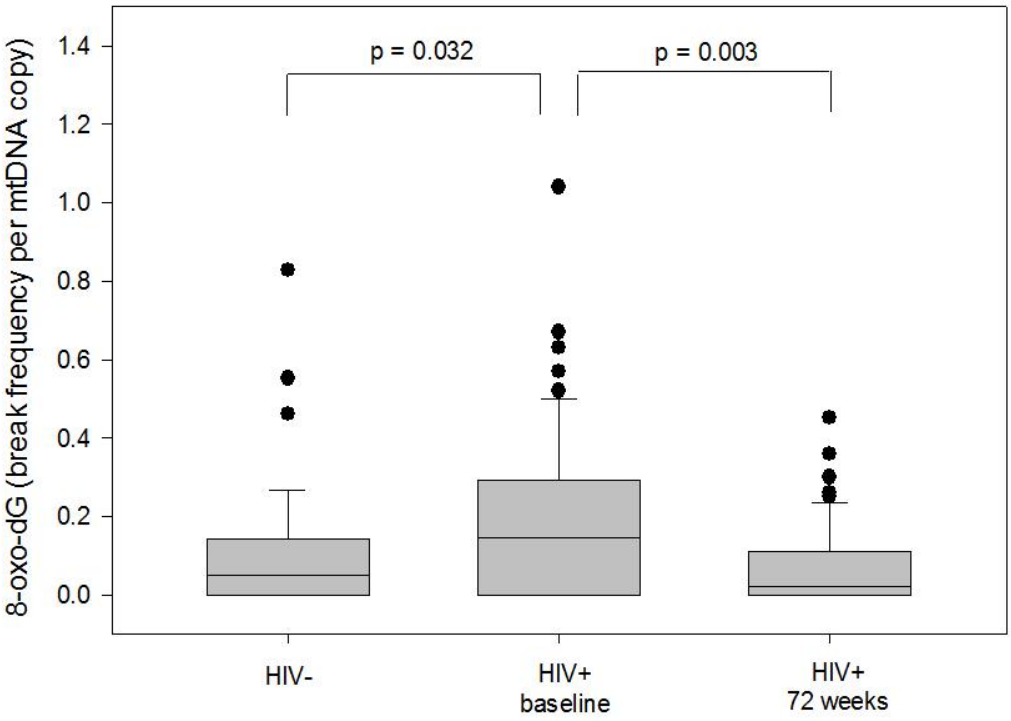

Figure 2.1. 8-oxo-dG is affected by HIV infection and ART. 8-oxo-dG break frequency in PBMC mtDNA is higher in HIV-positive patients (n=56) at baseline than after 72 weeks on ART and in HIV-seronegative participants (n=37). Boxes represent median and IQR, while whiskers represent SEM.

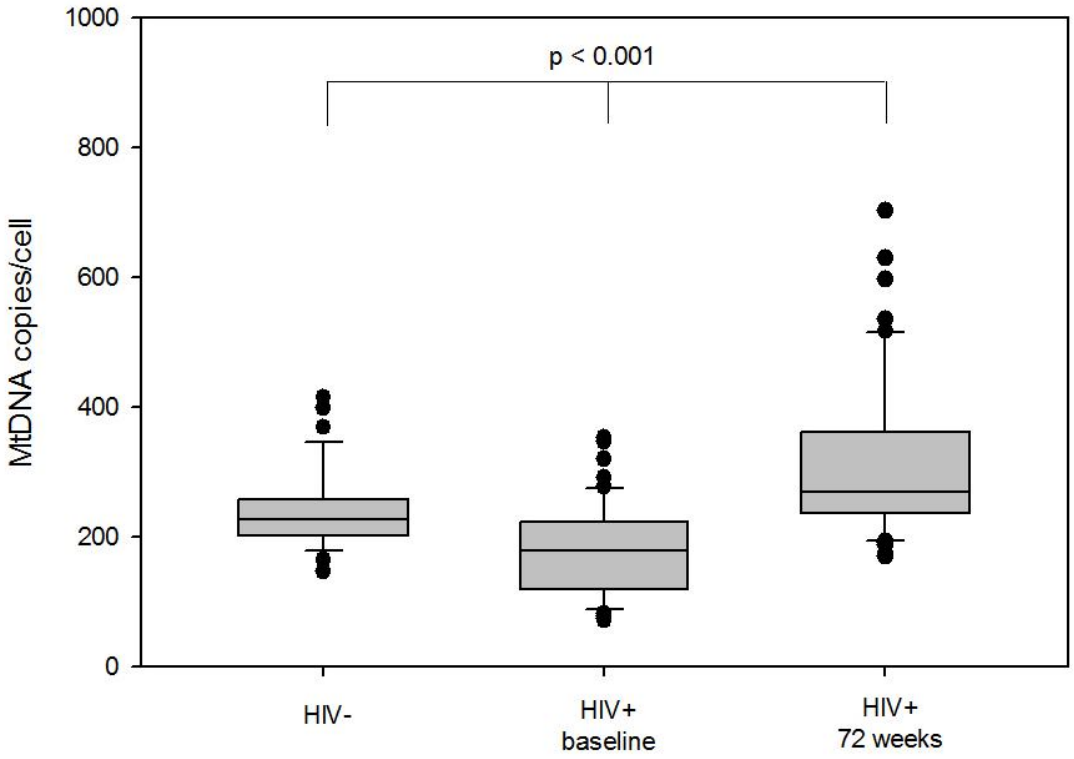

Figure 2.2. MtDNA content is affected by HIV infection and ART. MtDNA copies per cell in patient PBMCs is lower in HIV-positive patients (n=56) at baseline than after 72 weeks on ART and in HIV-seronegative participants (n=37). HIV-positive patients at 72 weeks had higher mtDNA content than either other group. Boxes represent median and IQR, while whiskers represent SEM.

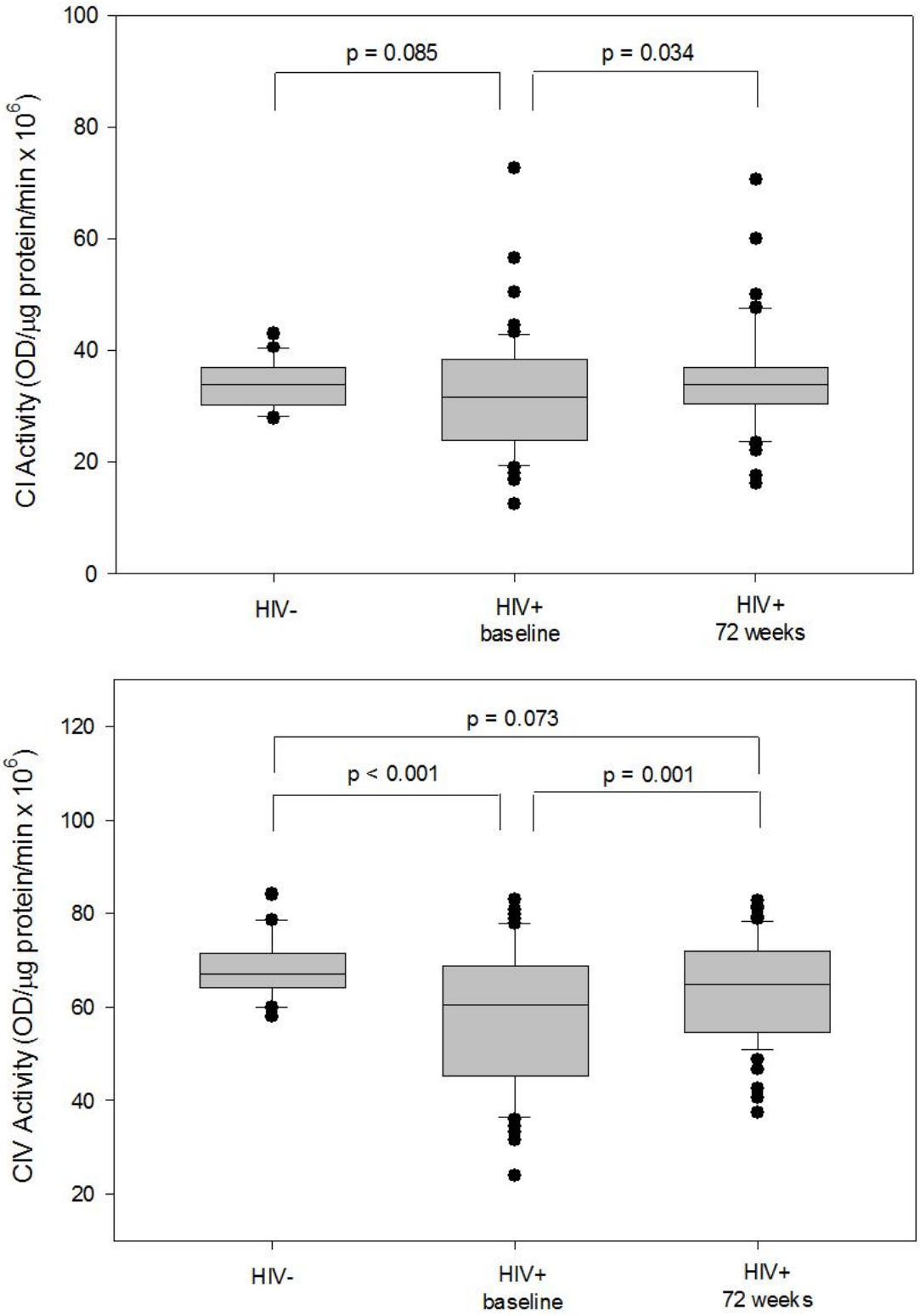

Figure 2.3. OXPHOS Complexes I and IV enzyme activities are affected by HIV infection and ART. Specific activities of CI and CIV were both lower in HIV-positive patients (n=56) at baseline than after 72 weeks on ART or in HIV-seronegative participants (n=37). Boxes represent median and IQR, while whiskers represent SEM.

2.4.3. MutYH and FEN1, but not OGG1, mRNA levels are affected by HIV and ART

OGG1 mRNA levels were not significantly different between the HIV- (1.40 ±1.46), baseline HIV+ (1.06 ±1.22), and 72-week HIV+ (1.11 ±1.10) participant groups (Fig. 2.4). Similar to the other mitochondrial parameters, MutYH mRNA was lower in HIV+ patients at baseline (4.41 ±2.26) than in the HIV- participants (6.23 ±2.36, $p<0.001$) but increased after 72 weeks of ART (6.73 ±2.62, $p<0.001$, Fig. 2.5). FEN1 mRNA levels were not significantly different between the HIV- and baseline HIV+ groups ($p=0.42$); however, FEN1 mRNA was significantly lower in HIV+ patients at 72 weeks (0.16 ±0.11) than in both the HIV+ patients at baseline (0.26 ±0.23, $p=0.002$) and the HIV- participants (0.26 ±0.16, $p=0.001$, Fig. 2.6)

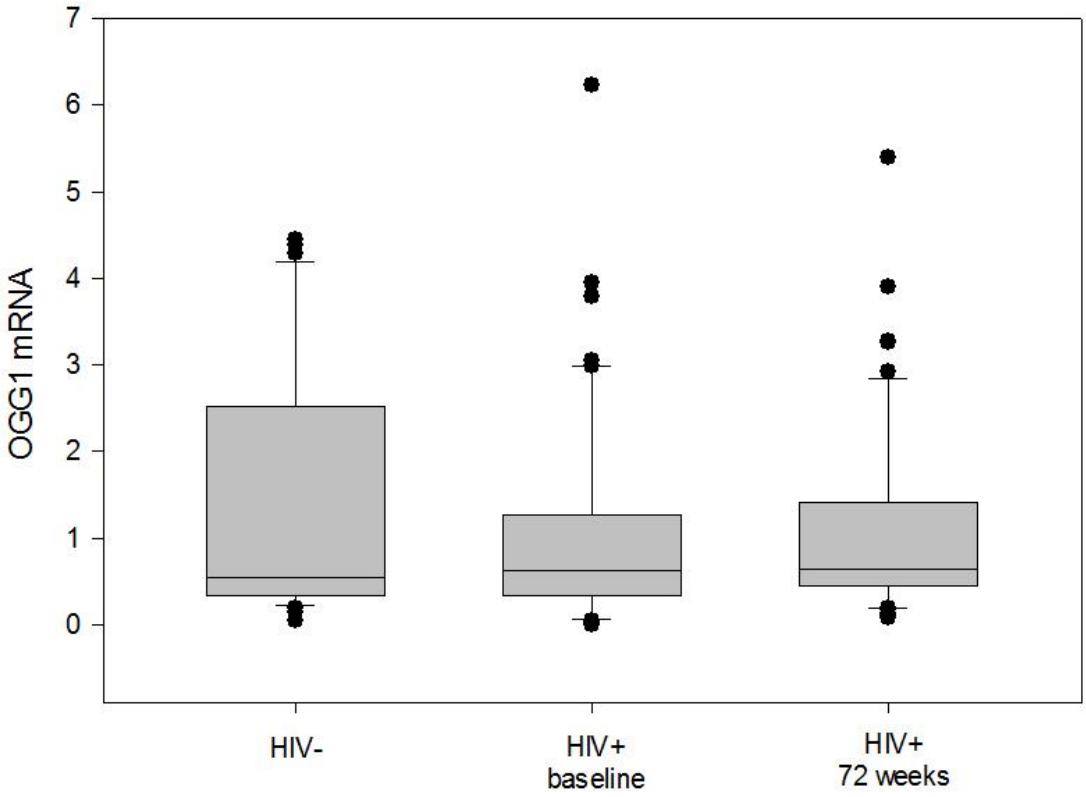

Figure 2.4. OGG1 mRNA was not significantly different among the study groups. No significant differences were found in PBMC OGG1 mRNA expression (given as a normalized ratio of OGG1/TBP mRNA in each sample) among the HIV-seronegative (n=37) and HIV-positive (n=56) groups at either time point. Boxes represent median and IQR, while whiskers represent SEM.

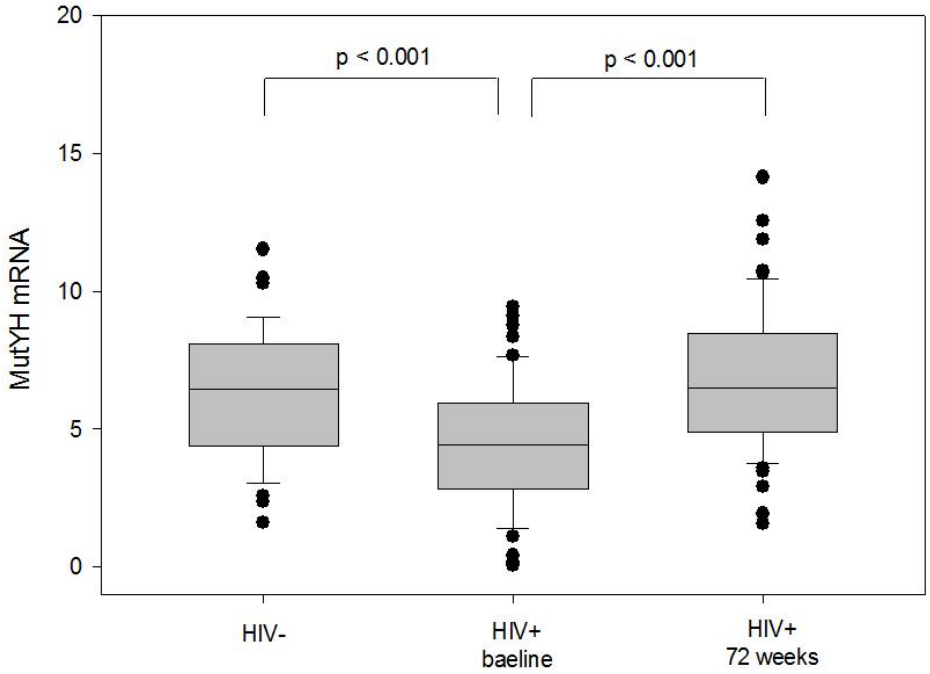

Figure 2.5. MutYH mRNA expression is affected by HIV infection and ART. PBMC MutYH mRNA (given as a normalized ratio of MutYH/TBP mRNA in each sample) is lower in HIV-positive patients (n=56) at baseline than after 72 weeks of ART and in HIV-seronegative participants (n=37). Boxes represent median and IQR, while whiskers represent SEM.

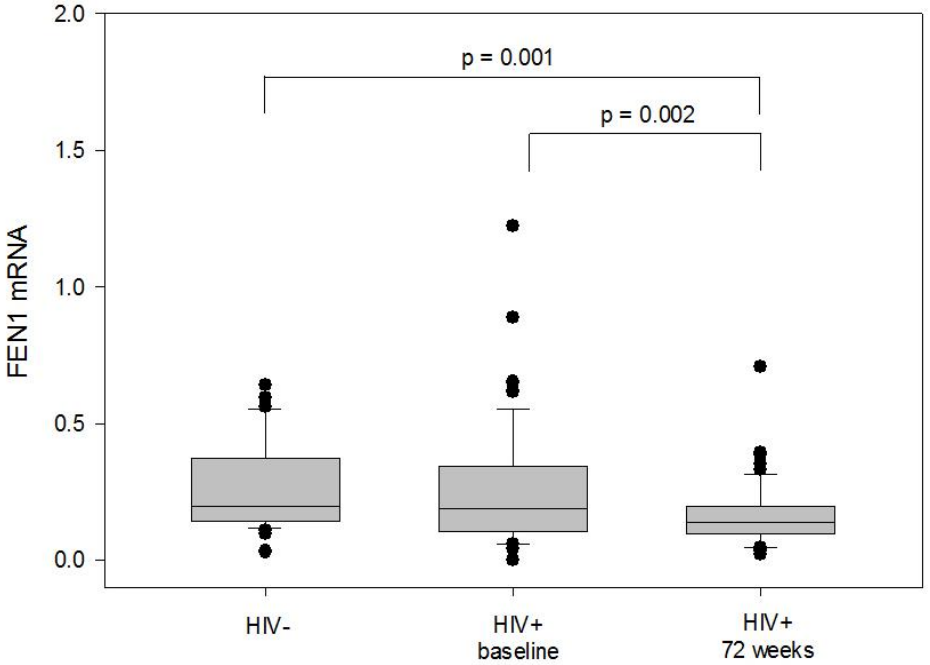

Figure 2.6. FEN1 mRNA expression is lower in HIV+ patients receiving ART. FEN1 mRNA values (given as a normalized ratio of FEN1/TBP mRNA in each sample) from participant PBMCs is lower in HIV-positive patients (n=56) after 72 weeks on ART than at baseline or in HIV-seronegative participants (n=37). Boxes represent median and IQR, while whiskers represent SEM.

2.4.4. In HIV-positive patients at baseline, 8-oxo-dG BF and mtDNA levels are negatively correlated

Patients who were HIV-positive and who were ART-naïve had the highest incidence of oxidative mtDNA damage out of the three study groups, having a 69.6% rate (39/56 samples) of non-zero PBMC 8-oxo-dG break frequencies, compared to 57.1% (32/56) after 72 weeks of ART and 59.5% (22/37) in HIV-negative participants. Among the HIV-positive baseline patients, a negative correlation was found between 8-oxo-dG BF and mtDNA copies per cell (ρ= -0.331, p=0.013). No correlations between 8-oxo-dG BF and mtDNA copies/cells were found in the HIV-seronegative or the ART-treated groups (p=0.36 and p=0.83, respectively).

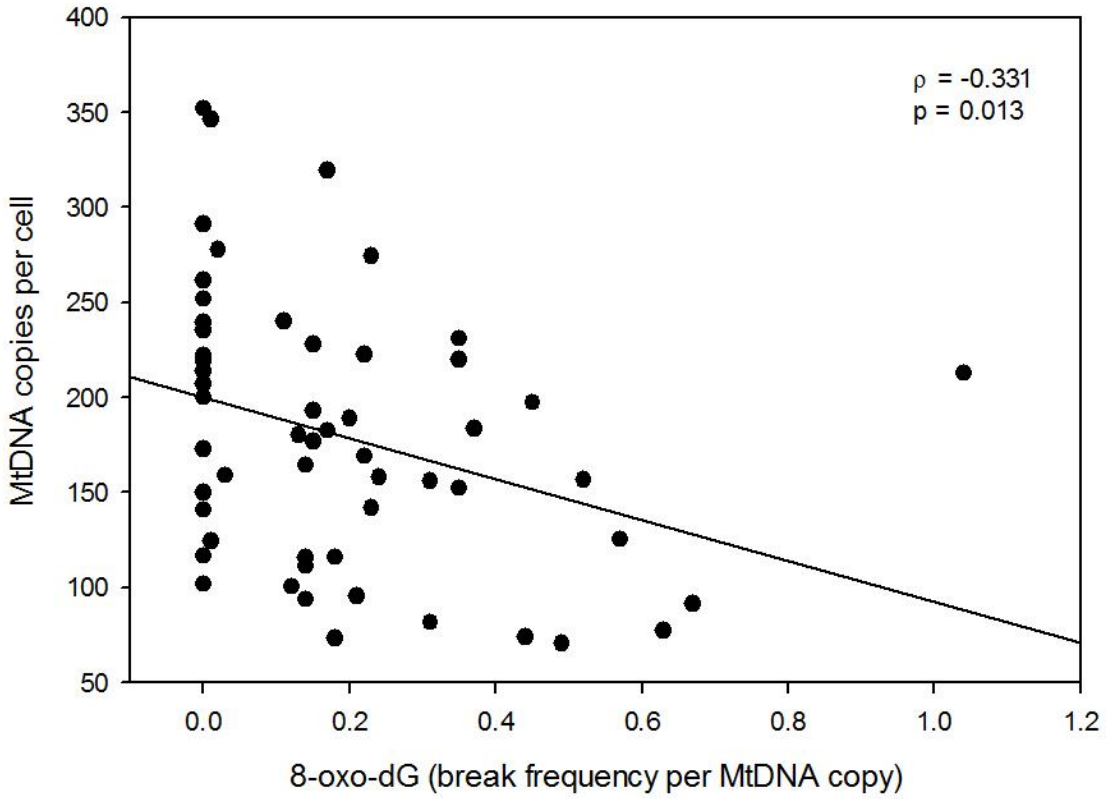

Figure 2.7. MtDNA content and 8-oxo-dG are negatively correlated in HIV-positive, ART-naïve patients. In PBMCs from HIV-infected patients not receiving ART, an inverse correlation exists between mtDNA copies per cell and 8-oxo-dG break frequency. The slope of the line represents the linear regression of mtDNA vs. 8-oxo-dG across all samples (n=56).

2.4.5. OGG1 and FEN1 mRNA correlate with each other and with 8-oxo-dG BF

OGG1 and FEN1 mRNA levels had a positive correlation in all three study groups: ρ=0.662, p<0.001 for HIV-negative participants; ρ=0.630, p<0.001 for HIV-positive patients at baseline; and ρ=0.496, p<0.001 for HIV-positive patients 72 weeks after ART initiation (Fig. 2.8). Relative mRNA values of OGG1 were positively correlated with 8-oxo-dG break frequency in both HIV-seronegative participants (ρ=0.369, p=0.025) and HIV-positive patients after 72 weeks of ART (ρ=0.322, p=0.016), though no correlation was found in the HIV-positive patients at baseline (p=0.65, Fig. 2.9). FEN1 mRNA likewise was positively correlated with 8-oxo-dG in HIV-seronegative individuals (ρ=0.354, p=0.032) though not in HIV-positive individuals at either time point (p=0.526 and p=0.46, Fig. 2.10).

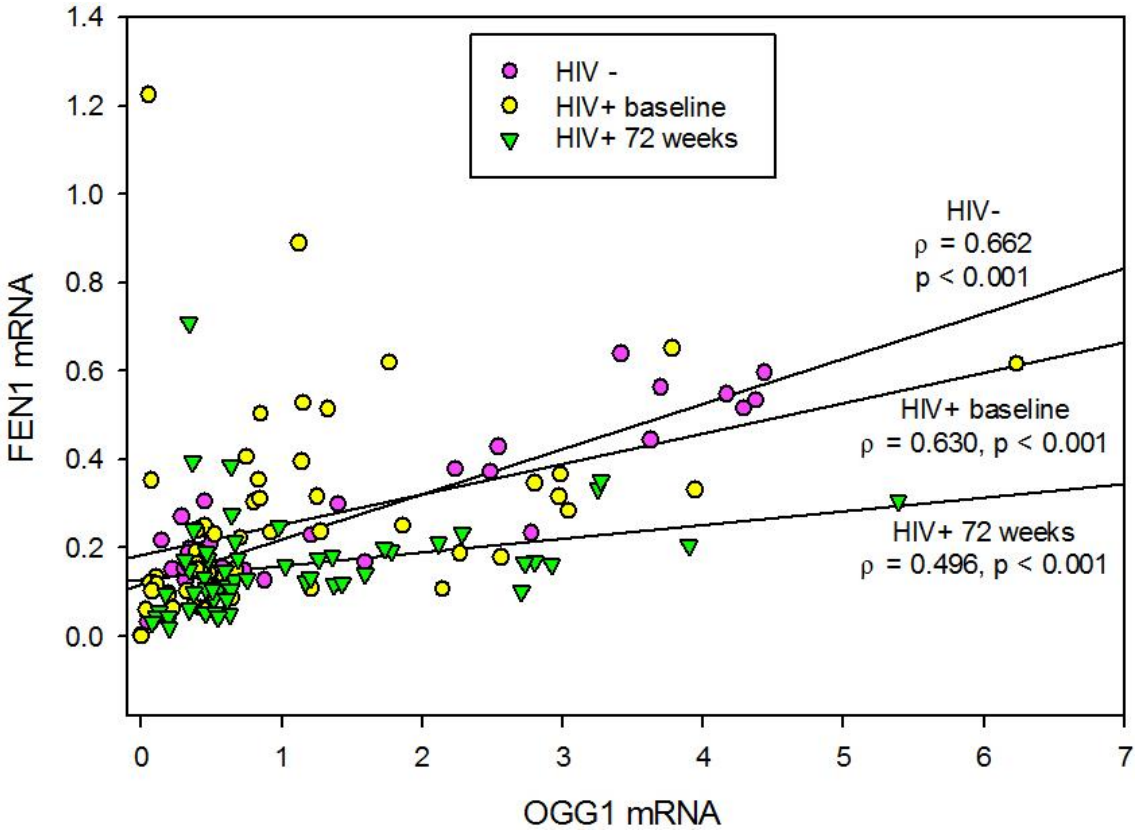

Figure 2.8. FEN1 and OGG1 mRNA levels are correlated. In PBMCs from the HIV-seronegative control participants (n=37) and HIV-positive patients at both baseline and 72 weeks (n=56), FEN1 and OGG1 mRNA values (given as a ratio of target/TBP mRNA for each sample) were positively correlated. The slope of the line represents the linear regression of FEN1 mRNA vs. OGG1 mRNA.

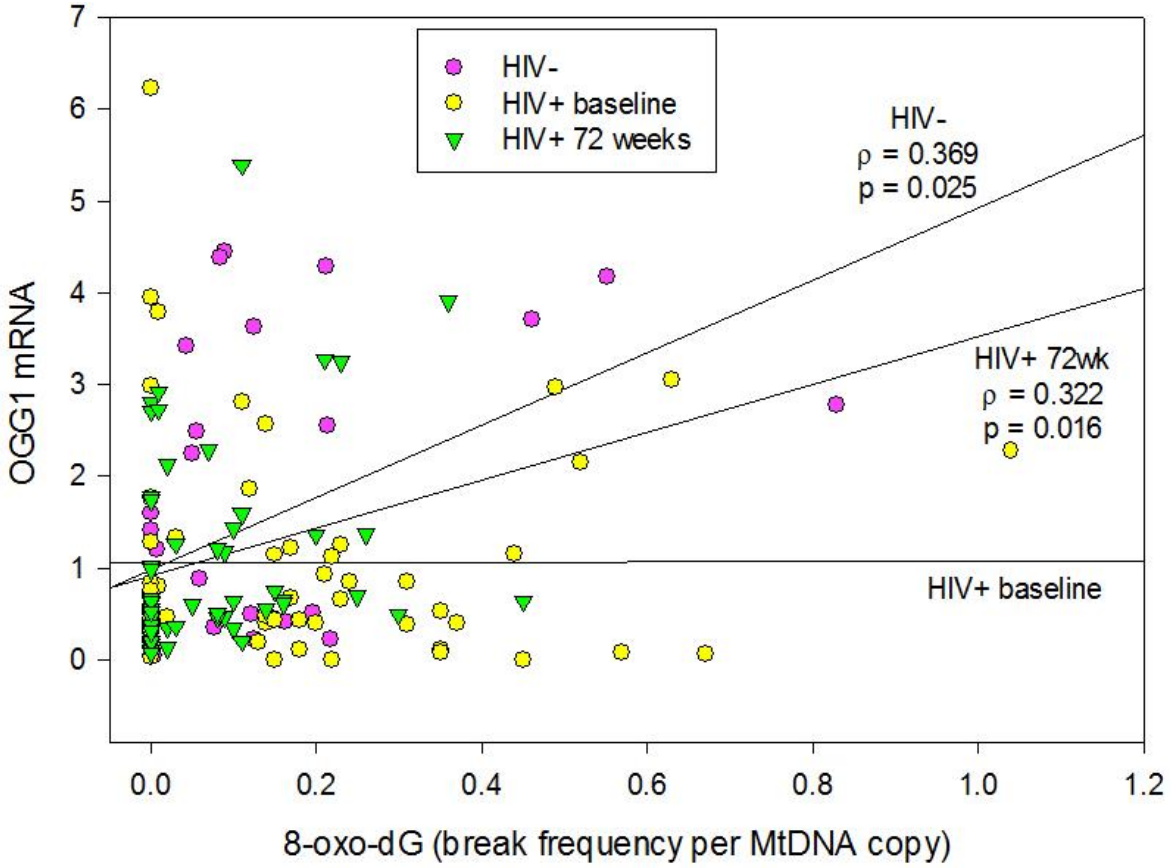

Figure 2.9. OGG1 mRNA level correlates with mtDNA oxidative damage. OGG1 mRNA levels were positively correlated with 8-oxo-dG in PBMCs from both HIV-seronegative participants (n=36) and HIV-positive patients after 72 weeks of ART (n=56). No correlation was found in HIV-positive patients at baseline (n-56). The slopes of the lines represent the linear regressions of OGG1 mRNA value (given as a ratio of OGG1/TBP mRNA for each sample) vs. 8-oxo-dG BF.

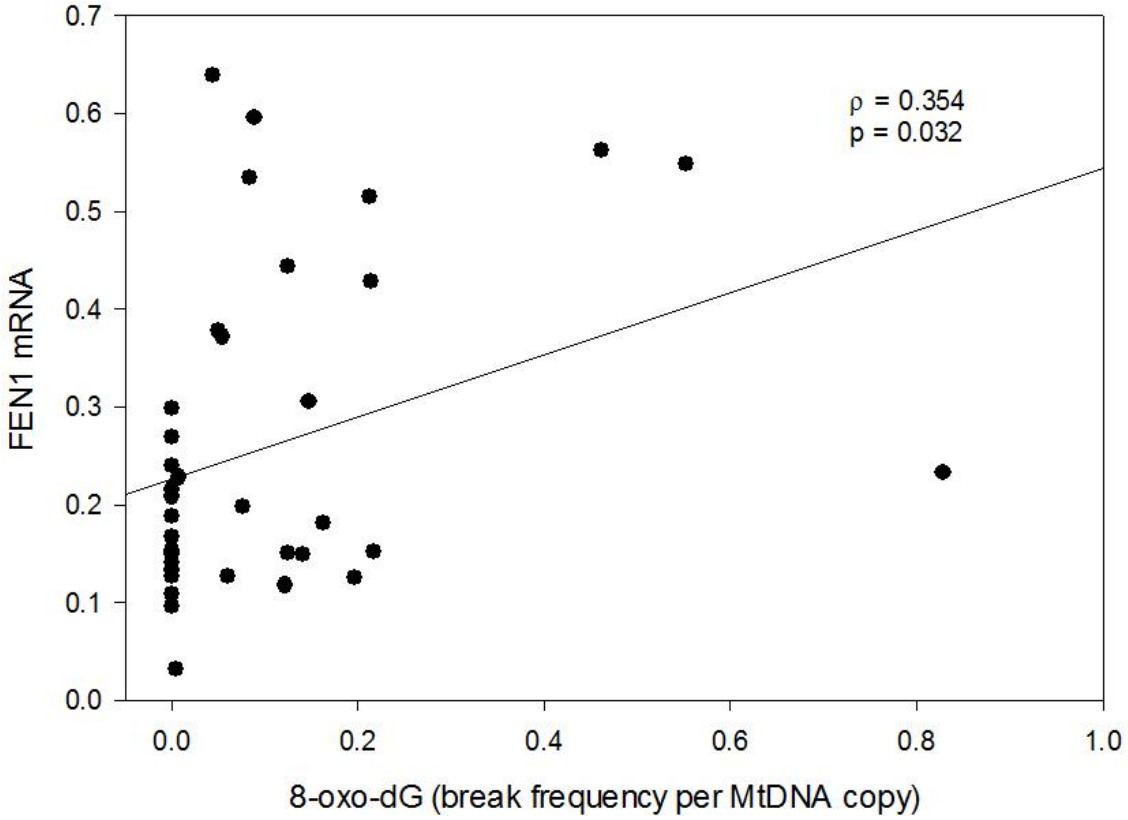

Figure 2.10. FEN1 mRNA correlates with mtDNA oxidative damage in HIV-positive, ART-naïve patients. FEN1 mRNA level was positively correlated with 8-oxo-dG BF in PBMCs from HIV-positive, ART-naïve patients (n=56). No correlation was found in HIV-positive patients (n=56) at either baseline or after 72 weeks on ART (data not shown). The slope of the line represents the linear regression of FEN1 mRNA value (given as a ratio of FEN1/TBP mRNA for each sample) vs. 8-oxo-dG BF.

2.4.6. 8-oxo-dG change and mtDNA content after 72 weeks of ART vary by drug arm

Out of the 56 participants from SEARCH 003 selected for this study, 17 were enrolled in Arm A, 20 were in Arm B, and 20 were in Arm C. Of patients who were considered to have a "high increase" in 8-oxo-dG (a change of ≤ -0.06 in break frequency from baseline to 72 weeks, n=15), 7 were from Arm A, 5 were from Arm B, and 3 were from arm C. Of those with a "high decrease," (a change in break frequency of ≥ 0.06, n=33), 9 were from Arm A, 10 were from Arm B, and 14 were from Arm C.

The amount of change in 8-oxo-dG break frequency experienced by patients from baseline to 72 weeks varied in each drug arm, with the mean ±SD change in break frequency of patients in Arm C (-0.23 ±0.30) being greater than that of patients in Arm A (-0.01 ±0.20, p=0.018). The change in 8-oxo-dG experienced by patients in Arm B (-0.10 ±0.16) was not significantly different from either Arm A or Arm C (Fig. 2.11, top panel).

Correspondingly, mtDNA content after 72 weeks of ART also varied by drug arm. The mean ±SD mtDNA copies per cell at 72 weeks was higher in patients in Arm C (382.7 ±119.2) than in patients in Arm A (246.7 ±56.5, p<0.001), though mtDNA content in Arm B (319.3 ±131.1) was not significantly different from the other drug arms (Fig. 2.11, bottom panel).

2.4.7. Baseline FEN1 mRNA is higher in patients who experienced an increase in 8-oxo-dG than those who experienced a decrease

The mRNA expression levels of OGG1, MutYH, and FEN1 were examined in patients who had either a high increase or high decrease in 8-oxo-dG BF at both baseline and at 72 weeks. OGG1 and MutYH mRNA values were not significantly different between the two groups at either time point. However, patients whose 8-oxo-dG BF increased by 0.06 or greater had a higher level of FEN1 at baseline (0.39 ±0.31) than those whose break frequency decreased by 0.06 or greater (0.22 ±0.18, p=0.045, Fig. 2.12). FEN1 mRNA at 72 weeks did not differ between the two groups. Expression of mRNA at either time point was not affected by drug arm.

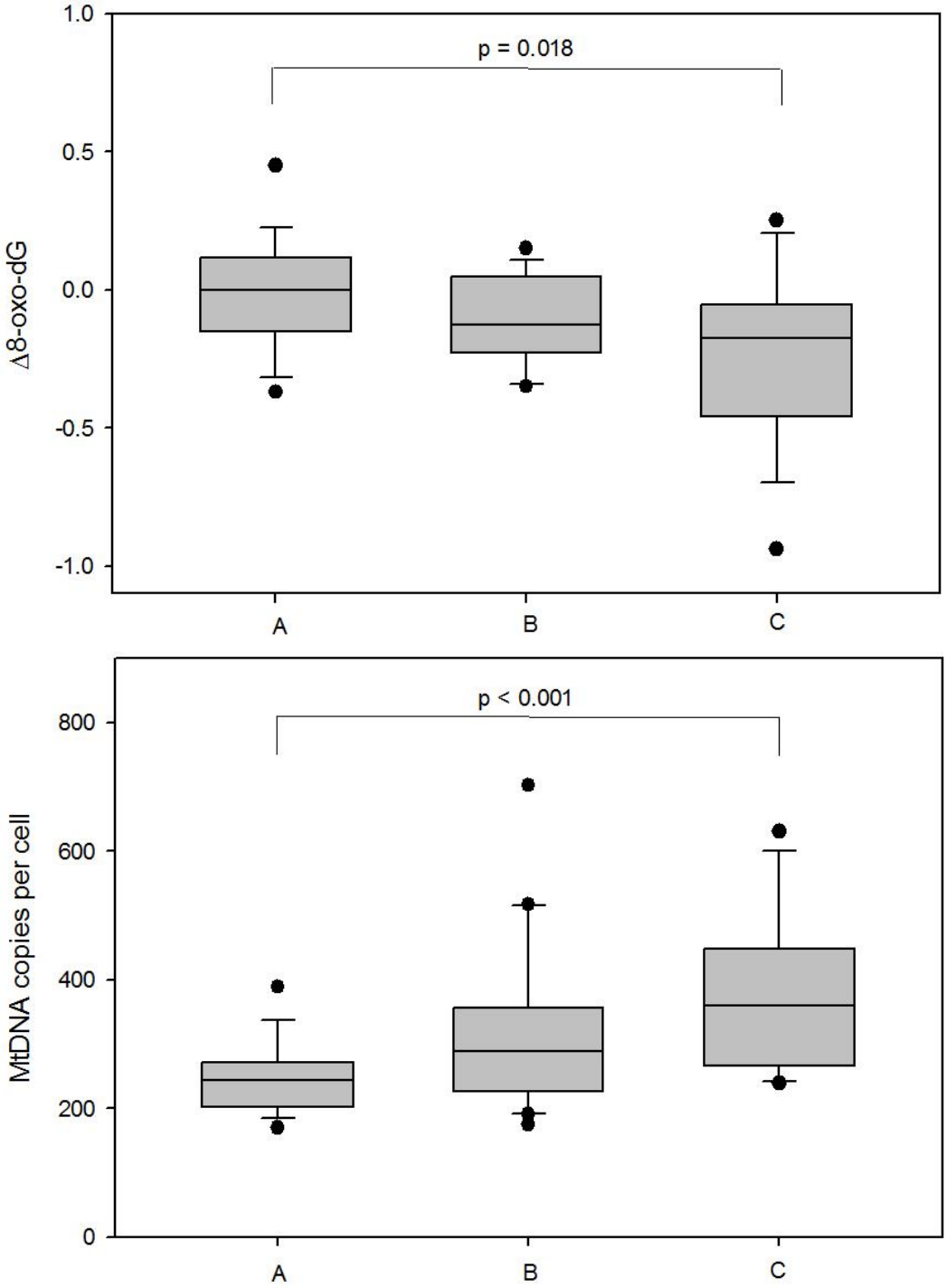

Figure 2.11. 8-oxo-dG BF change and mtDNA content vary by drug arm. Change in mitochondrial 8-oxo-dG BF from baseline to 72 weeks varied between Arm A (24 weeks on d4T +3TC/NVP then 48 weeks on ZDV +3TC/NVP), Arm B (72 weeks on ZDV +3TC/NVP) and Arm C (72 weeks on TDF/FTC +3TC/NVP), with the change significantly greater in Arm C than Arm A (top panel). MtDNA copies/cell at 72 weeks after ART initiation was higher in patients in Arm C than Arm A (bottom panel). Boxes represent median and IQR, while whiskers represent SEM.

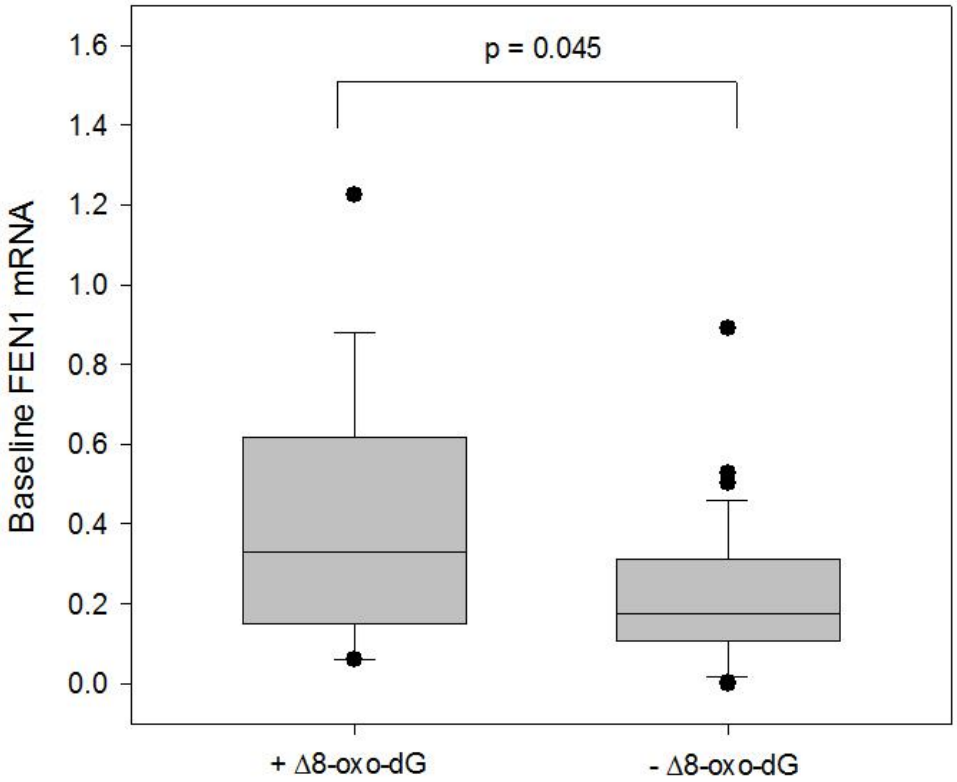

Figure 2.12. Baseline FEN1 mRNA levels are greater in patients whose 8-oxo-dG BF increased compared to those whose 8-oxo-dG BF decreased. Patients who experienced an increase in 8-oxo-dG BF of 0.06 or greater started with a higher level of FEN1 mRNA (given as a normalized ratio of FEN1/TBP mRNA for each sample) at baseline than patients who experienced a decrease in 8-oxo-dG BF of 0.06 or greater. Boxes represent median and IQR, while whiskers represent SEM.

2.5. DISCUSSION

This study aimed to elucidate the involvement of mitochondrial DNA base-excision repair in antiretroviral-induced toxicity in HIV patients. By utilizing specimens from the SEARCH 003 cohort from Thailand, it was possible to investigate the effects of ART and expression of DNA repair enzymes in the same HIV patients both before and after initiating NRTI/NNRTI-based combinational therapy. Often during the first few months to couple of years, patients newly placed on ART regimens undergo what is termed a "return to health," that is assessed by decreased viral load and reduced incidence of co-morbidities. After several years of ART, drug-related toxicities begin to occur [104]. Therefore, with the latest time point for which SEARCH 003 specimens are available being 72 weeks, the overall vitality improvement may make it difficult to discern any direct drug-induced effects from those caused by viral

elimination. The SEARCH 014 cohort, with age, gender, and ethnicity-matched HIV-seronegative participants, was included to determine any viral-related effects on mitochondrial function, oxidative damage, and DNA repair between HIV-negative and HIV-positive, ART-naïve patients, so these effects may be considered when investigating any ART-related changes.

Indeed, many of the mitochondrial changes seen from baseline to 72 weeks seem to be of the "return to health" nature: mitochondrial 8-oxo-dG BF, a measure of oxidative damage to mtDNA, was higher in HIV patients at baseline than the control participants, though decreased after 72 weeks of therapy. Likewise, mtDNA copies per cell, indicating mitochondrial biogenesis, and specific enzyme activities of NADH dehydrogenase (Complex I or CI) and cytochrome *c* oxidase (Complex IV or CIV), demonstrating OXPHOS and mitochondrial function, were lower in ART-naïve HIV patients than in the controls, but increased following 72 weeks of ART treatment. Thus, several parameters of mitochondrial function appear to be affected by HIV infection but improve in the first few months after ART initiation.

This pattern of altered mitochondrial health followed by improvement due to ART therapy is reflected in the expression of MutYH. MutYH is important for correcting incorrect base-pairing which arises from oxidative DNA damage which could otherwise lead to mutation, and though it did not show a correlation with 8-oxo-dG, its mRNA expression did decrease in HIV patients relative to controls and improve following 72 weeks of ART. Rather than increasing in response to higher levels of oxidative DNA damage, MutYH expression seems to be negatively impacted by HIV infection. It is possible that HIV regulatory proteins may be affecting MutYH expression directly, or may be indirectly altering the activity of transcription factors necessary for MutYH expression.

On the other hand, OGG1 and FEN1 mRNA transcript levels are related to oxidative DNA damage. OGG1, the first enzyme to act during repair of 8-oxo-dG base modifications, and FEN1, a later-event enzyme which functions during long-patch base-excision repair, show a strong positive correlation with each other in both the 014 and 003 cohorts at both time points examined. Among 014 participants, under what can be considered "normal" circumstances, both OGG1 and FEN1 mRNA positively correlate with mtDNA 8-oxo-dG break frequency, seeming to be up-regulated as need arises. However, despite a significant increase in 8-oxo-dG BF, expression of both enzymes is not different between the controls and the ART-naïve HIV patients, and OGG1 and FEN1 no longer correlate with 8-oxo-dG in HIV patients at baseline.

This could be due to HIV infection impacting the ability of the mtDNA BER pathway to adequately respond to oxidative DNA damage, or to additional regulations introduced by the virus. In previous *in vitro* studies, the HIV *tat* protein has been found to down-regulate OGG1 expression [35], while HIV integrase can stimulate FEN1 activity [43]; while the full extent of HIV regulation of these enzymes in currently unknown, it is possible these two phenomena may be responsible for the absence of a normal response seen here in HIV patients. After 72 weeks following ART-initiation, OGG1 once again responds normally to oxidative DNA damage, and OGG1 mRNA positively correlates with mitochondrial 8-oxo-dG BF.

Interestingly, FEN1 mRNA levels were found to decrease in HIV patients after 72 weeks of ART therapy, despite there being no differences in expression found as a result of HIV infection. This could be an effect of the antiretroviral drugs independent of the virus, especially as at 72 weeks when the viral load has been nearly eliminated and other parameters of mitochondrial health have improved, FEN1 does not regain its normal response to oxidative DNA damage, and unlike OGG1, FEN1 mRNA does not correlate with 8-oxo-dG after therapy initiation. Perhaps most intriguingly, FEN1 mRNA levels were found to be higher at baseline in patients who showed an increase in 8-oxo-dG after initiating therapy versus those who showed a decrease, regardless of drug arm or other mitochondrial factors. It is possible that antiretroviral drugs can interact with FEN1 directly or indirectly, as ART therapy seems to down-regulate or interfere with normal FEN1 expression, and the level of FEN1 expression at therapy initiation can have an effect on the outcome of antiretroviral treatment.

We have demonstrated that mitochondrial DNA repair enzymes are affected by both HIV infection and ART. Mechanistic studies to determine the means by which antiretroviral drugs cause these changes would be useful in understanding ART-induced cellular complications, and perhaps give better insight into means into mediating ART-induced mitochondrial toxicity. An *in vitro* cell model, which we explore in the next chapter, would enable finely-controlled mechanistic experiments to examine the mode of BER regulation by antiretroviral agents, and allow these phenomena to be investigated without the compounding effects of HIV.

CHAPTER 3

Effects of protease inhibitor-based antiretroviral cocktails on mitochondrial DNA oxidative damage and base-excision repair in cultured human renal cells

3.1. ABSTRACT

Long-term treatment of HIV with ART has been linked to various clinical complications; in NRTIs, many of these side effects are attributable to mitochondrial toxicity, though whether mitochondrial BER is involved in or affected by ART-induced toxicity is currently unknown. Likewise, whether the side effects of PI-based therapy, which include dyslipidemia and renal toxicity, are associated with mitochondrial dysfunction has also not been established. This study sought to investigate the molecular effects of PI-based ART on mitochondria in renal cells by measuring mitochondrial respiration, mtDNA oxidative damage and mitochondrial BER enzyme expression following treatment with two clinically-used PI-based regimens. The hypothesis to be tested was that ART treatment would increase mtDNA oxidative damage and expression of BER enzymes, while altering mitochondrial function.

The two drug cocktails used in this study were ritonavir-boosted atazanavir with a tenofovir/emtricitabine backbone (TDF/FTC +ATV/r), or ritonavir-boosted darunavir with tenofovir/emtricitabine (TDF/FTC +DRV/r), with cells given the vehicle, dimethyl sulfoxide (DMSO) as a control. Cells were treated for one week with patient sera-equivalent concentrations of the drugs, then oxidative stress was measured by mtDNA 8-oxo-dG BF. Transcript and protein levels of three mitochondrial BER enzymes: OGG1, MutYH, and FEN1 were assayed. Mitochondrial respiration was determined and non-mitochondrial respiration, proton leak, ATP production, and spare mitochondrial respiratory capacity were calculated. Paired *t*-tests were used to analyze normally-distributed data, and significance was set at $p < 0.05$.The oxygen consumption rate due to non-mitochondrial respiration and proton leak were slightly increased in cells treated with ART relative to DMSO. ATP production and spare respiratory capacity were not affected by treatment. Conversely, 8-oxo-dG BF and OGG1 mRNA and protein levels were lower in ATV-treated cells than those treated with DMSO. However, DMSO itself had an effect of increasing 8-oxo-dG and OGG1 compared to untreated cells, rendering the effects of the drugs themselves indistinguishable from the vehicle. What we have found, though, is that expression of the DNA repair enzyme OGG1 is elevated concurrently with mitochondrial 8-oxo-dG due to treatment (DMSO or ART) –induced oxidative damage.

3.2. INTRODUCTION

3.2.1. PI-based drug regimens

In current treatment of HIV/AIDS, PI-based drug regimens generally consist of a PI base, often boosted with ritonavir (RTV), and a backbone of two NRTIs. As RTV is a potent inhibitor of the liver enzyme cytochrome P450-3A4 (CYP3A4), RTV-boosting prevents rapid metabolism of co-administered PIs, increasing their serum concentrations and enhancing their efficacy [75]. Occasionally a newer CYP3A4 inhibitor, cobicistat (COBI), may be used as a pharmacokinetic enhancer in place of RTV [105]. As of 2014, the NIH recommends two PI-based regimens for therapy-naïve adolescents and adults: ritonavir-boosted atazanavir (ATV/r) or ritonavir-boosted darunavir (DRV/r), both in combination with tenofovir and emtricitabine (TDF/FTC). Alternative PI-based therapies, for patients with intolerance or HIV resistance towards the standard drugs, include using ritonavir-boosted lopinavir (LPV/r) as the base, abacavir with lamivudine (ABC/3TC) as the backbone, or DRV/r in combination with the integrase inhibitor raltegravir (RAL). Commercially-available antiretrovirals offer fixed doses of boosted PIs in single-pill form, and NRTI backbone combinations similarly, which only need to be taken once daily [78].

3.2.2. Side effects of drugs in currently-used PI-based drug regimens

Being the first class of antiretrovirals developed, more is known about the toxic side effects of NRTIs than the other types of drugs used in HIV treatment. Earlier NRTIs caused a range of complications, including myopathy, various metabolic disorders such as lipoatrophy and lactic acidosis, and neuropathy [106]. Due to the severity of toxicity, several of the oldest NRTIs are no longer offered as standard treatment in the United States (though continue to be used in developing countries because of their low cost) [73]. Much of the toxicity from earlier drugs can be traced to depletion of mtDNA due to inhibition of pol γ [106], though the newer, currently-used NRTIs have a lower affinity for pol γ and have not been found to induce mtDNA depletion. These drugs still have clinical side effects, so there may be another aspect of mitochondrial function they are interfering with [55].

Tenofovir (TDF) in particular is known to induce renal toxicity, including proximal renal tubular dysfunction in some patients [88], in addition to the more common gastrointestinal upset and dizziness. Symptoms include glucosuria, renal tubular acidosis, and hypophosphatemia, and

are much more prevalent in patients already exhibiting nephrotoxicity prior to treatment [82]. Specifically, TDF has been found to induce dysfunction in the renal proximal tubule [107, 108]. Emtricitabine (FTC), commonly administered in combination with TDF, has a lower rate of side effects, which are milder and may include gastrointestinal (GI) upset, rash, headache, and hyperpigmentation of the palms and soles. No significant mitochondrial toxicity has been attributed to FTC [82].

PIs have the benefit of lower toxicity compared to NRTIs as a class, although they do have a number of clinical complications associated with them. The two most common types of side effects that occur over the range of the PI class of drugs are rashes, GI upset, cardiovascular disease (CVD) risk, and metabolic disorders such as dyslipidemia, lipodystrophy, and insulin resistance [109]. While the mechanisms behind these toxicities are unknown, metabolic disorders in particular may be indicative of mitochondrial dysfunction, as has been the case for NRTI-induced metabolic disorders [81].

Atazanavir (ATV) has the most severe of the toxicities of currently-used PIs, with hepatotoxicity occurring in a small portion of patients, resulting in hyperbilirubinemia, caused by inhibition of the metabolic enzyme uridine 5'-diphospho-glucuronosyltransferase (UGT), as well as jaundice [110]. Long-term use of ATV can also lead to proximal renal tubular dysfunction [109]. Compared to ATV, darunavir (DRV) has relatively mild side effects, which include GI upset, headache, rash, and nasopharyngitis [111], with only minor increases in triglycerides and total cholesterol [112]. Ritonavir (RTV), as it is generally used as a pharmacokinetic enhancer, is not administered in viral-neutralizing doses, and so is associated with fewer long-term complications than other clinically-used PIs [82]. Clinical studies have linked RTV use to GI upset and hypertriglyceridemia, which may be due to its co-administration with other PIs [113].

3.3. MATERIALS AND METHODS

3.3.1. Cell culture

HeLa human cervical cells and HEK-293 human embryonic kidney cells were cultured in T-72 flasks or 15cm cell culture dishes (Corning, Corning, NY) using Gibco high-glucose DMEM supplemented with 10% FBS and 50U/mL penicillin/streptomycin (Life Technologies, Grand Island, NY). When cells reached a confluence of approximately 80%, they were passaged to a ¼ concentration by washing with 1X PBS (Amresco, Solon, OH) and incubating in 0.25%

trypsin-EDTA (Life Technologies) at 37°C for 1 minute or until detached, using gentle tapping or pipetting to lift cells.

Primary human renal proximal convoluted tubule (RPCT) epithelial cells were purchased from ZenBio (Research Triangle Park, NC). Upon thawing, each vial of cells was washed by spinning down for 5 minutes at 4°C in 14mL renal epithelial maintenance medium (ZenBio), aspirating the liquid and re-suspending the cells in renal epithelial plating medium (ZenBio). Cells were plated at a density of $5x10^3$cells/cm^2 onto T-25 flasks coated with 5μg/cm^2 rat tail collagen (Life Technologies) in renal epithelial plating medium and allowed to settle overnight. Once attached, cells were cultured in renal epithelial maintenance medium until a confluence of approximately 20% was reached before beginning any treatment.

3.3.2 Antiretroviral treatment

All antiretrovirals were obtained free of charge from the NIH AIDS Reagent Program (Germantown, MD). Reagents were received in lyophilized form, and then re-suspended as follows: 5mg/mL TDF in H_2O; 20mg/mL FTC in H_2O; 15mg/mL ATV in DMSO (Sigma-Aldrich, St. Louis, MO); 15mg/mL DRV in DMSO; and 10mg/mL RTV in DMSO. Once re-suspended, reagents were stored in working aliquots at -20°C. For cell treatment, media concentrations of the drugs were based on patient sera steady-state C_{max} levels on currently-recommended dosages as given in the Physicians' Desk Reference [114]: 0.3μg/mL TDF; 1.8μg/mL FTC; 6.13μg/mL ATV; 5.6μg/mL DRV; 0.9μg/mL RTV.

Treatment of HEK-293 and primary RPCT cells lasted for one week. Five treatment groups were established: untreated cells (cultured in normal maintenance media for duration of treatment), vehicle-treated cells (media with 0.038% DMSO, equivalent amount to DMSO used in drug-treated groups), ATV-based drug regimen (media with TDF/FTC + ATV/r in concentrations indicated above), DRV-based drug regimen (media with TDF/FTC + DRV/r), and H_2O_2-treated cells (HEK-293 cells only, used as a positive control: on last day of treatment, 2μM H_2O_2 [Sigma Aldrich] was added to media for 16 hours). For treated HEK-293 cells, a complete media change with fresh reagents was performed every other day; for treated primary RPCT cells, half of the media volume was replaced every day.

3.3.3. Seahorse mitochondrial respiration assay

Mitochondrial respiratory parameters were measured on a Seahorse XF^{e}96 Extracellular Flux Analyzer using the XF Cell Mito Stress Test Kit (Seahorse Bioscience, North Billerica, MA) (Fig. 3.1). Primary RPCT cells were detached with trypsin as described above and seeded at a density of $2x10^4$ cells/well in an XF cell culture plate coated with 5μg/cm^2 rat tail collagen (Life Technologies). Untreated HeLa cells were plated at a density of $3x10^4$cells/well in 3-6 wells as a control. Cells were allowed to attach overnight in renal epithelial maintenance medium in a 5% CO_2 incubator, then were switched to 175μL per well XF assay medium (RPMI-1640, no sodium bicarbonate, MP Biomedicals, Santa Ana, CA, with 2.5mM glucose, Sigma Aldrich) and de-gassed in a non-CO_2 incubator at 37°C for 30 minutes prior to starting the assay. Reagents from the XF Cell Mito Stress Test Kit were diluted into XF assay medium and loaded into an XF cartridge according to kit protocol to give the following in-well final concentrations: 2.0 μM oligomycin, 1.0 μM FCCP, and 2.0 μM antimycin/rotenone. The respiration assay was run using the following protocol: four measurement cycles at basal, then three measurement cycles following each reagent injection, with one cycle consisting of three minutes of mixing followed by three minutes of dissolved oxygen concentration readings at 13-second intervals to give the oxygen consumption rate (OCR) at each measurement [115].

Results from Seahorse assays were exported onto Excel for calculation of mitochondrial respiratory parameters. The first measurement from each run was eliminated, and the OCR under each experimental condition was obtained by averaging the three measurements at baseline and following each injection. Respiratory parameters were calculated as follows:

non-mitochondrial respiration = OCR after antimycin/rotenone injection

basal respiration = baseline OCR – non-mitochondrial respiration

proton leak = OCR after oligomycin injection – non-mitochondrial respiration

ATP production = basal respiration – proton leak

maximal respiration = OCR after FCCP injection – non-mitochondrial respiration

spare respiratory capacity = maximal respiration – basal respiration

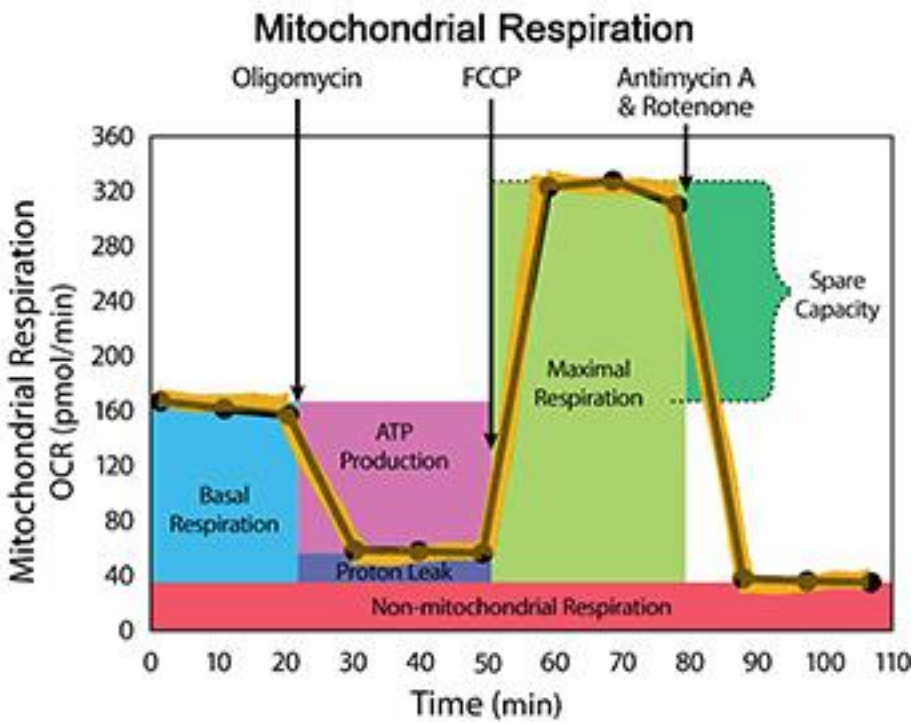

Figure 3.1. Schematic of a Seahorse XF Cell Mito Stress Test mitochondrial respiration assay. An example graph of oxygen consumption rate (OCR) for one well during the course of a typical mitochondrial respiration assay, showing the drug injection protocol and values used for calculating each mitochondrial respiratory parameter [116].

3.3.4. DNA and RNA extraction and quantification

Cells were harvested by washing with 1X PBS then lysing with buffer RLT+ (Qiagen, Valencia, CA) directly in-dish. DNA and RNA were purified jointly using Qiagen's AllPrep DNA/RNA Mini Kit according to manufacturer's instructions. DNA was eluted with TE buffer and stored at 4°C. RNA was eluted with RNAse-free H_2O and used directly for quantification and cDNA synthesis.

DNA concentrations were measured on a NanoDrop 2000 spectrophotometer (Thermo Scientific, Waltham, MA). RNA quantity and quality were measured on an Agilent 2100 Bioanalyzer using the RNA Nano or RNA Pico Lab-on-a-Chip Kits (Agilent Technologies, Santa Clara, CA) according to manufacturer's instructions. An RNA integrity number (RIN) of 7.0 or higher was the standard requirement for further RNA experimental use.

3.3.5. Mitochondrial 8-oxo-dG quantification by Southern blot

Oxidative damage to mtDNA was evaluated by measuring the number of 8-oxo-dG modifications per mtDNA strand using a gene-specific repair assay. For HEK-293 cells, 8µg total purified DNA per sample was used for the assay, while 2µg DNA pooled from two samples was used per blot for the primary RPCT cells. MtDNA was detected using a DNA probe specific for the mitochondrial gene encoding human cytochrome b, labelled with digoxygenin (DIG) by PCR amplification (primer sequences: DigFor: 5'-GCT ACC TTC ACG CCA A-3'; DigRev: 5'-CCG TTT CGT GCA AGA AT-3').

The following ethanol precipitation procedure was used for each DNA concentration step: 0.1 volume of 3.0M NaOAc (Sigma-Aldrich) then 2.5 volume cold 100% EtOH was added per sample. DNA was then incubated at -80°C for a minimum of 40 minutes (up to overnight), then centrifuged for 15 minutes, 16,000xg, 4°C. The supernatant was aspirated, then 500µL 70% EtOH was added followed by another centrifugation for 3 minutes, 16,000xg, room temperature. The supernatant was removed again, and the DNA pellet allowed to air-dry in a 40°C heat block before re-suspending in the desired solvent at the desired concentration.

After the appropriate amount of starting DNA was concentrated in DNase/RNase-free H_2O, mtDNA was linearized by a two-hour incubation at 37°C with 1X NEBuffer 2 and 20U/mL PVUII (New England BioLabs, Ipswich, MA). Samples were precipitated again, re-suspended in TE buffer (Qiagen), and divided equally into two parts. One half remained at 4°C while the other half was digested for one hour at 37°C with 1X NEBuffer 2.1, 200µg/mL BSA, and 100U/mL hOGG1 (New England BioLabs). The digestion reaction was terminated by incubating at 65°C for one hour, followed by another precipitation and re-suspension in TE buffer.

Both halves of each DNA sample were re-quantified, and equal amounts for each half were used for alkaline gel electrophoresis. Each sample pair was brought to equal volumes using TE+ (Tris-EDTA, Sigma-Aldrich, with extra 0.2mM EDTA, Amresco), mixed with 1X alkaline loading dye (Boston BioProducts, Ashland, MA), and dry-loaded onto a 0.75% SeaKem Gold agarose gel (Lonza Group Ltd., Basel, Switzerland) along with a DIG-labelled, HINDIII-digested λ DNA molecular weight marker (Roche Diagnostics Corporation, Indianapolis, IN). The gel was dry-run at 50V for 30 minutes until the loading dye had completely left the wells and entered the gel. Electrophoresis continued at 50V for another 3 hours after adding 1X

alkaline electrophoresis buffer (50mM NaOH, Fisher Scientific, 1mM EDTA, Amresco), using a Mini-pump Variable Flow recirculating system (Fisher Scientific) to keep cool. After the first two hours, DNA complimentary to the detection probe was loaded into an unused well as a positive control.

The DNA gel was transferred onto a Nylon+ membrane (Roche) using a Vacugene XL vacuum blotting unit (GE Healthcare Bio-Sciences, Pittsburg, PA) at 50mbar. A series of solutions was used to facilitate transfer: 15 minutes with depurination solution (0.25M HCl), 15 minutes with denaturation solution (1.5M NaCl, 0.5M NaOH), 7 minutes with neutralizing solution (1M Tris, 1.5M NaCl, pH 7.5), and 30 minutes with 20X SSC (Teknova, Hollister, CA). After transfer, the blot was auto-crosslinked with 1200μJ/cm^2 UV using a Stratalinker 1800 UV crosslinker (Stratagene, La Jolla, CA). The blot was incubated in pre-hybridization buffer (dissolved DIG Easy Hyb granules, Roche) at 45°C for 20 minutes in a Shake 'N' Bake hybridization oven (Boekel Scientific, Feasterville, PA), then incubated overnight at 45°C in DIG probe hybridization buffer (pre-hybridization buffer with 15μL denatured probe).

Prior to detection, the blot was washed twice for 5 minutes at room temperature with low-stringency wash buffer (2X SSC, 0.1% SDS, Sigma Aldrich) then twice for 20 minutes at 65°C with high-stringency wash buffer (0.5X SSC, 0.1% SDS), and rocked in 1X Blocking Buffer in 1X Maleic Acid Buffer (Roche DIG Wash and Block Buffer Set, Roche) between 30 minutes and 3 hours at room temperature. A solution of 0.15U anti-DIG Fab (Roche) in 1X Blocking Buffer , 1X Maleic Acid Buffer was added, and incubation proceeded for another 30 minutes. The blot was then washed and incubated in 1X Detection Buffer (Roche) for 5 minutes, then incubated under a thin layer of CSPD solution (Roche) 5 minutes at room temperature then 20 minutes at 37°C while blocked from light. Two overlaid images were taken at 30 minutes each on a G:BOX gel doc system using GeneSys software (SynGene, Cambridge, UK).

Band quantification by densitometry was performed using GeneTools software by SynGene. 8-oxo-dG modifications were quantified by calculating the mtDNA strand break frequency (BF) based on Poisson distributions of undigested and hOGG1-digested mtDNA using the following formula:

$$BF = l_n\left(\frac{undigested\ mtDNA}{hOGG1-digested\ mtDNA}\right)$$

3.3.6. cDNA synthesis

Purified RNA was converted into cDNA by reverse transcription PCR using the Transcriptor First Strand cDNA Synthesis Kit (Roche) according to manufacturer's instructions using the following parameters: for each reaction, 11µL RNA eluate was combined with 2µL Random Hexamer Primer, then denatured at 65°C for 10 minutes, followed by a 1 minute incubation on ice. Reverse transcription reaction protocol was: 25°C, 10 minutes; 50°C, 60 minutes; 85°C, 5 minutes. Two duplicate reactions were run separately per RNA sample, then combined and stored at -20°C.

3.3.7. OGG1, MutYH, and FEN1 mRNA quantification by real-time PCR

Quantification of OGG1, MutYH, and FEN1 mRNA was performed by real-time PCR with hydrolysis probes on a LightCycler 480 instrument using LightCycler 480 Software version 4.0 (Roche). Custom primers were ordered from Life Technologies (primer sequences: OGG1F: 5'-CCC CAG ACC AAC AAG GAA C-3'; OGG1R: 5'-AGG TCG GCA CTG AAC AGC-3'; MutYHF: 5'-AAC TAT GAG CCC GAG GCC TT-3'; MutYHR: 5'-AGC GGC TTC CCA GAG GTA G-3'; FEN1F: 5'-ACC CCG AAC CAA GCT TTA G-3'; FEN1R: 5'-GGG CCA CAT CAG CAA TTA GT-3'). Fluorescent hydrolysis probes from the Universal ProbeLibrary (Roche) used for each primer pair were: Probe #20 (OGG1), Probe #14 (MutYH), and Probe #82 (FEN1). The Universal ProbeLibrary Human PPIA Reference Gene Assay (Roche) was used for normalization. For each cDNA sample, four separate reactions, one for each target and reference gene, were run in duplicate on the same 96-well plate. Each reaction mixture was composed of the following: 25-100ng cDNA (diluted to 5µL in PCR-grade H_2O), 10µL ProbesMaster mix (Roche), 1µL (reference) or 2µL (target) primers (10µM forward and reverse primers in TE buffer, Sigma), 0.4µL probe, PCR-grade H_2O up to 20µL total volume per well. Cycling conditions were: a 10 minute pre-incubation at 95°C; amplification over 55 cycles of denaturing at 95°C for 10 seconds, annealing at 55°C for 30 seconds, and extension at 72°C for 1 second; and a final cool-down at 40°C for 30 seconds. Each target gene was normalized to PPIA for each sample, and calibrated to a control sample of cDNA from untreated HEK-293 or RPCT cells included on each plate.

3.3.8. Mitochondrial isolation

HEK-293 cells were prepared for fractionation by detaching cells from four 15cm dishes with trypsin as described above and combining into a 15cm falcon tube (Corning). Cells were then pelleted by brief centrifugation at 400xg, followed by a 1X PBS wash. Purification of mitochondria was performed with a dounce-homogenization method using the Mitochondria Isolation Kit for Cultured Cells (Abcam, Cambridge, MA) according to manufacturer's protocol with the following modifications: cell pellets were re-suspended in 6mL Reagent A without performing a snap-freeze step, and were not homogenized a second time (6mL Reagent B was added to the supernatant from the first dounce/spin step before proceeding with final centrifugation). The resulting mitochondrial pellets were re-suspended in 50µL Reagent C and stored at -80°C.

3.3.9. Protein collection and quantification

Whole-cell lysate (WCL) was obtained from HEK-293 and primary RPCT cells by washing cells with 1X PBS then lysing directly in-dish with RIPA buffer (Thermo Scientific, Rockford, IL). Lysates were passed through a QiaShredder column (Qiagen) via centrifugation at 16,000xg for 2 minutes to dislodge aggregates. Halt Protease Inhibitor Cocktail, EDTA-Free, 100X (Thermo Scientific) was added to lysates to 1% total volume. Lysates were stored at -80°C. Protein from both WCL and mitochondrial fractions (MF) was quantified using a Direct Detect infrared spectrometer (EMD Millipore, Billerica, MA) according to manufacturer's instructions.

3.3.10. OGG1, FEN1, and porin protein quantification by western blot

Depending on the total available amount of the smallest sample, 25-75µg protein from each WCL or MF (for HEK-293 cells) was used per blot. Samples were mixed with an equal volume SDS Loading Buffer and denatured for 2 minutes on an 85°C heating block before loading onto a 1.5mm, 15-well 10% Tris-glycine Novex gel (Life Technologies). Each gel was loaded in triplicate due to FEN1, porin, and β-tubulin having similar molecular weights. Thermo Scientific Spectra Multicolor Broad Range Protein Ladder, a pre-stained molecular weight marker, was added to the first and last wells of each blot. Electrophoresis proceeded for 1.75 hours at 125V on an XCell SureLock Mini-cell Electrophoresis System (Life Technologies).

Gels were transferred onto 0.45μM pore-size Whatman Nytran N nitrocellulose membrane (GE Healthcare Life Sciences, Pittsburg, PA) using the XCell SureLock system by electrophoresis at 25V for 1.5 hours. Presence of all pre-stained protein ladder bands on the membrane was checked to ensure complete transfer. Membranes were irradiated with 1200μJ/cm^2 UV on the Stratalinker 1800 UV crosslinker (Stratagene), then cut according to target and reference protein molecular weight and blocked in 5% Blotto in 1X PBST (PBS with 0.1% Tween-20, Sigma Aldrich) while rocking overnight at 4°C.

All antibodies were purchased from Abcam. Primary antibody incubation occurred at room temperature for 4 hours with the following dilutions in 1% Blotto in 1X PBST: 1:1000 rabbit anti-OGG1; 1:500 rabbit anti-FEN1; 1:1000 mouse anti-VDAC-1 (porin, mitochondrial loading control); 1:500 rabbit anti-lamin B (nuclear contamination indicator); 1:500 rabbit anti-β-tubulin (WCL loading control or cytoplasmic contamination indicator). Three 5-minute washes were done at room temperature in 1X PBST. Secondary antibody incubation occurred at room temperature for 2 hours with 1:10,000 HRP-conjugated goat anti-rabbit or anti-mouse IgG dilutions in 1% Blotto in 1X PBST, followed by three more 5-minute washes in 1X PBST.

Blots were incubated at room temperature with a thin layer of Pierce ECL Western Blotting Substrate (Thermo Fisher Scientific) for three minutes, then gently drained onto a paper towel. Three 10-second overlaid images and three 10-minute overlaid images were taken on a G:BOX gel doc system using GeneSys software (SynGene). Band quantification by densitometry was performed using GeneTools software (SynGene), and the relative quantity of OGG1 and FEN1 in each sample was calculated by dividing by the band intensity of β-tubulin (WCL) or porin (MF). Values of protein quantity were calibrated in each blot to a sample from untreated HEK-293 or RPCT cells.

3.3.11. Statistical analysis

Paired *t*-tests for normally-distributed data were run to compare OCR, 8-oxo-dG BF, mRNA ratios, and protein values between treatment groups across all treatment replications. Statistical probability values of $p \leq 0.05$ were considered significant while those of $0.06 \leq p \leq 0.10$ were considered a trend. N values for the primary RPCT cells resulted in powers of $\alpha < 0.80$, so there is a possibility of differences between groups being undetected. Analyses were performed using SigmaPlot version 12.0 software.

3.4. RESULTS

3.4.1. HEK-293 cells were not affected by ART after one week of treatment

Due to their quick growth rate and ease of culturing, HEK-293 immortalized human embryonic kidney cells were used to optimize procedures and establish controls for the *in vitro* ART treatment experiments. After treatment with antiretrovirals as described above for one week, no significant differences in 8-oxo-dG break frequency (n=4), mRNA expression of OGG1, MutYH, or FEN1, (n=11), or WCL or mitochondrial protein quantity of OGG1 or FEN1 (n=4) was found between the untreated, DMSO, TDF/FTC + ATV/r, TDF/FTC + DRV/r, or H_2O_2 treatment groups (data not shown).

3.4.2. Non-mitochondrial respiration and proton leak are slightly elevated in RPCT cells following one week of treatment with PI-based antiretroviral cocktails

RPCT cell treatment as described above and Seahorse analyses were performed three separate times. Values given are average OCR ±SD. Non-mitochondrial respiration was higher in the TDF/FTC +DRV/r treatment group (33.7 ±11.7pmol/min) than in the DMSO-treated group (29.7 ±11.4 pmol/min, p=0.031), although no differences were found between the TDF/FTC +ATV/r treatment group (30.6 ±4.5 pmol/min) and the vehicle (p=0.88) or TDF/FTC +DRV/r treatment groups (p=0.43, Fig. 3.2). Proton leak was elevated in the TDF/FTC +ATV/r treatment group (20.9 ±2.8 pmol/min) relative to the DMSO-treated group (16.9 ±3.6 pmol/min, p=0.036), although no differences were found between the TDF/FTC +DRV/r (29.3 ±15.8 pmol/min) treatment group and the vehicle (p=0.28) or TDF/FTC +ATV/r groups (p=0.48, Fig. 3.3).

3.4.3. ATP production and spare respiratory capacity were not affected by treatment

OCR due to ATP production was not found to differ significantly in primary RPCT cells following one week of treatment between the vehicle (69.3 ±15.7 pmol/min) and the TDF/FTC +ATV/r (78.2 ±13.3 pmol/min, p=0.069) or TDF/FTC +DRV/r (77.1 ±34.5 pmol/min, p=0.38) groups (Fig. 3.4, top panel). Likewise, no significant differences were found in spare respiratory capacity among the vehicle (144.0 ±68.6 pmol/min) and the TDF/FTC +ATV/r (157.6 ±59.0 pmol/min, p=0.13) or TDF/FTC +DRV/r (113.7 ±120.2 pmol/min, p=0.794) treatment groups (Fig. 3.4, bottom panel).

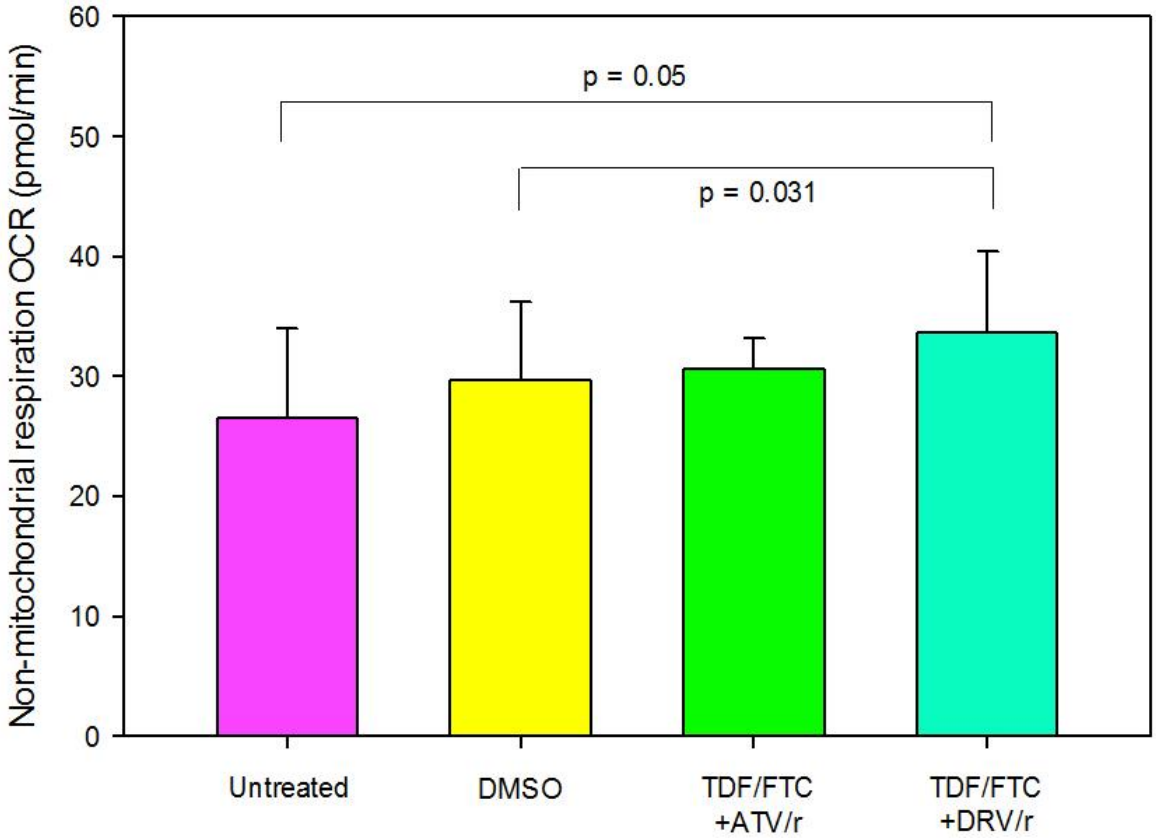

Figure 3.2. Non-mitochondrial respiration is increased in primary renal cells treated with a DRV-based antiretroviral cocktail. After one week of treatment, primary RPCT cells given the TDF/FTC +DRV/r drug regimen had higher non-mitochondrial respiration than untreated or DMSO-treated cells. No differences were found between the TDF/FTC +ATV/r treatment and the other groups. Bars indicate oxygen consumption rate (OCR) mean + standard error, n=3.

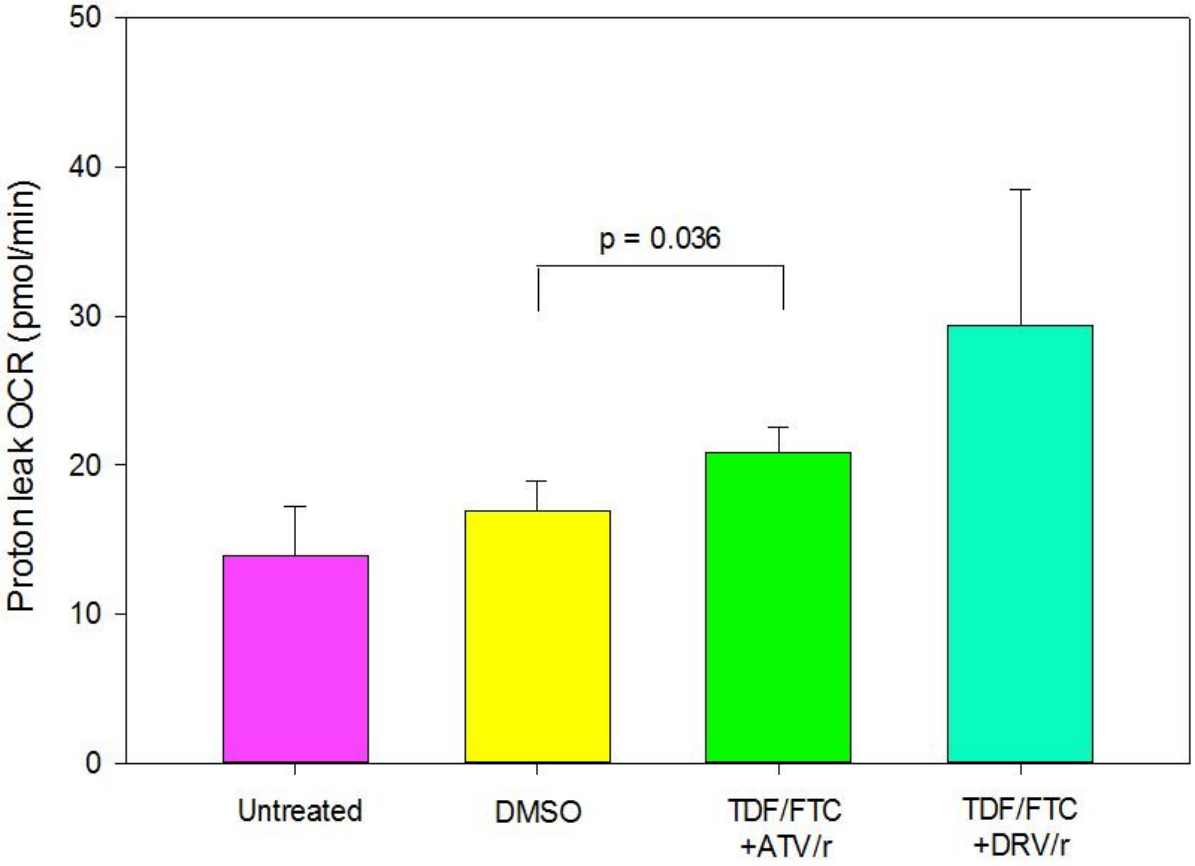

Figure 3.3. Proton leak is increased in primary renal cells treated with an ATV-based antiretroviral cocktail. After one week of treatment, primary RPCT cells given the TDF/FTC +ATV/r drug regimen had a higher amount of proton leak compared to DMSO-treated cells. No differences between untreated cells, cells given TDF/FTC +DRV/r, and the other treatment groups was found. Bars indicate oxygen consumption rate (OCR) mean + standard error, n=3.

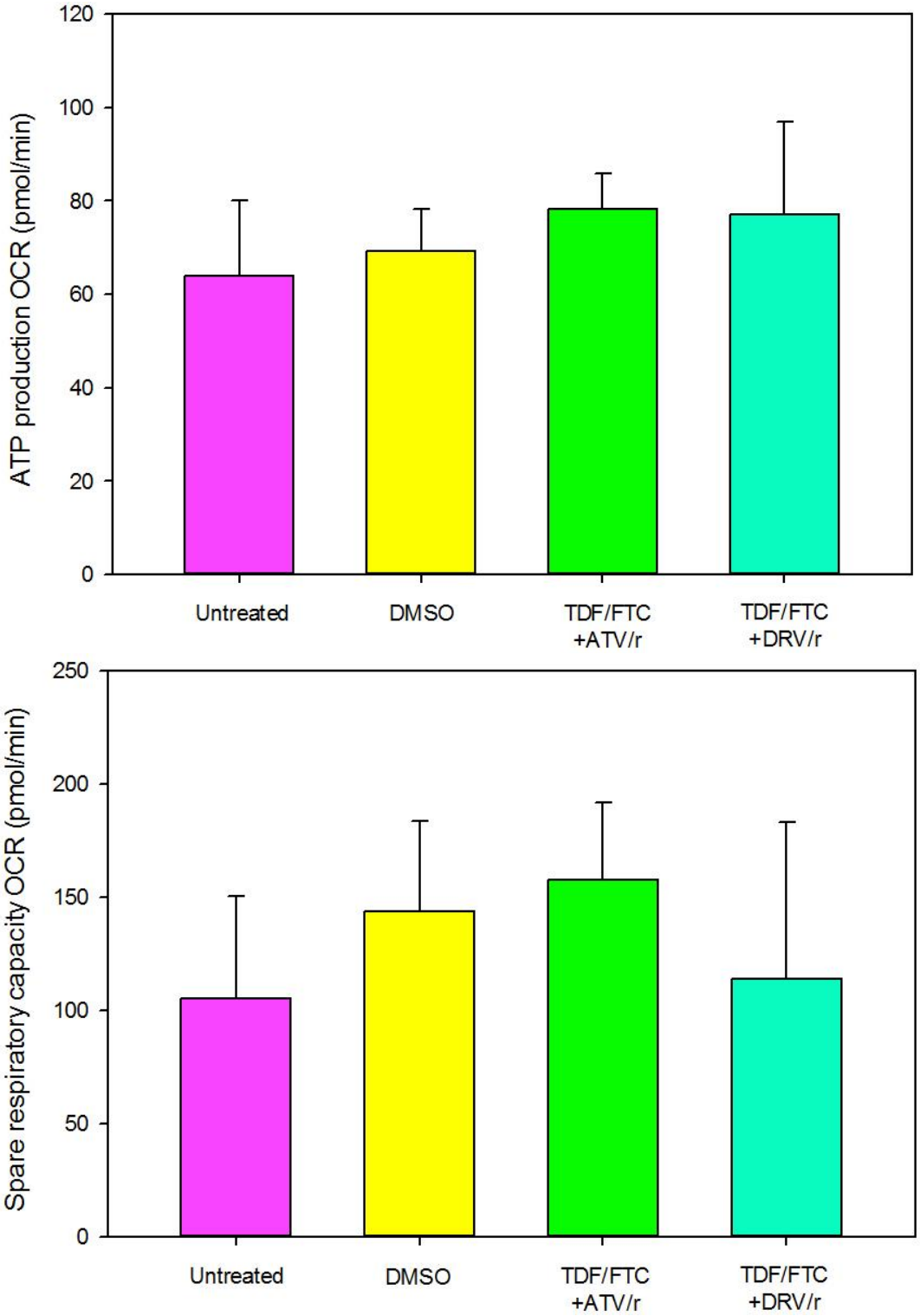

Figure 3.4. ATP production and spare capacity in primary renal cells did not differ by group. After one week of treatment with antiretrovirals, no differences in ATP production (top panel) or spare respiratory capacity (bottom panel) were found between untreated primary RPCT cells or cells given DMSO, TDF/FTC +ATV/r, or TDF/FTC +DRV/r. Bars indicate oxygen consumption rate (OCR) mean + standard error, n=3.

3.4.4. MtDNA oxidative damage is lower in ART-treated than vehicle-treated renal cells

From two sets of pooled primary RPCT cell DNA, the mtDNA 8-oxo-dG Southern blot assay showed lower break frequencies in both the TDF/FTC +ATV/r (average break frequency = 2.6 breaks/16.6kb) and TDF/FTC +DRV/r (1.8 breaks/16.6kb) treatment groups relative to the vehicle-treated cells (4.1 breaks/16.6kb). Vehicle (DMSO) and ART-treated cells all had higher break frequencies than untreated cells (1.2 breaks/16.6kb, Fig. 3.5), indicating an effect caused by the drug vehicle.

3.4.5. OGG1 mRNA and protein levels are lower in renal cells treated with antiretrovirals than in vehicle-treated cells

Quantitative real-time PCR showed lower OGG1 mRNA levels in primary RPCT cells treated with TDF/FTC +ATV/r (normalized mean ±SD: 1.66 ±0.38,) than in cells treated with the vehicle (2.25 ±0.4, p=0.02). OGG1 mRNA levels were not significantly different between cells treated with TDF/FTC +DRV/r (2.01 ±0.75) and the vehicle (p=0.14) or the TDF/FTC +ATV/r (p=0.69) treatment groups (Fig. 3.6). MutYH and FEN1 mRNA levels were not found to have significant differences between the vehicle-treated cells (1.22 ±0.16 and 0.82 ±0.02, respectively), and the cells given TDF/FTC +ATV/r (1.14 ±0.29, p=0.59; 0.72 ±0.15, p=0.18), or TDF/FTC +DRV/r (1.10 ±0.06, p=0.25; 0.83 ±0.08, p=0.88) after one week of treatment (Fig. 3.7).

Western blotting also found a decrease in OGG1 protein levels in cells treated with TDF/FTC +ATV/r (0.64 ±0.48) relative to DMSO-treated cells (1.48 ±1.11. p=0.046). Significant differences were not found between cells treated with TDF/FTC +DRV/r (0.81 ±1.04) and the vehicle (p=0.10) or TDF/FTC +ATV/r (p=0.54) treatment groups (Fig. 3.9). FEN1 protein levels also did not have any significant differences between the vehicle-treated cells (1.00 ±0.82), and the cells treated with TDF/FTC +ATV/r (0.67 ±0.56, p=0.19) or TDF/FTC +DRV/r (0.71 ±0.46, p=0.91). Porin protein levels, a measure of mitochondrial quantity, did not differ between the vehicle treatment group (1.65 ±0.89), and the TDF/FTC +ATV/r (1.84 ±2.18, p=0.56), or TDF/FTC +DRV/r (2.24 ±2.32, p=0.51) treatment groups (Fig. 3.10).

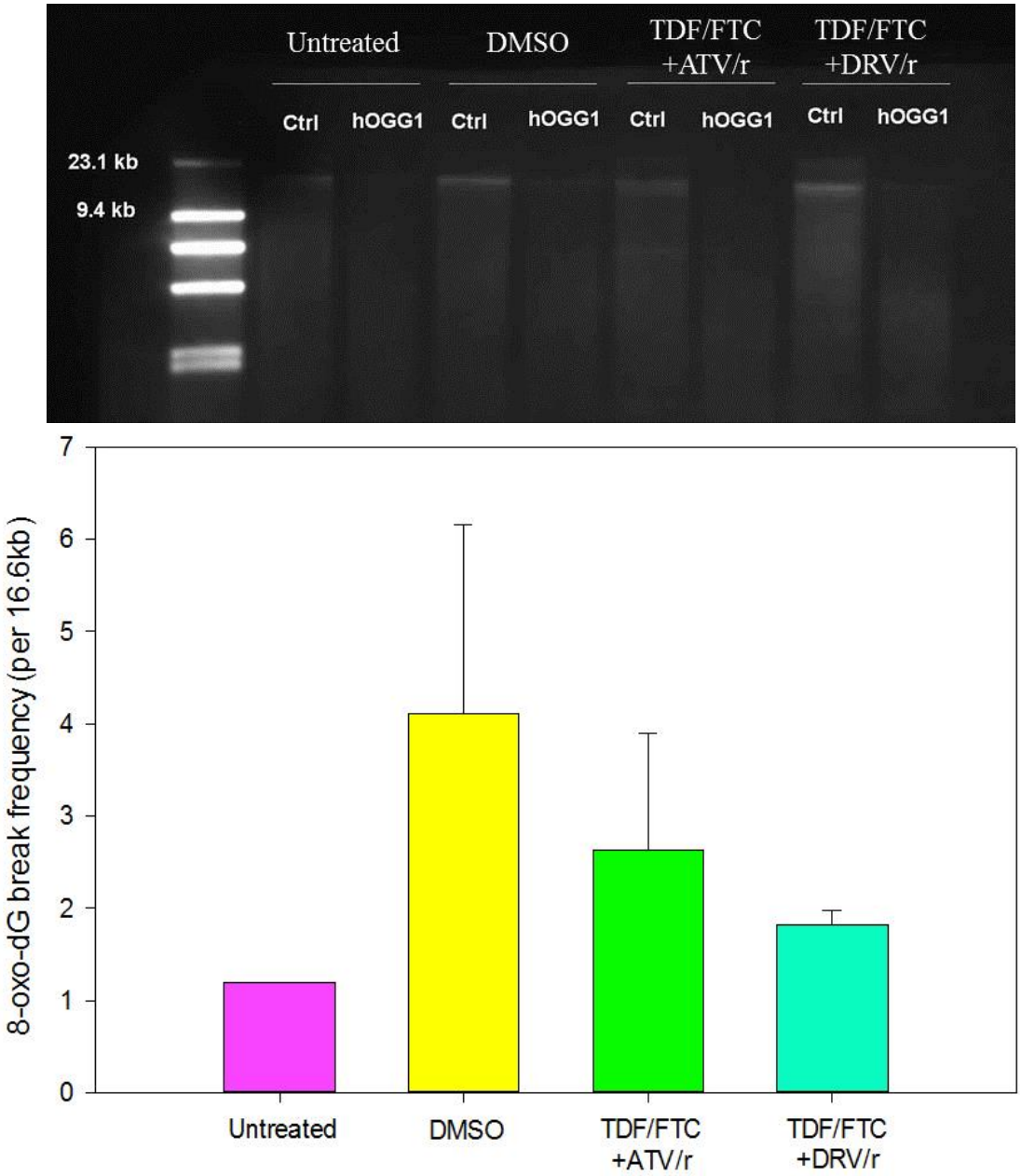

Figure 3.5. MtDNA 8-oxo-dG break frequency in ART-treated primary renal cells was higher than in untreated cells but lower than that of the vehicle-treated control. Top panel: a representative alkaline electrophoresis gel using DNA from primary RPCT cells. The difference in quantity of full-length mtDNA (16.6kb) between undigested (Ctrl) and hOGG1-digested (hOGG1) DNA in each sample pair is proportional to the number of 8-oxo-dG modifications per mtDNA strand. Bottom panel: break frequencies per treatment group, from four separate treatments pooled into two samples (untreated RPCT DNA was combined into one sample). Bars indicate mean break frequency ± standard error.

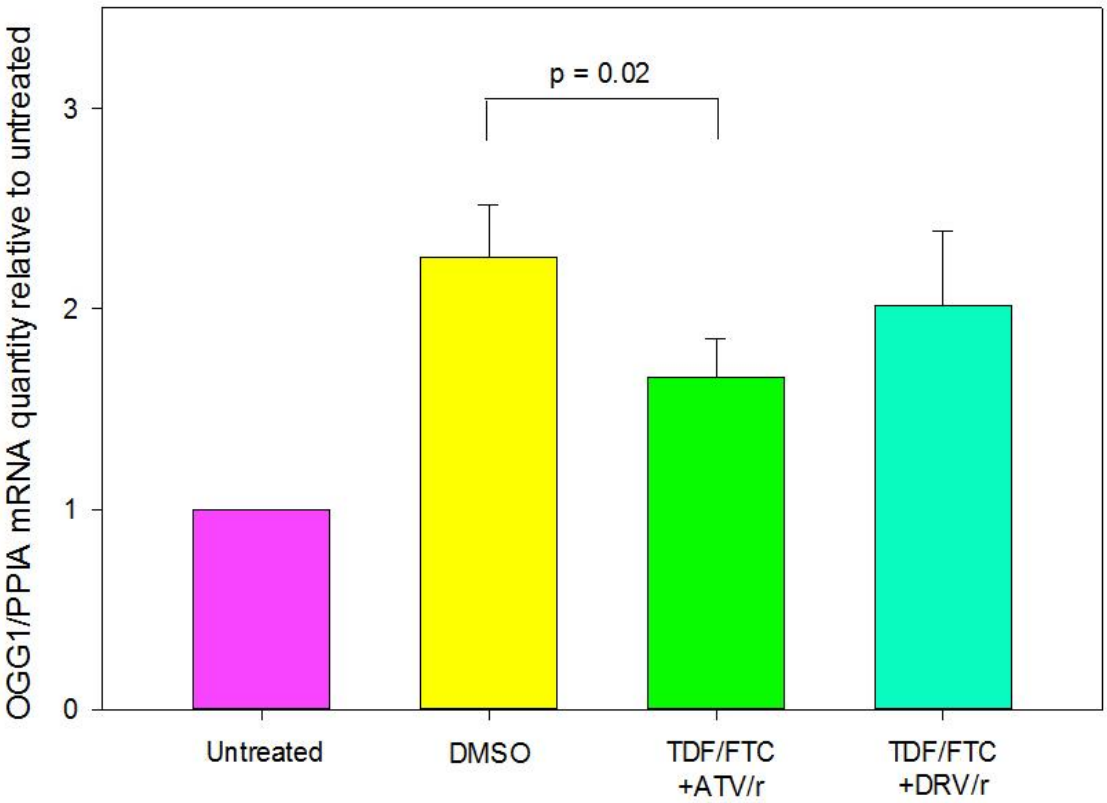

Figure 3.6. OGG1 mRNA is lower in primary renal cells treated with an ATV-based drug cocktail than in the vehicle-treated control. Primary RPCT cells treated with TDF/FTC +ATV/r for one week had lower OGG1 mRNA than DMSO-treated cells. No significant differences were seen between cells treated with TDF/FTC +DRV/r and the other treatment groups. Quantity of mRNA for each run was normalized to PPIA and calibrated cDNA from untreated cells. Bars indicate mean mRNA quantity + standard error, n=4.

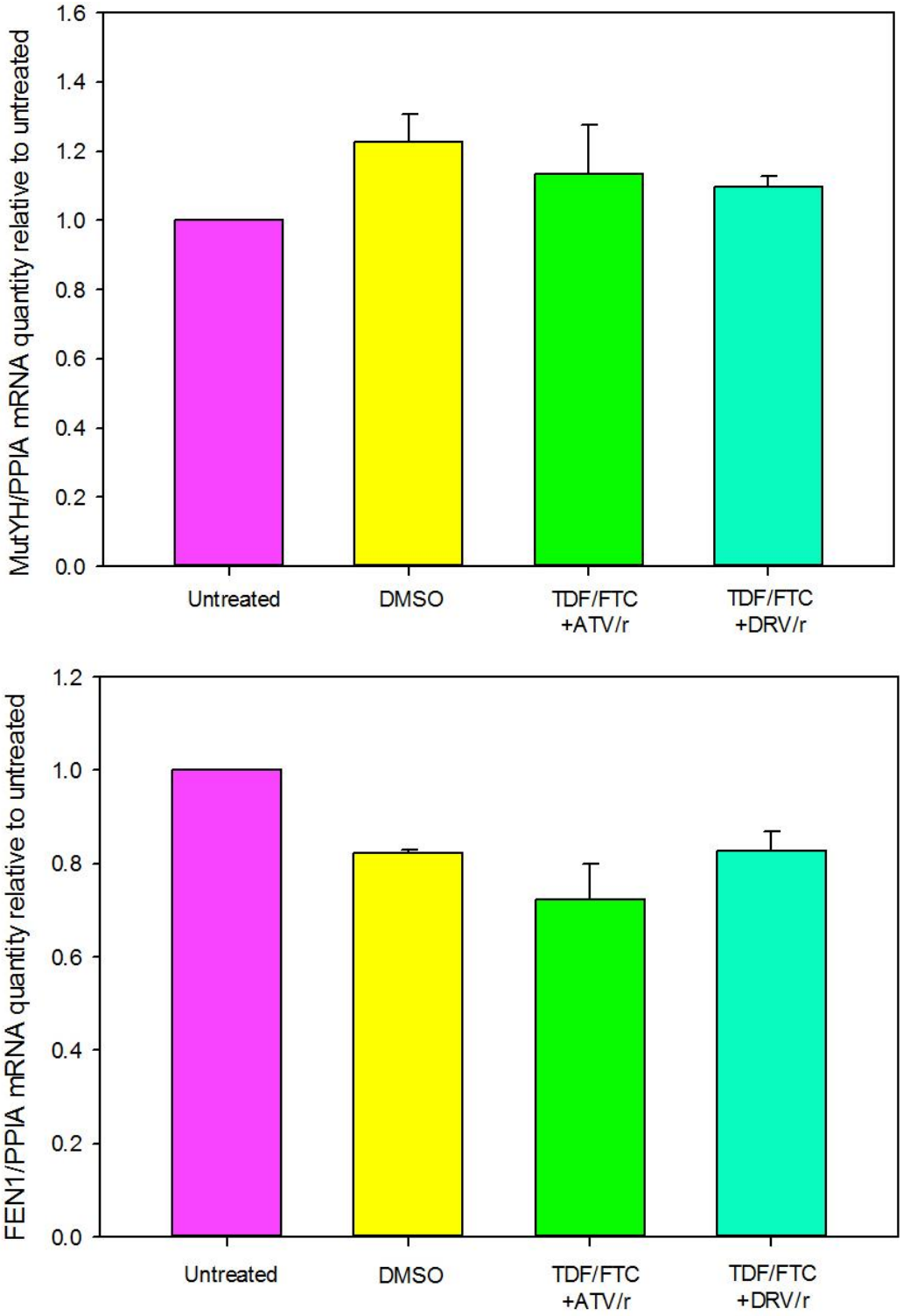

Figure 3.7. MutYH and FEN1 mRNA levels did not differ by treatment group. Primary RPCT cells treated for one week with TDF/FTC +ATV/r, TDF/FTC +DRV/r, or DMSO did not have significant differences in relative mRNA transcript levels of MutYH (top panel) or FEN1 (bottom panel). Quantity of mRNA for each run was normalized to PPIA and calibrated to cDNA from untreated cells. Bars indicate mean mRNA quantity + standard error, n=4.

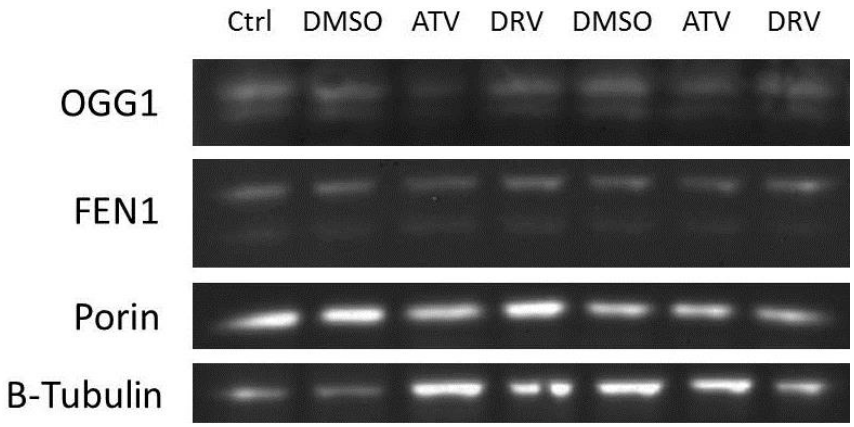

Figure 3.8. OGG1, FEN1, and porin protein levels in antiretroviral-treated primary renal cells. A representative western blot is shown depicting OGG1, FEN1, porin, and reference protein β-tubulin in untreated RPCT cells (Ctrl), and cells treated for one week with DMSO, TDF/FTC +ATV/r (ATV), or TDF/FTC +DRV/r (DRV).

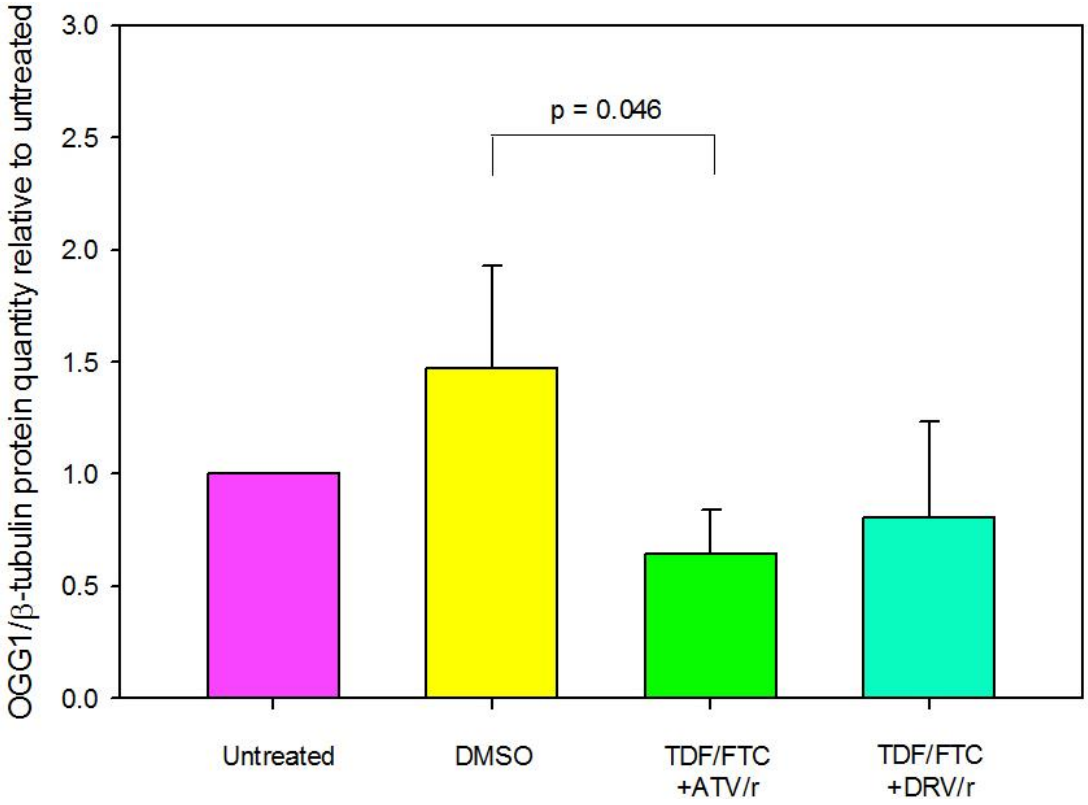

Figure 3.9. OGG1 protein level is lower in primary renal cells treated with an ATV-based drug cocktail than in the vehicle-treated control. Primary RPCT cells treated with TDF/FTC +ATV/r for one week had lower levels of OGG1 protein than DMSO-treated cells. No significant differences were seen between cells treated with TDF/FTC +DRV/r and the other treatment groups. Quantity of protein in each blot was normalized to β-tubulin and calibrated to untreated cell protein. Bars indicate mean protein quantity + standard error, n=6.

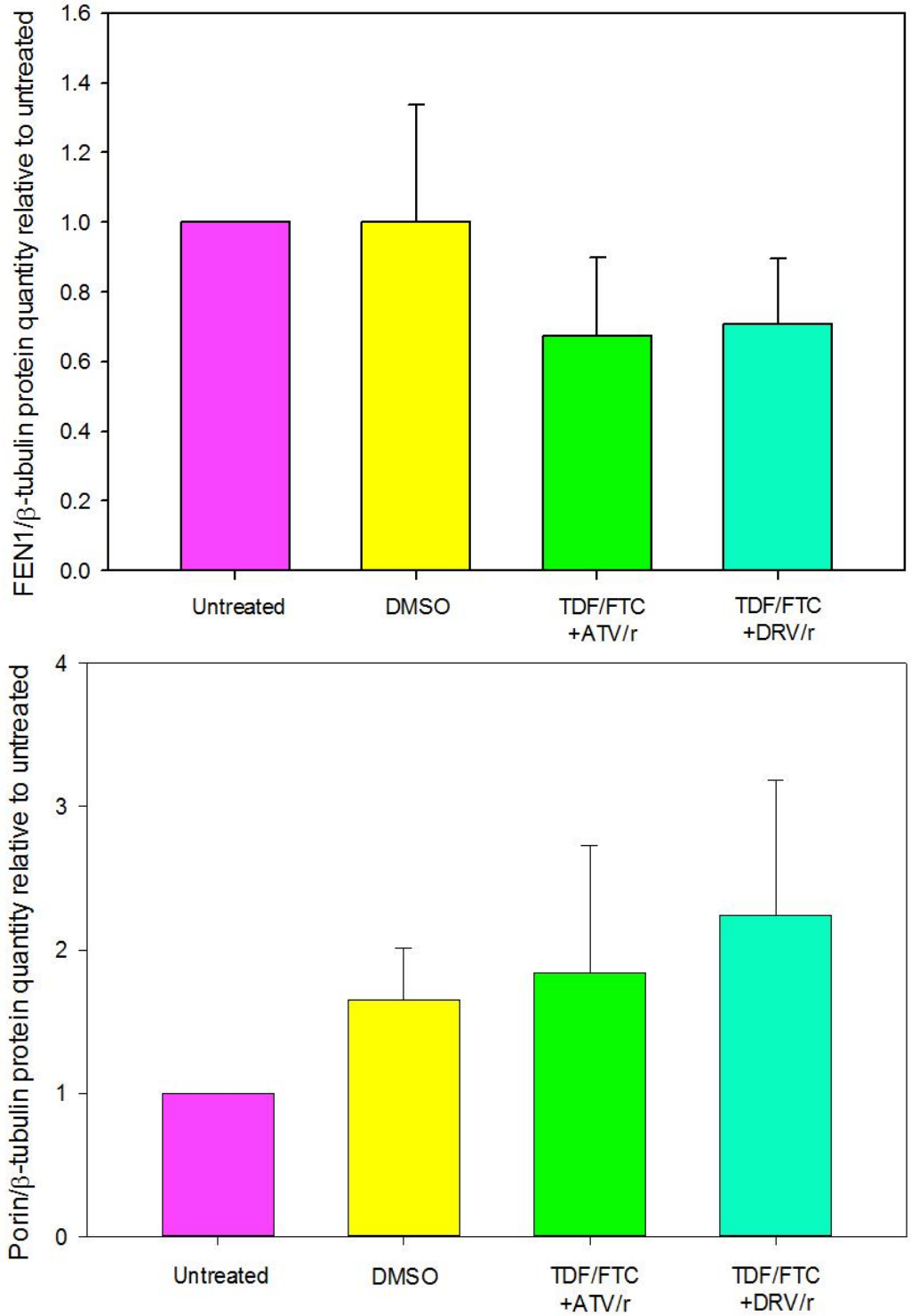

Figure 3.10. FEN1 protein level and mitochondrial quantity did not differ by treatment group. Primary RPCT cells treated for one week with TDF/FTC +ATV/r, TDF/FTC +DRV/r, or DMSO did not have significant differences in relative protein expression of FEN1 (top panel) or porin, a measure of mitochondrial quantity (bottom panel). Quantity of protein for each blot was normalized to β-tubulin and calibrated to untreated cells. Bars indicate mean protein quantity + standard error, n=6.

3.5. DISCUSSION

In this study, we examined the *in vitro* molecular effects of treatment of renal cells with two different clinically-used PI-based drug cocktails (TDF/FTC +ATV/r and TDF/FTC +DRV/r), specifically investigating any possible involvement of the mitochondrial base-excision repair pathway during antiretroviral-induced toxicity. We chose to use two types of renal cells, HEK-293 human embryonic kidney cells (a transformed, immortalized cell line) and primary human renal proximal convoluted tubule (RPCT) epithelial cells, due to the occurrence of renal toxicity in patients on current PI-based ART. The concentrations of drugs given to the cells were based on steady-state sera C_{max} values in patients given the indicated drug regimens. ATV, DRV, and RTV were all dissolved in DMSO; therefore, to control for effects of the solvent, a control set of cells was given an equivalent amount of DMSO as used as a vehicle in the drug-treated cells. The final concentration of DMSO in cell culture media was 0.038%; concentrations of DMSO less than 0.1% have not been found to cause significant mitochondrial toxicity [117].

After one week of treatment, no significant differences were found in HEK-293 cells in mtDNA oxidative damage or mRNA and protein levels of mitochondrial BER enzymes, total or mitochondria-localized. HEK-293 is a relatively hardy cell line that was chosen due to their quick growth rate and ease of culturing to optimize Southern blotting, qPCR, and western blotting conditions for the chosen genes in renal cells. It is possible that the lack of mitochondrial changes in these cells is due to a phenomenon known as the Crabtree effect, in which rapidly-proliferating cells, such as those from immortalized cell lines, produce ATP primarily through glycolysis despite having functional mitochondria [118]. This makes studying mitochondrial function difficult, and can mask effects of mitochondrial toxicity. Culturing cells in glucose-free media supplemented with galactose can ameliorate this; however, cells must be adapted to growth in glucose-free media first.

In primary RPCT cells, slight changes were found in two respiratory parameters: an increase in non-mitochondrial respiration in cells given TDF/FTC +ATV/r over DMSO-treated cells, and an increase in proton leak in cells given TDF/FTC +DRV/r over DMSO-treated cells. Changes to non-mitochondrial respiration, the combination of all cellular consumption of oxygen aside from OXPHOS [119], can be due to a number of factors not related to mitochondrial toxicity, such as cytoplasmic re-oxygenation of NADH, fatty acid desaturation, or activity of

detoxification enzymes. Likewise, a number of causes can lead to increased proton leak, such as altered proton-motive force or increased inner mitochondrial membrane permeability, which could be indicative of mitochondrial toxicity. However, since no significant changes were found in ATP production or spare respiratory capacity, such effects are likely negligible with regards to mitochondrial function. A limitation of the study was power, any undetected differences may become more pronounced if a greater number of treatment replicates was used. Power calculations found that to achieve a power of 0.80 to detect a difference with a significance probability of 0.05, a minimum of ten replicates was required.

When compared to untreated cells, DMSO has an effect of increasing 8-oxo-dG and OGG1, which is diminished by the addition of antiretrovirals. One compounding factor could be the storage conditions of DMSO: the vehicle-treated cells were provided with liquid DMSO that had been stored at ambient temperature, while the DMSO used as a solvent had been frozen and stored at -20°C following drug re-suspension; however, DMSO is known to be a very stable compound, and no changes to its structure or potency due to freezing have been described as of yet. Another possibility is a direct interaction between DMSO and the antiretroviral compounds used; DMSO is a commonly-used solvent in pharmacological research, but has on occasion been found to have an effect on the activity of the drug itself, such as in the case of acetaminophen [120]. For future studies involving *in vitro* use of protease inhibitors, a solvent selection study to identify a more suitable vehicle could prove beneficial.

Decreases in 8-oxo-dG BF and corresponding OGG1 mRNA and protein levels were found in primary RPCT cells treated with TDF/FTC +ATV/r relative to DMSO-treated cells, which would seemingly indicate a protective effect of antiretroviral drugs with regards to mitochondrial oxidative damage. As patients develop complications gradually over the course of several months or years, a longer treatment time or higher drug concentrations may have yielded more drastic results. Primary renal proximal convoluted tubule cells were used in this study as damage and dysfunction in the renal proximal tubule is a side effect of TDF and PI treatment. However, renal toxicity does not always occur, and future studies on other cell types, such as adipocytes or hepatocytes, may provide further insight into systemic ART toxicity.

CHAPTER 4

Discussion

4.1. Mitochondrial DNA damage repair in HIV patients before and after initiating ART

In the United States today, most patients who test positive for HIV are immediately placed on antiretroviral therapy (ART) regardless of their viral load or CD4 count [78], so while investigating the various complications that arise it can be difficult to discern which are due to treatment with the antiviral drugs and which are caused by the virus itself. Much is known about the HIV life cycle in the host cell and the effects of the virus on immune system function, but less has been learned about the influence of the virus on intercellular systems, such as the mitochondria and oxidative phosphorylation (OXPHOS). There exist *in vitro* and animal models to study HIV [121], but in the age of ART in the United States there are few cohorts of substantial size in which to study HIV independently from antiviral compounds.

My dissertation makes use of cohorts from the South East Asia Research Collaboration with Hawaii (SEARCH) in Thailand [102], in which patients newly diagnosed with HIV were enrolled in various drug trials and had clinical measurements and blood samples taken prior to beginning an antiretroviral regimen. I compared data from HIV-positive, ART-naïve patients from the SEARCH 003 cohort and HIV-seronegative participants from the SEARCH 014 cohort, I was able to determine virus-induced effects on the mitochondria. Previous studies by our laboratory on these patients found that epidermal nerve fiber densities (ENFD) in the upper thigh and lower leg, measures of proximal and distal nervous system health, was reduced in HIV-positive patients relative to the seronegative participants [103], and that plasma levels of the antioxidants superoxide dismutase 2 (SOD2), catalase, and peroxiredoxin 2 (PRX2) were elevated in HIV patients, indicating HIV-induced oxidative stress [122]. Various mitochondrial parameters, including mtDNA copies per cell, mtDNA 8-oxo-dG break frequency, and OXPHOS complexes CI and CIV specific enzyme activities were also previously measured from frozen patient peripheral blood mononuclear cells (PBMCs) [123].

I examined a sub-group of the SEARCH 003 and 014 cohorts PBMCs for mRNA expression of three enzymes involved in mitochondrial base-excision repair (BER): oxo-guanine DNA glycosylase 1 (OGG1), MutY homolog (MutYH) and flap structure-specific endonuclease 1 (FEN1). Among the selected participants, analysis of the previously-measured mitochondrial parameters revealed decreases in mtDNA content and CI and CIV enzyme activities in HIV-positive patients relative to the HIV-negative controls, showing genetic and functional consequences of HIV infection. Also, the HIV-positive patients showed higher PBMC

mitochondrial 8-oxo-dG break frequencies, as increased oxidative stress usually results from sub-optimal OXPHOS activity. The current study found no differences in OGG1 or FEN1 expression between the HIV-negative and HIV-positive groups, but did find a decrease in MutYH mRNA in the HIV-positive group, possibly indicating an impairment to BER due to HIV infection.

The next objective was to determine any alterations in mtDNA BER enzyme expression due to ART. After 72 weeks of ART, the patients' average viral load (mean viral RNA copies per mL) dropped from approximately 140,000 to 2,000, and CD4 counts (mean CD4+ cells per mm^3) rose from 174 to 372, above the AIDS-defining threshold. In our laboratory's previous SEARCH experiments, no changes in ENFD or antioxidant levels were found in HIV-positive patients between baseline readings and after 72 weeks of ART treatment. However, mitochondrial parameters did improve: mitochondrial 8-oxo-dG modifications had decreased while mtDNA content and CI and CIV enzyme activities increased 72 weeks after ART initiation. Likewise, the current study found that MutYH mRNA levels also increased from baseline to 72 weeks, showing a similar improvement following viral suppression. OGG1 expression did not change during the course of the trial; however, FEN1 mRNA expression interestingly decreased from baseline to 72 weeks, an effect which could be related to ART independently from HIV infection.

OGG1, which acts in the first step of 8-oxo-dG modified base repair, and FEN1, a later-event enzyme which functions during long-patch base-excision repair [25], show a strong positive correlation with each other in the control participants and in HIV-positive patients, both before and after starting ART. In HIV-seronegative individuals, under what can be considered normal circumstances, both OGG1 and FEN1 mRNA expression were found to positively correlate with mitochondrial 8-oxo-dG break frequency. OGG1 expression is controlled by a number of factors, including AP4 [34] and phosphorylated AKT [124], and this correlation with oxidative DNA damage may be due to a response to oxidative stress in general, as OGG1 transcription can be up-regulated by antioxidant-induced nuclear respiratory factor-2 (NRF2) [125]. Less is known about FEN1 regulation, though it seems to share a common regulatory pathway with OGG1.

In HIV-positive, ART-naïve patients, the correlation of these enzymes with 8-oxo-dG break frequency is no longer present. This could be due to HIV infection impacting the ability of

the mtDNA BER pathway to adequately respond to oxidative DNA damage, or to additional regulations introduced by the virus. In previous *in vitro* studies, the HIV *tat* protein has been found to down-regulate OGG1 expression [35], while HIV integrase can stimulate FEN1 activity [43]; while the full extent of HIV regulation of these enzymes in currently unknown, it is possible these two phenomena may be responsible for the absence of a normal response seen here in HIV patients. After 72 weeks of ART, the correlation with 8-oxo-dG is restored in OGG1 expression, though not in FEN1. As FEN1 did decline in expression during ART despite showing no differences in mRNA levels between HIV-positive and negative patients at baseline, it is possible this is due to a disruption in normal regulation caused by the antiretroviral agents.

Adding to this, when patients from SEARCH 003 were partitioned into groups based on whether they experienced an increase or a decrease in mitochondrial 8-oxo-dG break frequency from baseline to 72 weeks, those who ended up having an increase in 8-oxo-dG of 0.06 or higher started with higher levels of FEN1 mRNA at baseline than those who had a decrease of 0.06 or more. This difference was not affected by drug arm, viral load, or other variables. This further points to a role of FEN1 in ART-induced mitochondria toxicity, as patients' initial FEN1 mRNA expression may have an influence on the outcome of ART treatment, at least in terms of mitochondrial oxidative damage.

While the mechanism of mitochondrial toxicity from NRTIs through inhibition of polymerase γ and impairment of mtDNA replication has been described [106], the cause of the less-severe mitochondrial complications from lower-toxicity NRTIs and other classes of antiretrovirals is still not fully known. Certain antiretrovirals have been found to modulate the expression of other genes involved in mitochondrial function, as seen in the ZDV-induced decreased levels of thymidine kinase 2 (TK2) and deoxyguanosine kinase (dGK) in the mitochondria [126] and decreased mitochondrial RNA transcription in adipose tissue of subjects receiving ZDV/3TC or d4T/3TC [127]. A better understanding of BER enzyme regulation by antiretroviral agents would provide valuable insight into other mitochondrial off-target effects of these drugs, and could possibly lead to personalized drug regimens tailored to patients' individual mitochondrial profiles, including BER enzyme expression levels.

Ideal clinical trials for studying such long-term ART-induced BER regulation would involve either a longitudinal cohort of HIV patients beginning when they initiate ART and continuing for several years, able to measure cellular and metabolic changes that occur starting

once the viral load has been suppressed and CD4 count returns to normal, or a cross-sectional study of individuals at high risk for HIV infection and are receiving pre-exposure prophylaxis. Possible alternative methods to examine ART-specific effects include culturing human cells with antiretrovirals (as discussed in section 4.2) or using ART-treated animal models, which, while not perfect substitutes for human clinical studies, allow for mechanistic studies.

4.2. Base-excision repair enzyme expression in antiretroviral-treated renal cells

The next goal of the study was to further evaluate the ART-related mtDNA oxidative damage and the drug-induced effects on BER enzymes mechanistically. To accomplish this, we sought to develop an *in vitro* model for cellular toxicity caused by ART regimens currently in clinical use in the United States. Protease inhibitors (PIs) are a class of antiretroviral which is given to newly-diagnosed HIV patients who are ART-naïve [78], and although they have some clinical side effects [82], the mitochondrial complications of these drug regimens have not been investigated. One of the more severe complications associated with certain PIs is renal toxicity [88], and as damage to the renal proximal convoluted tubule (RPCT) has been documented in patients taking PIs [107, 108], we chose to use primary RPCT epithelial cells for our toxicity model.

Primary RPCT epithelial cells were cultured with patient sera steady-state C_{max} equivalent concentrations of two currently-recommended PI-based drug regimens: ritonavir-boosted atazanavir (TDF/FTC +ATV/r) or ritonavir-boosted darunavir (TDF/FTC +DRV/r). Vehicle (DMSO) –treated and untreated cells were used as controls. Treatment lasted for one week before harvesting the cells, as is common in primary culture antiretroviral research [117]. After treating, cells displayed no morphological differences between the treatment groups.

As expected, after one week the treated cells had higher mtDNA oxidative damage than the untreated cells. This was accompanied with an increase in OGG1 mRNA, indicating an upregulation in response to oxidative stress that is consistent with the results from the clinical study. No significant differences in protein levels were found, though as these data were calculated to be underpowered, a higher number of experimental replicates could possibly reveal subtler differences.

Two respiratory parameters were also found to be affected by drug treatment: cells treated with the ATV-based regimen had higher levels of non-mitochondrial respiration relative

to vehicle-treated cells, and cells treated with the DRV-based regimen had higher levels of proton leak than both the untreated and vehicle-treated cells. Non-mitochondrial respiration accounts for all cellular oxygen consumption that is not attributable to OXPHOS, and therefore cannot be pinpointed to a specific factor. These include cytoplasmic re-reduction of NADH, fatty acid desaturation, and activity of various detoxification enzymes [19]. Proton leak consists of hydrogen ions that slip back through the inner mitochondrial membrane from the inner membrane space into the matrix without passing through ATP synthase after being pumped across by the OXPHOS complexes [128]. This leakage results in a reduced efficiency of ATP production per NADH molecule oxidized, and can be due to increased membrane permeability. Overall ATP production and maximum capacity were not significantly affected by antiretroviral treatment. It is possible that higher glycolysis and NADH turnover rates could be fueling increased OXPHOS activity to make up for the ATP production lost through proton leak; further investigation into CI and CIV enzyme activity levels following treatment could yield greater insight.

Interestingly in these experiments, the vehicle, DMSO, had an effect on mtDNA oxidative damage and OGG1 mRNA levels itself. The concentration of DMSO used here is similar to that used in many other drug delivery experiments and well below the threshold that cellular toxicity is generally noted [117]. However, in addition to performing a higher number of replicates, identifying solvents for the PIs that have a lesser effect on mitochondrial oxidative stress and response could help discern significant differences between the treatments and improve the power of *in vitro* studies using this renal model.

Possible future studies using this RPCT system would be to identify the toxicities of the individual drugs in these regimens. For example, TDF is known to induce renal toxicity among other complications, although its affinity for pol γ and therefore its potential to inhibit this mtDNA replication enzyme are low [106]. Recently, REV3 DNA polymerase has been identified in the mitochondria and found to be protective of mitochondrial function [129]; following this, it would be worthwhile to investigate whether TDF or other NRTIs have inhibitory effects on this polymerase as well. Further, the precise targets of PIs that cause the observed oxidative stress have not yet been identified. Any inhibitory effects of PIs against human proteases would be worth investigating. Particularly, the protease inhibitor Wss1 in yeast is involved in repair of DNA-protein crosslinks, and the human translesion synthesis protein

SPRTN has recently been identified as a potential homolog [130]. If PIs are capable of binding to human proteases such as SPRTN in addition to the viral protease, this could increase DNA damage and mutation due to unresolved DNA-protein crosslinks, such as can happen between guanine and the tri-lysine moiety of transcription factor A, mitochondrial (TFAM) as a result of oxidation [25].

4.3. Conclusions

From both of these studies, it is clear that base-excision repair plays a role in cellular toxicity due to HIV infection and ART treatment. While OGG1 is upregulated in response to the mtDNA oxidative damage that results from ART, its expression is impacted by HIV in a manner that impairs its proper response to oxidative stress. MutYH mRNA was not found to correlate with 8-oxo-dG break frequency *in vitro* or *ex vivo*, but its reduction in HIV-positive, ART-naïve patients may be a factor in the increased amounts of mtDNA oxidative damage they show. FEN1 mRNA levels were not affected by HIV status but did decrease after patients had been on ART for 72 weeks, indicating a long-term impact of antiretrovirals on FEN1 expression. As higher FEN1 levels were found at baseline in patients who experienced increases in mtDNA 8-oxo-dG break frequency after 72 weeks of ART relative to those who experienced a decrease further suggests an interaction between FEN1 regulation and antiretroviral therapy, as patients initial FEN1 expression may influence how they respond to drug treatment.

4.4. Future directions

Additional research should include mitochondrial respirational analysis between the patient groups. This could be accomplished in the viable PBMCs from SEARCH 014 specimens. Utilizing specimens from Group 3 of the SEARCH 014 cohort (HIV-positive patients on ART without peripheral neuropathy) would allow for a comparison of mitochondrial respiratory parameters in individuals on long-term ART to the HIV-seronegative controls, and to determine any relationship between altered BER enzyme expression and reduced mitochondrial function. Likewise, Groups 1 and 4 (HIV-positive patients on ART with symptomatic or asymptomatic peripheral neuropathy) would provide further insight into the cause of ART-induced peripheral neuropathy, another serious treatment complication, by examining

mitochondrial respiratory parameters and BER enzyme regulation in relation to neuropathy-linked mtDNA oxidative damage and decreased OXPHOS enzyme activity.

Transcriptional regulation of the repair enzymes is only part of the story. While we have shown in both *ex vivo* and *in vitro* systems that the enzymes that repair oxidatively-modified bases in mtDNA have altered mRNA levels in response to treatment-induced oxidative mtDNA damage, the protein and enzymatic specific activity levels of OGG1, MutYH, or FEN1 would be better indicative of any changes in BER function. Obtaining sufficient quantities of patient PBMCs to perform western blotting or flow cytometry could be beneficial for a more thorough understanding of BER expression regulation during HIV-infection and ART. While protein levels were not significantly different in the *in vitro* ART-treatment experiment, it is possible that the enzyme activity levels have been impacted by ART. A recently-developed fluorescently-labeled DNA repair assay [131] could work well with our *in vitro* system to determine any actual BER functional consequences to ART treatment.

Additionally, as these proteins are not involved solely in DNA repair in the mitochondria, further investigation into protein levels should include cellular compartmentalization. The different splice variants of these genes, which could be detected at the mRNA level through qPCR, preferentially localize to either the nucleus or the mitochondria [29, 31], and analysis of these variants could indicate whether regulation of one type or the other is being more strongly affected by ART. However, these splice variants are not exclusively transported into either organelle [132, 133]. Thus, the mitochondria contains some full-length proteins containing nuclear localization sequences, and the nucleus contains some truncated proteins with exposed mitochondrial localization sequences [25], and the transcription levels of each variant alone are not enough to determine whether nuclear or mitochondrial DNA repair specifically is being affected by protein expression changes. Due to the slow growth rate of primary RPCT cells, a test for mitochondrial localization using low cell counts would be useful; this could possibly be accomplished through fluorescent microscopy.

As mtDNA BER has been shown here to be involved in mitochondrial toxicity as a result of HIV infection and antiretroviral treatment, it would be worth investigating whether this repair pathway has a role in other mitochondria-related diseases or syndromes. For example, a link has recently been described between mitochondrial dysfunction and diabetes, particularly in the cases of HIV infection and ART as HIV-positive individuals have elevated rates of insulin

resistance [134]. In pediatric HIV patients, mtDNA copies per cell were found to be lower in children with insulin resistance, and CI enzyme activity was inversely correlated with fasting serum glucose levels [135]. Mitochondrial BER would be needed to counter the oxidative damage incurred by impaired mitochondrial function, and the ability of OGG1, MutYH, FEN1, and other BER enzymes to respond properly in diabetic patients would be informative of the etiology of this metabolic disease.

FEN1 in particular appeared to be affected by ART treatment, and the degree of patients' changes in 8-oxo-dG following treatment initiation corresponded with their expression levels of this gene at baseline. Mitochondrial base-excision repair is not the only function of FEN1, however. In addition to processing the 5'-overhang as a result of long-patch BER in the nucleus as well as the mitochondria, FEN1 also processes the Okazaki fragments that are formed during nuclear DNA replication [41] and plays a role in leading-strand telomere replication [39].

Often, patients suffering from HIV-related chronic inflammation experience accelerated aging and associated complications [136]. One of the hallmarks of advanced age, in addition to high amounts of oxidative stress, is shortened telomeres [137], which ultimately lead to degradation of coding DNA adjacent to the telomeres and cellular senescence [138]. Recently, shortened telomeres have been found in HIV patients [139], especially those with chronic inflammation and age-associated syndromes such as chronic obstructive pulmonary disease (COPD) [140]. It is possible that the decreased expression of FEN1 following ART initiation could have an effect on telomere replication, causing a reduction in telomere length and contributing to age-associated ART-induced health issues, including fatigue, cardiovascular disease risk, and neuropathy.

In the modern age of health, personalized medicine is beginning to become a reality in the treatment of complicated diseases and disorders, as many of today's health challenges are multifaceted and heavily influenced by a person's own lifestyle, health history, and genetic makeup. For example, patients with breast cancer are currently assigned a particular chemotherapeutic treatment based on whether their tumors express estrogen, progesterone, or her2 receptors, allowing for a therapy that better targets their particular tumor type and results in fewer toxicities that can arise from a broader generalized chemotherapy strategy [141]. In the case of HIV/AIDS treatment, there are a number of first-line drug options available, though a patient may be placed on an alternative drug regimen such as an abacavir (ABC)-containing

regimen if they are negative for the human leukocyte antigen (HLA)-B*5701 expression [142] or a cobicistat-boosted PI-based regimen if they have a sufficiently high creatine clearance rate (CrCl) [143].

The expression of certain genes, such as FEN1, may influence a patient's response to ART. This would open up the possibility of better fine-tuning a patient's ART regimen based on their genetics and current health status. This would give better control over viral load reduction while avoiding or at least diminishing some of the more serious complications of ART treatment. For example, a patient who has a FEN1 expression level below a certain threshold could possible fare relatively well on a drug that can cause a moderate amount of oxidative damage, while those with a FEN1 level above the threshold might be best on a less oxidative stress-inducing regimen.

The continued development of novel antiretrovirals will provide a greater repertoire of ART agents to select from when choosing an ideal regimen for a patient. With this, however, a thorough understanding of their molecular effects is essential to designing personalized therapies. Also critical is the ability to rapidly and accurately test a patient's expression levels of multiple genes. Here we have developed a quick method to evaluate mitochondrial BER enzyme expression in easily-obtained blood samples using quantitative real-time PCR. High throughput qPCR systems now in use enable multiplexing of dozens or even hundreds of genes simultaneously [144], which could be used to analyze a wide array of genes of interest for mitochondrial toxicity studies including BER enzymes, OXPHOS enzymes, pol γ, antioxidants, and others involved in or affected by ART-induced toxicity. Technology is advancing for the use of gene chips to analyze mRNA transcripts of hundreds of genes from a relatively small sample quantity [145]; such chips could be produced which would include readings of FEN1 and the other genes mentioned above. These, along with an extensive bioinformatic database of drug responses, could be used for timely screening of patient genetic profiles and prescription of the best corresponding antiretroviral combination.

REFERENCES

1. Di Benedetto, G., et al., *Ca2+ and cAMP cross-talk in mitochondria.* J Physiol, 2014. **592**(Pt 2): p. 305-12.
2. Lill, R., et al., *The role of mitochondria in cellular iron-sulfur protein biogenesis and iron metabolism.* Biochim Biophys Acta, 2012. **1823**(9): p. 1491-508.
3. Bastin, J., *Regulation of mitochondrial fatty acid beta-oxidation in human: what can we learn from inborn fatty acid beta-oxidation deficiencies?* Biochimie, 2014. **96**: p. 113-20.
4. Nunes-Nesi, A., et al., *Regulation of the mitochondrial tricarboxylic acid cycle.* Curr Opin Plant Biol, 2013. **16**(3): p. 335-43.
5. Martinez, F., et al., *Multiple functions of syncytiotrophoblast mitochondria.* Steroids, 2015. **103**: p. 11-22.
6. Li, M.X. and G. Dewson, *Mitochondria and apoptosis: emerging concepts.* F1000Prime Rep, 2015. **7**: p. 42.
7. Sherratt, H.S., *Mitochondria: structure and function.* Rev Neurol (Paris), 1991. **147**(6-7): p. 417-30.
8. Raha, S. and B.H. Robinson, *Mitochondria, oxygen free radicals, disease and ageing.* Trends Biochem Sci, 2000. **25**(10): p. 502-8.
9. Alberts, B., et al., *Molecular Biology of the Cell*. 5th ed. 2007: Garland Science.
10. Giorgi, C., et al., *Mitochondria-associated membranes: composition, molecular mechanisms, and physiopathological implications.* Antioxid Redox Signal, 2015. **22**(12): p. 995-1019.
11. Christian, B.E. and L.L. Spremulli, *Mechanism of protein biosynthesis in mammalian mitochondria.* Biochim Biophys Acta, 2012. **1819**(9-10): p. 1035-54.
12. Varabyova, A., D. Stojanovski, and A. Chacinska, *Mitochondrial protein homeostasis.* IUBMB Life, 2013. **65**(3): p. 191-201.
13. Falkenberg, M., N.G. Larsson, and C.M. Gustafsson, *DNA replication and transcription in mammalian mitochondria.* Annu Rev Biochem, 2007. **76**: p. 679-99.
14. Wallace, D.C., *Why do we still have a maternally inherited mitochondrial DNA? Insights from evolutionary medicine.* Annu Rev Biochem, 2007. **76**: p. 781-821.
15. Ryan, M.T. and N.J. Hoogenraad, *Mitochondrial-nuclear communications.* Annu Rev Biochem, 2007. **76**: p. 701-22.
16. Pearson, N. *Mitochondria*. TutorVista.com 2016 [cited 2016 March 11]; Available from: tutorvista.com.
17. Shapira, A.H.V., *Mitochondrial Function and Dysfunction*. International Review of Neurobiology. Vol. 53. 2002: Academic Press.
18. Borsch, M. and T.M. Duncan, *Spotlighting motors and controls of single FoF1-ATP synthase.* Biochem Soc Trans, 2013. **41**(5): p. 1219-26.
19. Salin, K., et al., *Variation in the link between oxygen consumption and ATP production, and its relevance for animal performance.* Proc Biol Sci, 2015. **282**(1812): p. 20151028.
20. Drose, S. and U. Brandt, *Molecular mechanisms of superoxide production by the mitochondrial respiratory chain.* Adv Exp Med Biol, 2012. **748**: p. 145-69.
21. Imlay, J.A., *Pathways of oxidative damage.* Annu Rev Microbiol, 2003. **57**: p. 395-418.
22. Netto, L.E. and F. Antunes, *The Roles of Peroxiredoxin and Thioredoxin in Hydrogen Peroxide Sensing and in Signal Transduction.* Mol Cells, 2016. **39**(1): p. 65-71.
23. Wolff, J.N., et al., *Mitonuclear interactions: evolutionary consequences over multiple biological scales.* Philos Trans R Soc Lond B Biol Sci, 2014. **369**(1646): p. 20130443.

24. Dumont, E. and A. Monari, *Understanding DNA under oxidative stress and sensitization: the role of molecular modeling.* Front Chem, 2015. **3**: p. 43.
25. Muftuoglu, M., M.P. Mori, and N.C. de Souza-Pinto, *Formation and repair of oxidative damage in the mitochondrial DNA.* Mitochondrion, 2014. **17**: p. 164-81.
26. Klungland, A. and S. Bjelland, *Oxidative damage to purines in DNA: role of mammalian Ogg1.* DNA Repair (Amst), 2007. **6**(4): p. 481-8.
27. Hwang, B.J., G. Shi, and A.L. Lu, *Mammalian MutY homolog (MYH or MUTYH) protects cells from oxidative DNA damage.* DNA Repair (Amst), 2014. **13**: p. 10-21.
28. Scheibye-Knudsen, M., et al., *Protecting the mitochondrial powerhouse.* Trends Cell Biol, 2015. **25**(3): p. 158-70.
29. Nishioka, K., et al., *Expression and differential intracellular localization of two major forms of human 8-oxoguanine DNA glycosylase encoded by alternatively spliced OGG1 mRNAs.* Mol Biol Cell, 1999. **10**(5): p. 1637-52.
30. Ohtsubo, T., et al., *Identification of human MutY homolog (hMYH) as a repair enzyme for 2-hydroxyadenine in DNA and detection of multiple forms of hMYH located in nuclei and mitochondria.* Nucleic Acids Res, 2000. **28**(6): p. 1355-64.
31. Kazak, L., et al., *A cryptic targeting signal creates a mitochondrial FEN1 isoform with tailed R-Loop binding properties.* PLoS One, 2013. **8**(5): p. e62340.
32. Marsin, S., et al., *Role of XRCC1 in the coordination and stimulation of oxidative DNA damage repair initiated by the DNA glycosylase hOGG1.* J Biol Chem, 2003. **278**(45): p. 44068-74.
33. Ba, X., et al., *The role of 8-oxoguanine DNA glycosylase-1 in inflammation.* Int J Mol Sci, 2014. **15**(9): p. 16975-97.
34. Habib, S.L., et al., *Novel mechanism of regulation of the DNA repair enzyme OGG1 in tuberin-deficient cells.* Carcinogenesis, 2010. **31**(11): p. 2022-30.
35. Imai, K., et al., *Induction of OGG1 gene expression by HIV-1 Tat.* J Biol Chem, 2005. **280**(29): p. 26701-13.
36. Dorn, J., et al., *Regulation of human MutYH DNA glycosylase by the E3 ubiquitin ligase mule.* J Biol Chem, 2014. **289**(10): p. 7049-58.
37. Mason, P.A. and L.S. Cox, *The role of DNA exonucleases in protecting genome stability and their impact on ageing.* Age (Dordr), 2012. **34**(6): p. 1317-40.
38. Uhler, J.P. and M. Falkenberg, *Primer removal during mammalian mitochondrial DNA replication.* DNA Repair (Amst), 2015. **34**: p. 28-38.
39. Teasley, D.C., et al., *Flap Endonuclease 1 Limits Telomere Fragility on the Leading Strand.* J Biol Chem, 2015. **290**(24): p. 15133-45.
40. Qian, L., et al., *Human Fanconi anemia complementation group a protein stimulates the 5' flap endonuclease activity of FEN1.* PLoS One, 2013. **8**(12): p. e82666.
41. Henneke, G., S. Koundrioukoff, and U. Hubscher, *Phosphorylation of human Fen1 by cyclin-dependent kinase modulates its role in replication fork regulation.* Oncogene, 2003. **22**(28): p. 4301-13.
42. Hasan, S., et al., *Regulation of human flap endonuclease-1 activity by acetylation through the transcriptional coactivator p300.* Mol Cell, 2001. **7**(6): p. 1221-31.
43. Faust, E.A. and H. Triller, *Stimulation of human flap endonuclease 1 by human immunodeficiency virus type 1 integrase: possible role for flap endonuclease 1 in 5'-end processing of human immunodeficiency virus type 1 integration intermediates.* J Biomed Sci, 2002. **9**(3): p. 273-87.
44. Peeters, M., M. Jung, and A. Ayouba, *The origin and molecular epidemiology of HIV.* Expert Rev Anti Infect Ther, 2013. **11**(9): p. 885-96.
45. Chermann, J.C. and F. Barre-Sinoussi, *Role of the human immunodeficiency virus in the physiopathology of AIDS.* Antibiot Chemother (1971), 1987. **38**: p. 13-20.

46. Hill, A. and A. Balkin, *Risk factors for gastrointestinal adverse events in HIV treated and untreated patients.* AIDS Rev, 2009. **11**(1): p. 30-8.
47. Kaku, M. and D.M. Simpson, *HIV neuropathy.* Curr Opin HIV AIDS, 2014. **9**(6): p. 521-6.
48. Organization, W.H. *HIV/AIDS*. 2015 1/8/2016]; Available from: http://www.who.int/mediacentre/factsheets/fs360/en/.
49. Rubens, M., et al., *HIV Vaccine: Recent Advances, Current Roadblocks, and Future Directions.* J Immunol Res, 2015. **2015**: p. 560347.
50. Campbell, E.M. and T.J. Hope, *HIV-1 capsid: the multifaceted key player in HIV-1 infection.* Nat Rev Microbiol, 2015. **13**(8): p. 471-83.
51. Brandenberg, O.F., et al., *The HIV-1 Entry Process: A Stoichiometric View.* Trends Microbiol, 2015. **23**(12): p. 763-74.
52. Cary, D.C., K. Fujinaga, and B.M. Peterlin, *Molecular mechanisms of HIV latency.* J Clin Invest, 2016: p. 1-7.
53. Orenstein, J.M., *Replication of HIV-1 in vivo and in vitro.* Ultrastruct Pathol, 2007. **31**(2): p. 151-67.
54. Freed, E.O., *HIV-1 assembly, release and maturation.* Nat Rev Microbiol, 2015. **13**(8): p. 484-96.
55. Apostolova, N., A. Blas-Garcia, and J.V. Esplugues, *Mitochondrial interference by anti-HIV drugs: mechanisms beyond Pol-gamma inhibition.* Trends Pharmacol Sci, 2011. **32**(12): p. 715-25.
56. Hulgan, T. and M. Gerschenson, *HIV and mitochondria: more than just drug toxicity.* J Infect Dis, 2012. **205**(12): p. 1769-71.
57. McComsey, G.A., et al., *Changes in fat mitochondrial DNA and function in subjects randomized to abacavir-lamivudine or tenofovir DF-emtricitabine with atazanavir-ritonavir or efavirenz: AIDS Clinical Trials Group study A5224s, substudy of A5202.* J Infect Dis, 2013. **207**(4): p. 604-11.
58. Perez-Matute, P., et al., *Role of mitochondria in HIV infection and associated metabolic disorders: focus on nonalcoholic fatty liver disease and lipodystrophy syndrome.* Oxid Med Cell Longev, 2013. **2013**: p. 493413.
59. Ouellet, D.L., et al., *Regulation of host gene expression by HIV-1 TAR microRNAs.* Retrovirology, 2013. **10**: p. 86.
60. Zauli, G., et al., *Human immunodeficiency virus type 1 Tat protein protects lymphoid, epithelial, and neuronal cell lines from death by apoptosis.* Cancer Res, 1993. **53**(19): p. 4481-5.
61. Bailey, A.C. and M. Fisher, *Current use of antiretroviral treatment.* Br Med Bull, 2008. **87**: p. 175-92.
62. Este, J.A. and T. Cihlar, *Current status and challenges of antiretroviral research and therapy.* Antiviral Res, 2010. **85**(1): p. 25-33.
63. Arribas, J.R. and J. Eron, *Advances in antiretroviral therapy.* Curr Opin HIV AIDS, 2013. **8**(4): p. 341-9.
64. Wynn, G.H., et al., *Antiretrovirals, part 1: overview, history, and focus on protease inhibitors.* Psychosomatics, 2004. **45**(3): p. 262-70.
65. Blanco, J.L., et al., *HIV integrase inhibitors: a new era in the treatment of HIV.* Expert Opin Pharmacother, 2015. **16**(9): p. 1313-24.
66. Haqqani, A.A. and J.C. Tilton, *Entry inhibitors and their use in the treatment of HIV-1 infection.* Antiviral Res, 2013. **98**(2): p. 158-70.
67. Benson, C.A., *Structured treatment interruptions--new findings.* Top HIV Med, 2006. **14**(3): p. 107-11.
68. Collins, S.E., P.M. Grant, and R.W. Shafer, *Modifying Antiretroviral Therapy in Virologically Suppressed HIV-1-Infected Patients.* Drugs, 2015.

69. Taylor, L.E., T. Swan, and G.V. Matthews, *Management of hepatitis C virus/HIV coinfection among people who use drugs in the era of direct-acting antiviral-based therapy.* Clin Infect Dis, 2013. **57 Suppl 2**: p. S118-24.
70. Anglemyer, A., et al., *Antiretroviral therapy for prevention of HIV transmission in HIV-discordant couples.* Cochrane Database Syst Rev, 2013. **4**: p. Cd009153.
71. Sturt, A.S. and J.S. Read, *Antiretroviral use during pregnancy for treatment or prophylaxis.* Expert Opin Pharmacother, 2011. **12**(12): p. 1875-85.
72. Cohen, M.S. and C.L. Gay, *Treatment to prevent transmission of HIV-1.* Clin Infect Dis, 2010. **50 Suppl 3**: p. S85-95.
73. Cihlar, T. and A.S. Ray, *Nucleoside and nucleotide HIV reverse transcriptase inhibitors: 25 years after zidovudine.* Antiviral Res, 2010. **85**(1): p. 39-58.
74. Arts, E.J. and D.J. Hazuda, *HIV-1 antiretroviral drug therapy.* Cold Spring Harb Perspect Med, 2012. **2**(4): p. a007161.
75. National Institutes of Health. *FDA-Approved HIV Medicines*. AIDSinfo 2015 12/1/2015 [cited 2016 1/5/2016]; Available from: https://aidsinfo.nih.gov/education-materials/fact-sheets/21/58/fda-approved-hiv-medicines.
76. World Health Organization, *WHO Guidelines Approved by the Guidelines Review Committee*, in *Guidelines for the Prevention, Care and Treatment of Persons with Chronic Hepatitis B Infection*. 2015, Copyright (c) World Health Organization 2015.: Geneva.
77. Zapor, M.J., et al., *Antiretrovirals, Part II: focus on non-protease inhibitor antiretrovirals (NRTIs, NNRTIs, and fusion inhibitors).* Psychosomatics, 2004. **45**(6): p. 524-35.
78. National Institutes of Health. *Guidelines for the Use of Antiretroviral Agents in HIV-1-Infected Adults and Adolescents*. AIDSinfo 2015 4/8/2015 1/5/2016].
79. Wensing, A.M., N.M. van Maarseveen, and M. Nijhuis, *Fifteen years of HIV Protease Inhibitors: raising the barrier to resistance.* Antiviral Res, 2010. **85**(1): p. 59-74.
80. Hull, M.W. and J.S. Montaner, *Ritonavir-boosted protease inhibitors in HIV therapy.* Ann Med, 2011. **43**(5): p. 375-88.
81. Gerschenson, M. and K. Brinkman, *Mitochondrial dysfunction in AIDS and its treatment.* Mitochondrion, 2004. **4**(5-6): p. 763-77.
82. Margolis, A.M., et al., *A review of the toxicity of HIV medications.* J Med Toxicol, 2014. **10**(1): p. 26-39.
83. Helbert, M., et al., *Zidovudine-associated myopathy.* Lancet, 1988. **2**(8612): p. 689-90.
84. Mhiri, C., et al., *Zidovudine myopathy: a distinctive disorder associated with mitochondrial dysfunction.* Ann Neurol, 1991. **29**(6): p. 606-14.
85. Lim, S.E. and W.C. Copeland, *Differential incorporation and removal of antiviral deoxynucleotides by human DNA polymerase gamma.* J Biol Chem, 2001. **276**(26): p. 23616-23.
86. Gardner, K., et al., *HIV treatment and associated mitochondrial pathology: review of 25 years of in vitro, animal, and human studies.* Toxicol Pathol, 2014. **42**(5): p. 811-22.
87. Apostolova, N., A. Blas-Garcia, and J.V. Esplugues, *Mitochondrial toxicity in HAART: an overview of in vitro evidence.* Curr Pharm Des, 2011. **17**(20): p. 2130-44.
88. Izzedine, H., M. Harris, and M.A. Perazella, *The nephrotoxic effects of HAART.* Nat Rev Nephrol, 2009. **5**(10): p. 563-73.
89. Dykens, J.A., L.D. Marroquin, and Y. Will, *Strategies to reduce late-stage drug attrition due to mitochondrial toxicity.* Expert Rev Mol Diagn, 2007. **7**(2): p. 161-75.
90. Porter, K.M. and R.L. Sutliff, *HIV-1, reactive oxygen species, and vascular complications.* Free Radic Biol Med, 2012. **53**(1): p. 143-59.
91. Sharma, B., *Oxidative stress in HIV patients receiving antiretroviral therapy.* Curr HIV Res, 2014. **12**(1): p. 13-21.

92. Kallianpur, K.J., et al., *Oxidative mitochondrial DNA damage in peripheral blood mononuclear cells is associated with reduced volumes of hippocampus and subcortical gray matter in chronically HIV-infected patients.* Mitochondrion, 2016. **28**: p. 8-15.
93. Parikh, N.I., et al., *Lipoprotein concentration, particle number, size and cholesterol efflux capacity are associated with mitochondrial oxidative stress and function in an HIV positive cohort.* Atherosclerosis, 2015. **239**(1): p. 50-4.
94. Shoumilina, T. *Thailand*. UNAIDS 2014 [cited 2016 January 27]; Available from: http://www.unaids.org/en/regionscountries/countries/thailand.
95. AVERT. *HIV and AIDS in Thailand*. Global information and advice on HIV and AIDS 2015 [cited 2016 January 27]; Available from: http://www.avert.org/professionals/hiv-around-world/asia-pacific/thailand.
96. Division, I.B. *The Government Pharmaceutical Organization*. 2012; Available from: http://www.intergpomed.com/.
97. Organization, W.H. *Thailand statistics summary (2002-present)*. Global Health Observatory country views 2015 [cited 2016 January 27]; Available from: http://apps.who.int/gho/data/node.country.country-THA.
98. Sungkanuparph, S., et al., *Guidelines for antiretroviral therapy in HIV-1 infected adults and adolescents: the recommendations of the Thai AIDS Society (TAS) 2008.* J Med Assoc Thai, 2008. **91**(12): p. 1925-35.
99. Organization, W.H., *Transaction prices for antiretroviral medicines from 2010 to 2013: global price reporting mechanism*, in *WHO AIDS medicines and diagnostics services*. 2013.
100. Phanuphak, S.S.W.T.C.U.S.C.S.B.M.L.K.R.P., *Thai national guidelines for antiretroviral therapy in HIV-1 infected adults and adolescents 2010.* Asian Biomedicine, 2010. **4**(4): p. 14.
101. SEARCH. *SEARCH Thailand*. 2006 [cited 2016 January 27]; Available from: http://www.searchthailand.org/.
102. Phanuphak, N., et al., *A 72-week randomized study of the safety and efficacy of a stavudine to zidovudine switch at 24 weeks compared to zidovudine or tenofovir disoproxil fumarate when given with lamivudine and nevirapine.* Antivir Ther, 2012. **17**(8): p. 1521-31.
103. Shikuma, C.M., et al., *Distal leg epidermal nerve fiber density as a surrogate marker of HIV-associated sensory neuropathy risk: risk factors and change following initial antiretroviral therapy.* J Neurovirol, 2015. **21**(5): p. 525-34.
104. Al-Dakkak, I., et al., *The impact of specific HIV treatment-related adverse events on adherence to antiretroviral therapy: a systematic review and meta-analysis.* AIDS Care, 2013. **25**(4): p. 400-14.
105. von Hentig, N., *Clinical use of cobicistat as a pharmacoenhancer of human immunodeficiency virus therapy.* HIV AIDS (Auckl), 2016. **8**: p. 1-16.
106. Kohler, J.J. and W. Lewis, *A brief overview of mechanisms of mitochondrial toxicity from NRTIs.* Environ Mol Mutagen, 2007. **48**(3-4): p. 166-72.
107. Waheed, S., et al., *Proximal tubular dysfunction and kidney injury associated with tenofovir in HIV patients: a case series.* Clin Kidney J, 2015. **8**(4): p. 420-5.
108. Casado, J.L., et al., *Prevalence and significance of proximal renal tubular abnormalities in HIV-infected patients receiving tenofovir.* Aids, 2016. **30**(2): p. 231-9.
109. Lv, Z., Y. Chu, and Y. Wang, *HIV protease inhibitors: a review of molecular selectivity and toxicity.* HIV AIDS (Auckl), 2015. **7**: p. 95-104.
110. McDonald, C., et al., *Clinical significance of hyperbilirubinemia among HIV-1-infected patients treated with atazanavir/ritonavir through 96 weeks in the CASTLE study.* AIDS Patient Care STDS, 2012. **26**(5): p. 259-64.

111. Molina, J.M., et al., *Safety and efficacy of darunavir (TMC114) with low-dose ritonavir in treatment-experienced patients: 24-week results of POWER 3.* J Acquir Immune Defic Syndr, 2007. **46**(1): p. 24-31.
112. Mills, A.M., et al., *Once-daily darunavir/ritonavir vs. lopinavir/ritonavir in treatment-naive, HIV-1-infected patients: 96-week analysis.* Aids, 2009. **23**(13): p. 1679-88.
113. Kotler, D.P., *HIV and antiretroviral therapy: lipid abnormalities and associated cardiovascular risk in HIV-infected patients.* J Acquir Immune Defic Syndr, 2008. **49 Suppl 2**: p. S79-85.
114. *Physicians' Desk Reference*. [cited 2014 9/1/2014]; Available from: www.pdr.net.
115. Gerencser, A.A., et al., *Quantitative microplate-based respirometry with correction for oxygen diffusion.* Anal Chem, 2009. **81**(16): p. 6868-78.
116. Seahorse Bioscience. *Seahorse XF Cell Mito Stress Test Kit*. 2015 [cited 2016 1/25/2016].
117. Robertson, K., J. Liner, and R.B. Meeker, *Antiretroviral neurotoxicity.* J Neurovirol, 2012. **18**(5): p. 388-99.
118. Marroquin, L.D., et al., *Circumventing the Crabtree effect: replacing media glucose with galactose increases susceptibility of HepG2 cells to mitochondrial toxicants.* Toxicol Sci, 2007. **97**(2): p. 539-47.
119. Brand, M.D. and D.G. Nicholls, *Assessing mitochondrial dysfunction in cells.* Biochem J, 2011. **435**(2): p. 297-312.
120. Kelava, T., I. Cavar, and F. Culo, *Influence of small doses of various drug vehicles on acetaminophen-induced liver injury.* Can J Physiol Pharmacol, 2010. **88**(10): p. 960-7.
121. Policicchio, B.B., I. Pandrea, and C. Apetrei, *Animal Models for HIV Cure Research.* Front Immunol, 2016. **7**: p. 12.
122. Anderson, L.M., *The effects of chemotherapeutic or antiretroviral drugs on mitochondrial function*, in *Cell and Molecular Biology*. 2013, University of Hawaii at Manoa.
123. Hulgan, T., et al., *Epidermal nerve fiber density, oxidative stress, and mitochondrial haplogroups in HIV-infected Thais initiating therapy.* AIDS, 2014. **28**(11): p. 1625-33.
124. Kang, K.A., et al., *Butin decreases oxidative stress-induced 8-hydroxy-2'-deoxyguanosine levels via activation of oxoguanine glycosylase 1.* Chem Biol Interact, 2009. **181**(3): p. 338-42.
125. Singh, B., et al., *Antioxidant-mediated up-regulation of OGG1 via NRF2 induction is associated with inhibition of oxidative DNA damage in estrogen-induced breast cancer.* BMC Cancer, 2013. **13**: p. 253.
126. Sun, R., S. Eriksson, and L. Wang, *Zidovudine induces downregulation of mitochondrial deoxynucleoside kinases: implications for mitochondrial toxicity of antiviral nucleoside analogs.* Antimicrob Agents Chemother, 2014. **58**(11): p. 6758-66.
127. Mallon, P.W., et al., *In vivo, nucleoside reverse-transcriptase inhibitors alter expression of both mitochondrial and lipid metabolism genes in the absence of depletion of mitochondrial DNA.* J Infect Dis, 2005. **191**(10): p. 1686-96.
128. Brand, M.D., et al., *The causes and functions of mitochondrial proton leak.* Biochim Biophys Acta, 1994. **1187**(2): p. 132-9.
129. Singh, B., et al., *Human REV3 DNA Polymerase Zeta Localizes to Mitochondria and Protects the Mitochondrial Genome.* PLoS One, 2015. **10**(10): p. e0140409.
130. Stingele, J., B. Habermann, and S. Jentsch, *DNA-protein crosslink repair: proteases as DNA repair enzymes.* Trends Biochem Sci, 2015. **40**(2): p. 67-71.
131. Edwards, S.K., et al., *In Vitro Fluorogenic Real-Time Assay of the Repair of Oxidative DNA Damage.* Chembiochem, 2015. **16**(11): p. 1637-46.
132. Nakabeppu, Y., *Regulation of intracellular localization of human MTH1, OGG1, and MYH proteins for repair of oxidative DNA damage.* Prog Nucleic Acid Res Mol Biol, 2001. **68**: p. 75-94.

133. Kalifa, L., et al., *Evidence for a role of FEN1 in maintaining mitochondrial DNA integrity.* DNA Repair (Amst), 2009. **8**(10): p. 1242-9.
134. Nix, L.M. and P.C. Tien, *Metabolic syndrome, diabetes, and cardiovascular risk in HIV.* Curr HIV/AIDS Rep, 2014. **11**(3): p. 271-8.
135. Sharma, T.S., et al., *Short communication: The relationship between mitochondrial dysfunction and insulin resistance in HIV-infected children receiving antiretroviral therapy.* AIDS Res Hum Retroviruses, 2013. **29**(9): p. 1211-7.
136. Aberg, J.A., *Aging, inflammation, and HIV infection.* Top Antivir Med, 2012. **20**(3): p. 101-5.
137. Rizvi, S., S.T. Raza, and F. Mahdi, *Telomere length variations in aging and age-related diseases.* Curr Aging Sci, 2014. **7**(3): p. 161-7.
138. Bernadotte, A., V.M. Mikhelson, and I.M. Spivak, *Markers of cellular senescence. Telomere shortening as a marker of cellular senescence.* Aging (Albany NY), 2016. **8**(1): p. 3-11.
139. Hearps, A.C., et al., *HIV infection induces age-related changes to monocytes and innate immune activation in young men that persist despite combination antiretroviral therapy.* Aids, 2012. **26**(7): p. 843-53.
140. Liu, J.C., et al., *Absolute leukocyte telomere length in HIV-infected and uninfected individuals: evidence of accelerated cell senescence in HIV-associated chronic obstructive pulmonary disease.* PLoS One, 2015. **10**(4): p. e0124426.
141. Myers, M.B., *Targeted therapies with companion diagnostics in the management of breast cancer: current perspectives.* Pharmgenomics Pers Med, 2016. **9**: p. 7-16.
142. Guo, Y., et al., *Studies on abacavir-induced hypersensitivity reaction: a successful example of translation of pharmacogenetics to personalized medicine.* Sci China Life Sci, 2013. **56**(2): p. 119-24.
143. McDonald, C.K., et al., *Cobicistat-boosted protease inhibitors in HIV-infected patients with mild to moderate renal impairment.* HIV Clin Trials, 2014. **15**(6): p. 269-73.
144. Mamanova, L., et al., *Target-enrichment strategies for next-generation sequencing.* Nat Methods, 2010. **7**(2): p. 111-8.
145. Lim, G.S., et al., *A lab-on-a-chip system integrating tissue sample preparation and multiplex RT-qPCR for gene expression analysis in point-of-care hepatotoxicity assessment.* Lab Chip, 2015. **15**(20): p. 4032-43.